To The Graduate Council:

I am submitting herewith a dissertation written by Bahram Zandi entitled "Novel Approaches in the Thermal Management of Electronics Involving Coupled Electrical, Thermal and CFD Analysis." I have examined the final paper copy of this dissertation for form and content and recommend that it be accepted in partial fulfillment of the requirements for the degree of Doctor of Philosophy, with a major in Mechanical Engineering.

Majid Keyhani

Majid Keyhani, Major Professor

We have read this dissertation
and recommend its acceptance:

Masood Parang

William Johnson

Marion Hansen

Accepted for the Council:

Vice Chancellor and Dean of
Graduate Studies

Thesis
2005b
.Z26

Novel Approaches in the Thermal Management of Electronics Involving Coupled Electrical, Thermal and CFD Analysis

A Dissertation Presented for The

Doctor of Philosophy Degree

The University of Tennessee, Knoxville

Bahram Zandi

May, 2005

ACKNOWLEDGEMENTS

My foremost gratitude goes to my advisor, Professor Majid Keyhani, for his guidance, continual encouragement and friendship. I sincerely hope that we will continue our collaboration on many future projects.

My appreciation also goes to my other committee members- Professor Masood Parang, Professor William S. Johnson and Professor Marion Hansen- for their valuable suggestions and guidance.

I would also like to thank my good friend and business partner, Dr. Jeffrey Lewis. His suggestions greatly improved my dissertation, and his encouragements were extremely effective in completion of this study.

Finally, no words can express my heartfelt gratitude to my beloved family – my wife Dawn Zandi and my mother Giti Beheshti - for their love and support.

ABSTRACT

The cooling of electronic components is one of the most important tasks in the design and packaging of electronic equipments as insufficient thermal control can lead to low reliability, short life and failure of the electronic components. According to a study conducted by Philips Corporation, every ten degree Celsius increase in temperature causes a fifty percent decrease in the operating life of many integrated circuits.

With the increasing design complexities and reliability requirements, today's electronic design engineers rely significantly on software packages (often based on methods of Computational Fluid Dynamics, or CFD) for the prediction of electronics operational temperature. In the early to intermediate product design phase, numerical analysis is used to select a cooling strategy and refine a thermal design by parametric analysis. In the final design phase, detailed analysis of product thermal performance is carried out for performance and reliability predictions. However, it is recognized that, for a large class of electronics applications, progress in reliability prediction is currently hampered by the lack of accurate prediction methods. This is especially true for problems in which there is significant heat generation due to the flow of electrical currents in traces and conductors. The main difficulty comes from the fact that the majority of the heat is dissipated as a result of the flow of electrical current in various conductors. In order to predict temperatures accurately, the important mechanisms for heat generation and heat

transfer must be adequately considered. The issue that complicates matters is that the amount of heat generated by the electric current flowing through the board is itself dependent on temperature, thus requiring an approach that considers the coupling between the electrical and thermal aspects of the model.

This study is aimed at this class of electronics cooling applications. Its objective is to present a novel approach to the thermal management of electronic systems that focuses on the multi-physics nature of these problems by coupling electrical, thermal and CFD effects.

Following the presentation of relevant, governing, partial differential equations, a numerical approach is presented that centrally addresses various coupled mechanisms involved, namely:

- Conjugate convection and conduction throughout the region of interest
- Surface-to-surface thermal radiation
- Calculation of the coupled flow field using the techniques of computational fluid dynamics.
- Solution of electrical field and the resulting current densities for determination of heat dissipation in electrical connectors.

The software package ElectroFlo is developed by the author for the thermal management of electronic devices using this methodology.

In Chapter six, the software is used to predict the temperature rise resulting from the flow of electrical current in an embedded trace. The predicted temperature rise is shown to be in excellent agreement with the experimental data reported by the IPC researchers. In Chapter seven, a far more complex transient problem involving electrical current flow in a multi-layer board with connecting vias is studied. This type of board is frequently encountered in aircraft electronics boxes and it requires the solution of the voltage field to obtain the power dissipation distribution. The results of these simulations demonstrate the effect of coupling the electrical and thermal solutions. It is shown that failure to recognize this effect would result in an inaccurate model prediction; the coupled analysis predicts failure, whereas the uncoupled analysis predicts acceptable temperature levels.

Table of Contents

I. INTRODUCTION 1

1.1 Electrical Current Flow in Traces and Connectors 1

1.1.1 Circuit Boards Trace Heating (Current Carrying Capacity of Traces) 2

1.1.2 Straps and Connectors 2

1.1.3 Bussed Electrical Centers (Junction Boxes, Power Distribution Boxes) 5

1.2 Objective 7

II. BACKGROUND AND LITERATURE REVIEW 8

2.1 Background 8

2.2 Approach 13

2.2.1 Experimental Investigation 14

2.2.2 Theoretical Calculation 15

2.3 Literature Review 17

2.3.1 Natural Convection in Enclosures 18

2.3.2 Combined Natural Convection and Radiation 26

2.3.3 Cooling of Electronic Equipment 30

2.3.4 Coupled Thermal-Electrical Analysis 40

III. GOVERNING EQUATIONS 44

3.1 Conservation of Mass (Continuity Equation) 45

3.1.1 Continuity Equation for Incompressible Fluids 45

3.2 Momentum Equation (Newton's Second Law of Motion) 46

3.2.1 The Navier-Stokes Equations 46

3.2.2 Fluid Motion Pressure 48

3.2.3 Boussinesq Approximation 49

3.3 Conservation of Energy (First Law of Thermodynamics) 50

3.3.1 Simplifying Assumptions for Energy Equation 51

3.4 Voltage Field Equation 51

3.5 Thermal Radiation 52

3.5.1 Surface-to-surface radiation 52

IV. NUMERICAL PROCEDURE 54

4.1 General Differential Balance Equation 54

4.2 Discretization 57

4.3 Control Volume Formulation 59

4.3.1 One-Dimensional Steady-State Heat Conduction 60

4.3.2 A General Convection-Diffusion Formulation 61

4.3.3 General Expressions for ϕ on Control Volume Faces 64

4.3.4 Discretization Equation for Convection-Diffusion 66

4.3.5 Solution of the Flow Field 68

4.3.6 The SIMPLER Algorithm 75

4.4 Coupled Thermal / Electrical Analysis 81

4.5 Boundary Conditions 82

4.6 The Computational Details 83

V. Description of the Analysis Package 86

5.1 General Description 86

5.2 Model Creation ____ *87*

5.3 Meshing ____ *93*

5.4 Material Properties ____ *94*

5.5 Boundary Conditions ____ *95*

5.5.1 Temperature ____ *97*

5.5.2 Heat Flux ____ *97*

5.5.3 Heated Volume ____ *97*

5.5.4 Convection ____ *97*

5.5.5 Radiation ____ *98*

5.5.5.1 Radiation to Ambient ____ *98*

5.5.5.2 Radiation Network ____ *98*

5.5.6 Point Source ____ *101*

5.5.7 Velocity ____ *101*

5.5.8 Plane Resistance ____ *102*

5.5.9 Voltage ____ *102*

5.5.10 Current ____ *102*

5.5.11 Heat Exchanger ____ *102*

5.6 Analysis Options ____ *103*

VI. Validation Using IPC Design Rules and Limitations to IPC-2221 ____ 104

6.1 IPC-2221 Background ____ *104*

6.2 Single Board with a Trace ____ *107*

6.2.1 Cases Analyzed ____ *107*

6.2.2 Material Properties ____ *107*

6.2.3 Model Details and Boundary Conditions ____ *109*

6.2.4 Comparison with Test Data ____ *113*

6.3 Problems with IPC Design Rules 115

6.4 Single Board inside Enclosure 116

6.4.1 Model Details 118

6.4.1 Boundary Conditions 118

6.4.2 Analysis 118

6.4.3 Results 120

6.5 Multiple Boards inside Enclosure 120

6.5.1 Analysis 123

6.5.2 Results 123

6.6 Closing Remarks 126

VII. Transient Coupled Analysis - Six-Layer Board 127

7.1 Problem Statement 129

7.2 Board Geometrical Details 131

7.3 Modeling Details 133

7.4 Boundary Conditions 133

7.5 Material Properties 133

7.6 Review of Theory and Governing Equations 136

7.7 Results 137

7.7.1 Steady-State Results 137

7.7.2 Transient Results 139

7.8 Conclusions 142

VIII. CLOSING REMARKS 143

8.1 Conclusions ____ *143*

8.2 Recommendations for Future Work ____ *144*

LIST OF REFERENCES ____ **146**

APPENDICES ____ **159**

Divergence Theorem – Definition and Interpretation ____ *160*

Interface conductivity ____ *161*

Correlations Used for Natural Convection Boundary Condition ____ *163*

VITA ____ **165**

List of Tables

Table 4.1: Function $A(|P|)$ Expressions for Various Schemes 69

Table 7.1: Material Properties 135

List of Figures

Figure 1.1: Flex Board with Traces 3

Figure 1.2: Strap and Bus Bar 4

Figure 1.3: Typical Multi-board Junction Box 6

Figure 1.4: Network of Connectors and Traces 6

Figure 2.1: Automotive Electronics Packaging Attributes 10

Figure 2.2: Automotive Electronics Reliability Demand 10

Figure 2.3: A View Beneath the Sheet Metal 11

Figure 4.1: Arbitrary Control Volume with Fluxes 55

Figure 4.2: Cluster of Nodes Surrounding Center Node, P 58

Figure 4.3: Total Flux on Interface Between Two Grid Points 62

Figure 4.4: Two-Dimensional Control Volume 65

Figure 4.5: Staggered Grid Locations for u and v 73

Figure 4.6: Flow Diagram for SIMPLER Algorithm Steady-State 80

Figure 5.1: EFlo Interface with Treeview and Listview Tools 88

Figure 5.2: Definition Form for Functional Variati 96

Figure 6.1: Conductor Sizing Guidelines Based on NBS Testing 106

Figure 6.2: Vertical Board with a Single Trace 108

Figure 6.3: Mesh Used for Vertical Board with a Single Trace 110

Figure 6.4: Temperature and Velocity Field – Vertical Board w/ No Back Plane 111

Figure 6.5: Temperature and Velocity Field – Vertical Board - with Back Plane 112

Figure 6.6: Comparison between Numerical and Experimental Results 114

Figure 6.7: Enclosure and Board Geometry 117

Figure 6.8: Finite Volume Mesh 119

Figure 6.9 : Simulation Results 121

Figure 6.10: Enclosure with Two Boards 122

Figure 6.11: Finite Volume Mesh – Two Boards in Enclosure 124

Figure 6.12: Simulation Results – Two Boards in Enclosure 125

Figure 7.1: Board and Enclosure 130

Figure 7.2: Board Details 132

Figure 7.3: Control Volume Mesh 134

Figure 7.4: Steady-State Temperature and Velocity 138

Figure 7.5: Transient Temperature Rise 139

Figure 7.6: Temperature Distribution after 2 Minutes 140

Figure 7.7: Voltage Distribution Load and Return Layers 141

Figure B.1: Adjacent Control Volumes with Associated Distances 161

Nomenclature

English Symbols

a_i	Coefficient for discretization equation (side i)
b	Constant term for discretization equation
c_p	specific heat at constant pressure
D_e	Elemental diffusion term (on east side)
$\vec{E}$	Electrical Field
F	Body force term in momentum equation
F_e	Elemental mass flow rate (on east side)
F_{k-j}	Viewfactor surface k to j
g	Gravitational acceleration
i	Enthalpy
i	Unit vector in x direction
j	Unit vector in y direction
k	Unit vector in z direction
$\vec{J}$	Current density
k	Thermal Conductivity
P	Fluid static Pressure
P'	Pressure correction (velocity corrector pressure)
P_d	Fluid motion pressure

P_a	Fluid hydrostatic pressure
P_e	Peclet number (on east side)
q'''	Volumetric heat generation
q_r^j	Radiosity for surface j
R_i	Elemental resistance (i direction)
$\vec{V}$	Velocity Vector
V	Volume
u	Velocity component in x direction
S	Source term in governing partial differential equation
t	Time
T	Temperature
T_0	Reference temperature
u	Velocity component in x direction
v	Velocity component in y direction
w	Velocity component in z direction
x	Cartesian x Coordinate
y	Cartesian y Coordinate
z	Cartesian z Coordinate

Greek Symbols

α	Resistance temperature coefficient

β	Coefficient of volumetric expansion
Γ	General diffusion coefficient
K	Electrical conductivity
$\delta_{k,j}$	Kronecker delta
∇	Gradient Operator
ε_k	Emissivity for radiative surface, k
ρ	Fluid Density
ρ_e	Electrical resistivity
λ	Bulk Viscosity
μ	Dynamic viscosity
ϕ	Voltage
Φ	Viscous dissipation function
σ	Normal stress
τ	Shear stress

Chapter One

I. INTRODUCTION

1.1 Electrical Current Flow in Traces and Connectors

Today's electronic design engineers are faced with challenging thermal management problems resulting from high current densities in increasingly small boxes packed with temperature-sensitive electronic components. Proper evaluation and treatment of heat dissipation as a result of the flow of electrical current in traces and conductors is of utmost importance in thermal management of many classes of electronics designs. Unfortunately, no software programs capable of centrally addressing the thermal issues relating to the electrical current flow in traces and conductors are available.

Flow of electrical current in traces and conductors is always accompanied by the generation of heat in them. This effect, in honor of its discoverer, James Joule, is called Joule heating (or Joulian heat dissipation.) Joule heating plays an eminent role in the thermal design of many classes of electronic equipment. These problems cannot be solved using traditional heat transfer methods - they require the coupled solution of the voltage field that is needed to obtain the local rate of Joulian heat dissipation through all conductors in the field. The need for the coupling of electrical and thermal aspects of the

model is due to the fact that the amount of heat generated by the electric current flowing through the device is itself dependent on temperature. The significance of temperature-dependent effects is well documented and will be addressed in this study. These problems can be divided into three general classes.

1.1.1 Circuit Boards Trace Heating (Current Carrying Capacity of Traces)

Here the objective is to determine the temperature rise in traces and planes that conduct electrical current throughout the board. Typically, these traces exist as copper layers embedded in the board. The power dissipation in a copper plane is not a trivial problem to be solved. Often the copper plane is of irregular shape and has multiple through-holes, almost giving it a Swiss-cheese appearance. Moreover, vias are often used to provide electrical connection between various layers. Figure 1.1 provides an example of a flex-board with irregular embedded traces.

1.1.2 Straps and Connectors

These pieces are used to connect wires and busses to electrical devices such as relays, contactors and generators. One of the main concerns in the design of electronic systems is whether these straps can survive on overload. A typical simulation involves a transient analysis starting from a steady-state solution with the electrical current suddenly raised to its "worst case" value. It is usually desired to know how long it would take until the strap temperature reaches a critical value. Figure 1.2 shows a typical strap attaching a buss-bar to a generator.

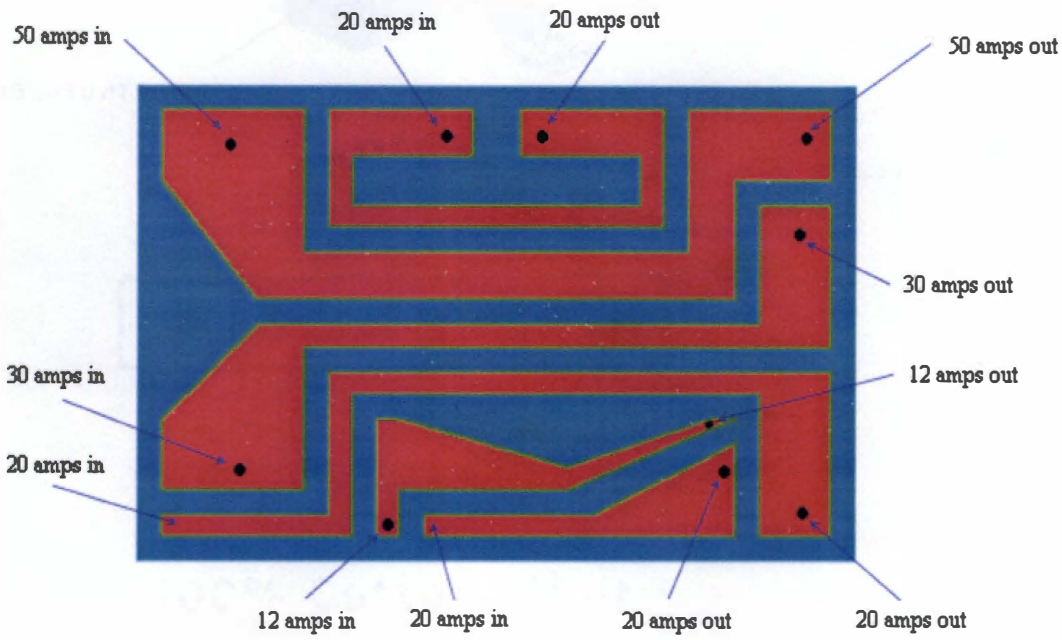


Figure 1.1: Flex Board with Traces

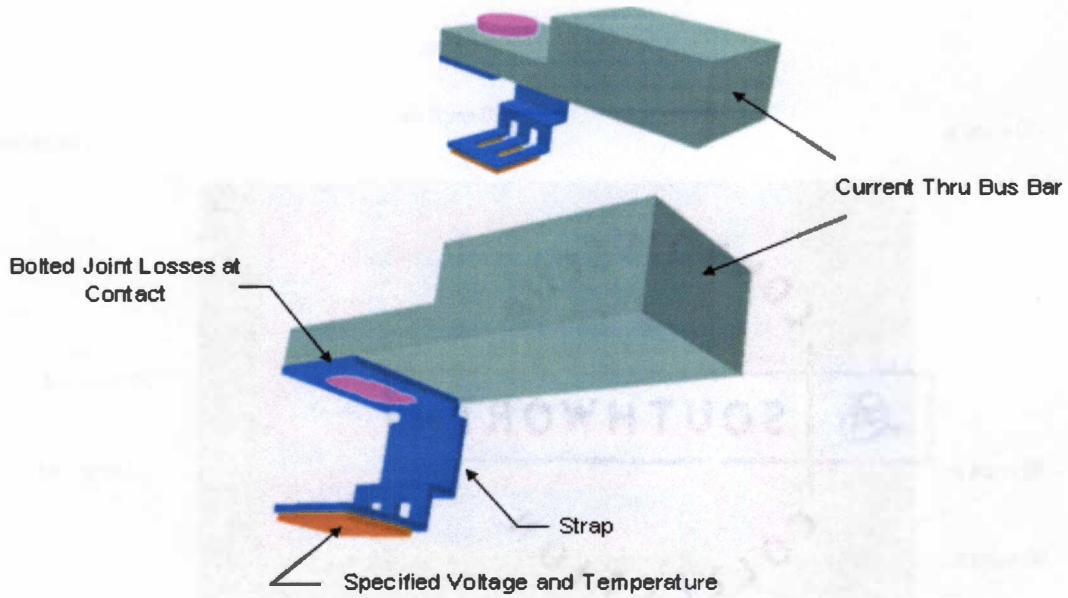


Figure 1.2: Strap and Bus Bar

1.1.3 Bussed Electrical Centers (Junction Boxes, Power Distribution Boxes)

A Bussed Electrical Center (BEC) is a power and signal distribution device where electrical switching and circuit protection components are combined into a single system. These designs contain components such as relays, fuses and circuit breakers, which are connected through an array of stamped metal bussing, traces and routed wires. The housing is made of variety of molded plastic parts. It is estimated that Joulian heating is responsible for close to half of the total heat dissipated in these devices. The heat dissipation distribution is not known prior to the solution and must be evaluated by simultaneously solving the electrical field. This can be accomplished through a "coupled electrical/thermal solution" scheme, where the voltage field is solved throughout the region knowing electrical loads and boundary conditions (in addition to thermal and flow fields) during each iteration. The most recent temperature field is used to update the electrical resistivity of the conductors in the model. The power dissipation is then calculated for all elements.

Figure 1.3 illustrates a typical BEC with multiple boards and components (i.e., relays, fuses, diodes). Figure 1.4 shows the electrical circuitry for this system. Typically, between 100 to 200 amps flow trough various circuitries, which leads to significant amount of Joulian heat dissipation.

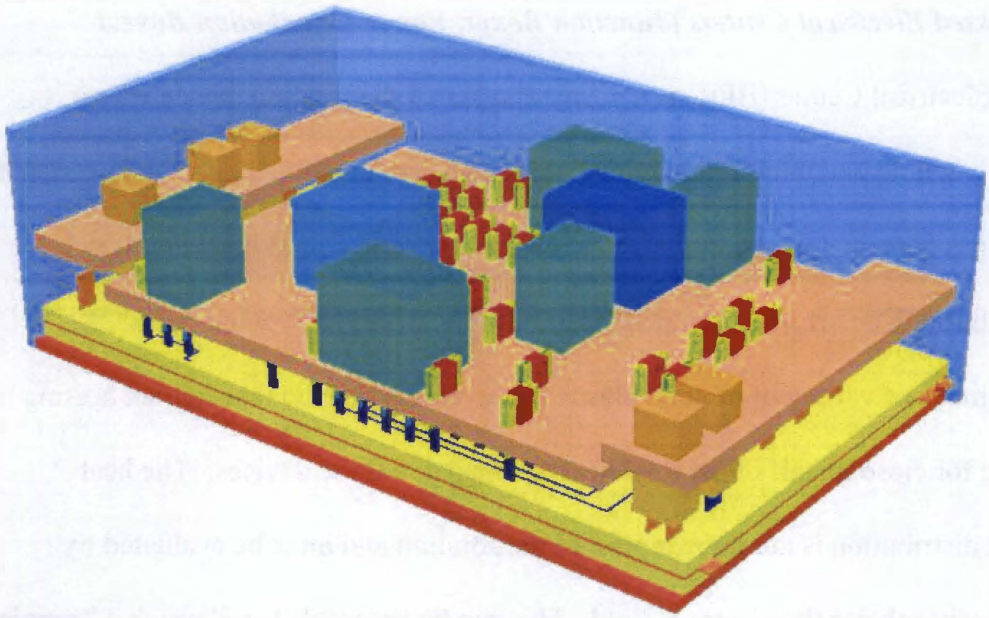


Figure 1.3: Typical Multi-board Junction Box

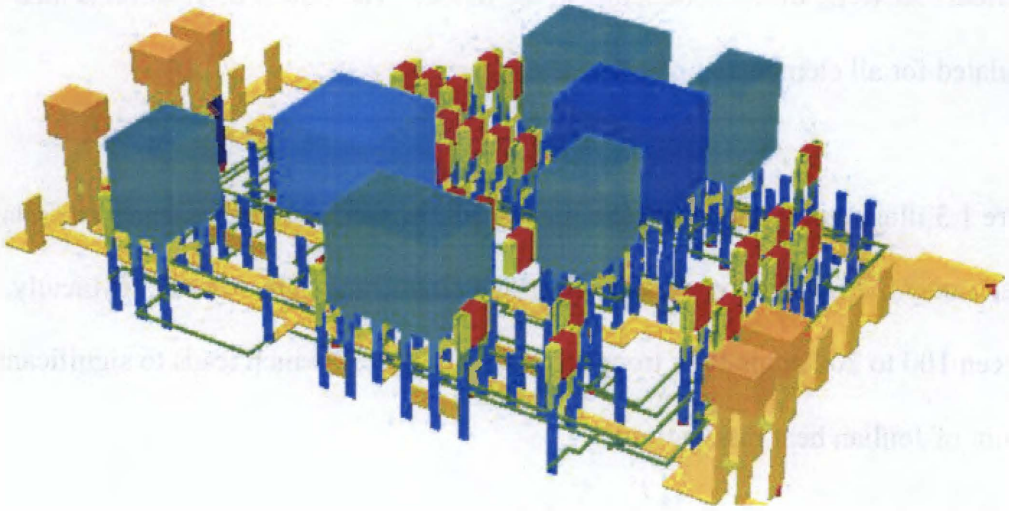


Figure 1.4: Network of Connectors and Traces

1.2 Objective

The objective of this study is to present a novel approach to the thermal management of electronic systems utilizing Computational Fluid Dynamics (CFD) and focusing on the multi-physics nature of these problems. The following areas are of paramount interest:

- Natural convection
- Conduction
- Surface-to-surface thermal radiation
- Coupled thermal/electrical effects

The product of this study is a numerical procedure for the prediction of temperature and flow fields commonly encountered in electronics applications, which addresses all the phenomena listed above concurrently.

Chapter Two

II. BACKGROUND AND LITERATURE REVIEW

2.1 Background

The cooling of electronic components is one of the most important tasks in the design and packaging of electronic equipment. In some equipment, the thermal (cooling) design is as important as the electronic design. Insufficient thermal control can lead to low reliability, short life and failure of the electronic components.

The importance of thermal management and the rate at which the market has grown, track closely the development of technology in the semiconductor, microprocessor and computer industries. The basic formula is that for every advance that these industries introduce to improve the performance of their systems, there has been a corresponding increase in the operating heat generated by the system. To satisfy consumer demands for more compact and sophisticated electronic devices, advances in semiconductor technology have achieved increased Integrated Circuit (IC) functionality and miniaturization. However, the continuous increase of both switching speed and transistor density have inadvertently resulted in rising die heat fluxes, which, if not efficiently removed from the device, may impact product performance and reliability.

Typical IC heat densities over the last few years have risen from between 2 and 5 W/cm^2 to currently between 10 and 20 W/cm^2, and are projected to reach 40 W/cm^2 within the next five years. This trend is even more dramatic for automotive and aircraft industries, where the major business drivers are lower cost, smaller size, higher reliability and lower mass. Additionally, the electronics modules are frequently placed in very hostile environments (ambient temperature of 105 °C, high humidity, oil and gasoline, etc.).

Figures 2.1 and 2.2 illustrate the predicted trends for packaging and reliability – a reduction in size and cost of the electronics and, at the same time, a dramatic increase in reliability. Figure 2.3 provides a view of the underhood environment and shows some of the common types of electronics encountered.

The increasing IC power densities, combined with even more stringent performance and reliability constraints in the future, pose challenges that will make thermal management a key enabling technology in the development of microelectronics systems in the next decade.

The operating temperatures of electronic components must be controlled through appropriate thermal management strategies that require increasing levels of engineering expertise and sophistication due to these rising heat loads. The challenge is further exacerbated by the ever-reducing product development cycle times.

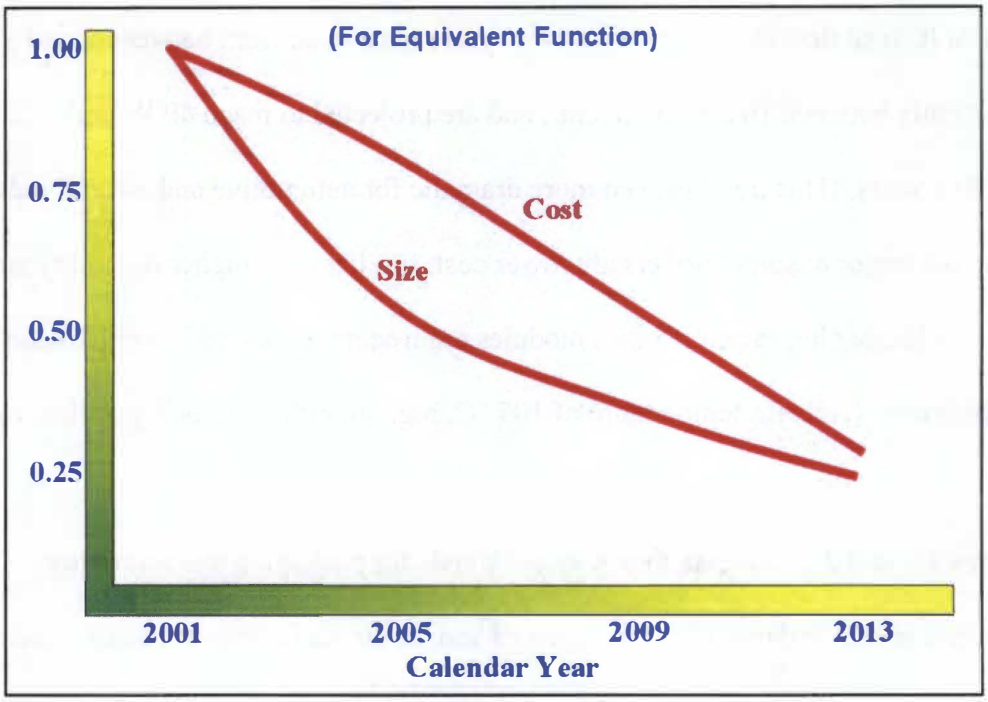


Figure 2.1: Automotive Electronics Packaging Attributes

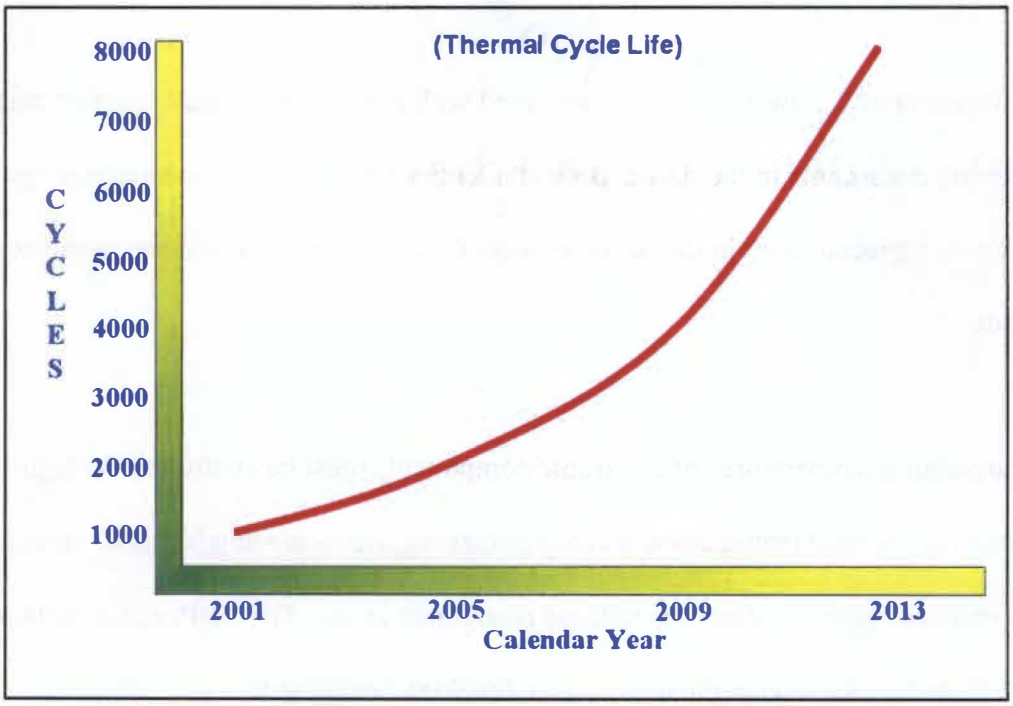


Figure 2.2: Automotive Electronics Reliability Demand

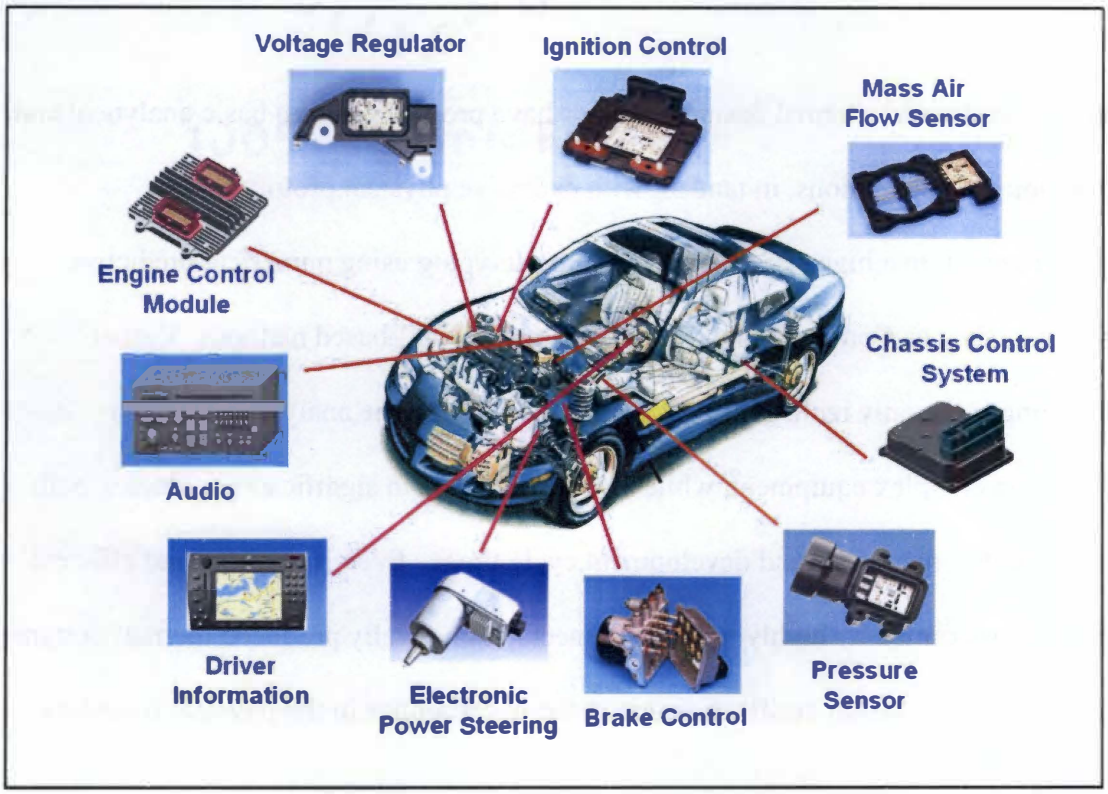


Figure 2.3: A View Beneath the Sheet Metal

An efficient thermal design strategy requires a balanced combination of both experimental and numerical efforts with an awareness of the latest developments in thermal cooling technologies. Such expertise is a pre-requisite to permit high-quality, cost-effective, thermal design solutions to be implemented in the shortest possible turnaround time.

Over the last decade, thermal design practices have progressed from basic analytical and semi-empirical calculations, in tandem with extensive physical prototype characterization, to a high reliance on virtual prototyping using numerical predictive techniques, such as Computational Fluid Dynamics (CFD)-based methods. Virtual prototyping is the only realistic design approach to permit the analysis of today's increasingly complex equipment, while also contributing to significantly reducing both physical prototyping costs and development cycle times. Even if accurate and efficient analysis is performed by highly trained engineers, numerically produced thermal designs still require experimental verification due to the uncertainties in the physical boundary conditions.

In this regard, high levels of heat dissipation require more accurate experimental characterization of thermal performance than in the past, where vendor-supplied, component junction-to-reference thermal resistances were used to calculate component-operating temperature. This approach is now recognized as leading to significant underestimation of operating temperatures and, hence, catastrophic product field failures. Electrical sensing methods and infrared thermography are the preferred methods to

quantify component and board operating temperatures, respectively.

The combination of a high level of engineering expertise with adequate experimental facilities and computing resources is needed. For many companies within the electronics industry, outsourcing their thermal design projects can be the most cost-effective and time-efficient solution. In addition to reducing both development and managerial costs, and in many instances time to market, this approach can also enable companies to better focus on their primary activity. Factors involved in the choice to outsource depend on the availability of resources in-house and the frequency of the thermal design needs. Even leaders within the electronics industry, who already have in-house thermal design capabilities, increasingly tend to outsource both electronics cooling design and research to specialized consulting firms and academic institutions, respectively, rather than further developing their capabilities in this area.

2.2 Approach

The prediction of heat transfer and fluid-flow processes requires an understanding of the values of the relevant variables (temperature, velocity, pressure, etc.) throughout the domain of interest. There are two main methods of prediction available: experimental investigation and theoretical calculation.

2.2.1 Experimental Investigation

Until relatively recently studies of fluids in motion were confined to the laboratory, but with the rapid growth in processing power of the personal computer, software applications now bring numerical analysis and solutions of flow problems to the desktop. It is commonly believed that the most reliable information about a physical process is obtained by directly measuring it. However, the following facts must be kept in mind in all heat transfer and fluid-flow laboratory testing situations:

- There is no such thing as an easy experiment. It can also be said that there is no substitute for careful experimentation for investigating a new basic phenomenon or validation of a numerical study.
- When performing experiments on small-scale models, the resulting information must be extrapolated; however, there are no general rules available for this. Furthermore, the small-scale prototype does not always simulate all the features of the full-scale device.
- There is always a risk that one can change the very quantity being measured by insertion of probes required for its measurement or by other compromises made to allow measurement.
- A properly conducted experimental investigation can be very costly.
- It is very difficult to perform parametric (what if) studies.

Baker, et al [1] present various techniques for measurement of temperature in engineering situations. A number of flow visualization techniques are presented by Merzkirch [2]. Also, practical flow visualization experiments are given by Mallinson and Graham [3].

2.2.2 Theoretical Calculation

In theoretical prediction a mathematical model replaces the actual physical model. For processes involving fluid-flow and heat transfer, the mathematical model consists of a set of five non-linear, coupled partial differential equations, although this number increases as one includes a coupled thermal/electrical field and turbulence. As there are no closed form solutions available for such equations, one must resort to numerical techniques (Computational Fluid Dynamics, or CFD). Over the past 30 years, with the rapid growth in the processing power of personal computers, numerical prediction methods have acquired significant importance to engineers dealing with heat transfer and fluid-flow processes. The general acceptance of numerical prediction methods in these areas is underscored by the various programs that are now available for these purposes. It is fair to say that numerical methods can now be employed to substantially reduce both the cost and time required for the analysis of heat transfer and fluid flow problems. The utility of a numerical prediction arises from the fact that the outcome is a detailed description of the variations of temperature, pressure and velocity components in the region of interest. Such a detailed description can provide clear insights into the phenomena and facilitate the design of a system for a set of performance specifications. Some of the advantages of numerical prediction methods are:

- Low Cost: In most cases, the cost of a computer analysis is much lower than the cost of a corresponding experimental study. This will become an even more important factor in the future since, as the price of most items are increasing, computing cost will continue to decrease.
- Speed: With today's personal computers, a computer simulation can be performed astonishingly quickly. The analyst can investigate many different scenarios (which may be impossible to do experimentally) and choose the best possible design.
- Completeness of results: As mentioned earlier, the outcome of a computer simulation is the values of all the relevant variables throughout the domain of interest (and for all times, in a transient process). Contrary to an experiment, there are no inaccessible locations and no inaccuracies as a result of probe interference.
- Ability to Model Difficult Conditions: Modeling toxic or flammable substances and very large-scale problems can be carried out with no additional difficulties. Moreover, an existing numerical model can be slightly modified to study worst case and many other scenarios.

Classification of Numerical Methods:

The two most widely used numerical techniques are finite element methods and finite difference methods. The primary advantage of the finite element method is its ability to model irregular boundaries. They have been used extensively with a great deal of success in structural engineering applications. However, they are known to exhibit

convergence difficulties in CFD problems, and as a result, they are rarely used in those applications. Details of formulation and application of finite element methods are presented in Baker [4] and Martin and Cary [5].

Finite difference methods are much easier to formulate, and they have been investigated more thoroughly. The main drawback of this approach is the difficulty encountered in modeling of complex geometries. A thorough discussion of finite difference methods can be found in the book by Anderson, et al [6] and Hornbeck [7].

The so-called "finite volume" technique of Patankar and Spalding [8,9] is basically a finite difference type approach. This method is the most preferred method for the analysis of CFD application and is the method of choice in the current study. It will be discussed in depth in the next section. Ferziger and Peric [10] present a thorough discussion of computational methods for fluid dynamics using both finite difference and finite volume techniques.

2.3 Literature Review

As stated earlier, the ultimate objective of the current study is to develop and present a computational procedure that can be used to address the main difficulties encountered in practical electronics cooling applications. In the open literature, no references could be found to centrally address the key issues raised in this proposal. There are numerous

closely related references, however, on many aspects of electronics cooling. These references are discussed below.

2.3.1 Natural Convection in Enclosures

Numerous experimental and numerical studies exist dealing with natural convection in rectangular enclosures. Many of these studies are discussed in the review papers by Ostrach [12, 13], Catton [14].

Ozoe, Sayama and Churchill [15] performed experimental and numerical studies to evaluate the Nusselt number for natural convection heat transfer in an inclined square channel. They studied the case in which one inclined wall was maintained at a uniform temperature, and the opposing inclined wall was held at a lower uniform temperature while the remaining two walls were kept insulated. The authors found complete agreement between their numerical and experimental results and determined that the maximum rate of heat transfer occurs at about 50 degrees of inclination. In a different paper, Ozoe, Sayama and Churchill [16] experimentally measured the rate of heat transfer for laminar natural convection in long rectangular enclosures. The channel was heated from below and cooled from above while the other two walls were insulated. The authors studied the effect of varying the aspect ratio, the Rayleigh Number and the angle of inclination on the rate of heat transfer.

In a similar study, Arnold, Catton and Edwards [17] performed a series of experiments to study the natural convection heat transfer in rectangular regions of various aspect ratios.

The bottom surface of the enclosure was kept at a fixed temperature while the upper surface was kept at a higher uniform temperature, and the sides were insulated. The Rayleigh number was varied between 10^3 and 10^6, and the angle of inclination was varied from 0 degrees (heated from above) to 180 degrees (heated from below).

A numerical investigation of three-dimensional, natural convection in an enclosure heated from below was performed by Ozoe et al [18]. The governing equations were solved by a finite difference technique along with the general three-dimensional Alternating Direction Implicit (ADI) method. The results of the numerical method were next checked against the prior experimental and theoretical results and showed good agreement.

Mallinson and Davis [19] obtained a numerical solution for the steady, three-dimensional, natural convection problem in a rectangular cavity as a result of differential side heating. The authors, using the finite difference technique, found solutions for a range of Rayleigh numbers. Their results for high values of Ra ($Ra > 10^4$) show multiple longitudinal flows that are a function of the Rayleigh number and the Prandtl number indicating spatial oscillations of the temperature field in the y-direction.

The effect of a non-uniform surface temperature on laminar natural convection in rectangular enclosures was studied by Chao et al. [20]. A three-dimensional numerical model for natural convection was developed, and a set of solutions was obtained using the finite difference approach. Their results indicated that the circulation patterns do not

change significantly with the surface temperature distributions; however, the magnitude of the Nusselt number increased with the amplitude of the surface temperature variations.

Krane and Jessee [21] performed an experimental study to measure the velocity and temperature distributions as well as the local heat flux distributions on the enclosure walls of a vertical square enclosure for a Rayleigh number of 1.89×10^5. The horizontal walls of the enclosures were kept insulated, and the vertical walls were isothermal surfaces. The measured results compared favorably with those obtained from similar experiments at 13 slightly different Rayleigh numbers.

Kim and Viskanta [22] numerically and experimentally investigated the buoyancy-induced flow in a two- dimensional enclosure and studied the effect of wall conduction on natural convection heat transfer. The air temperature inside the cavity was measured using a Mach-Zehnder interferometer. The Alternating Direction Implicit (A.D. I.) method was employed for the numerical solution of the system of transient equations. The results were obtained using a 26 by 26 grid.

Keyhani, Kulacki and Christensen [23] experimentally studied free convection in two vertical enclosed rod bundles for a wide range of Rayleigh numbers. Each rod was supplied with uniform power dissipation, and the enclosing outer cylinder was maintained at constant temperature. Nusselt numbers for individual rods, as well as an overall value for each bundle, were obtained as a function of the Rayleigh number. Experiments were conducted with air and water as the working fluid. The results indicate

that, for a fixed Rayleigh number, an increase in the Prandtl number produces a reduction in the Nusselt number. This trend is contrary to what has been reported for vertical cavities, and it is attributed to the curvature effects. Also, it was observed that, as the Rayleigh number increased, the rods each tend to assume nearly the same heat transfer coefficient. A correlation for the overall convective Nusselt number was developed in terms of the Rayleigh number and geometric parameters.

A numerical study based on a three-dimensional finite difference method utilizing the QUICK scheme was carried out to predict the critical tilt angle (the angle corresponding to a minimum heat transfer rate, and at which the flow changes from a two-dimensional unicell structure to a three-dimensional oblique roll) for a differentially heated, rectangular enclosure, heated from below by Yang, Yang and Lloyd [24]. The results showed good agreement with the known experimental results for air. Also, many details of the flow transition process at the critical tilt angle are apparent from the results.

Keyhani, Prasad and Cox [25] experimentally investigated natural convection heat transfer in a tall vertical cavity with one isothermal vertical wall (heat sink) and eleven alternately unheated and flush-heated sections of equal height on the opposing vertical wall using ethylene glycol as the working fluid. The flow visualization results reveal a flow pattern consisting of primary, secondary and tertiary flows. The heat transfer and flow visualization data indicate that the stratification is the primary factor influencing the temperature of the heated section. Detail analysis of the photographs suggests that the flow turbulence occurs at the local modified Rayleigh number in the range of 9.3×10^{11} to

$1.9x10^{12}$. Additionally, the authors observed that discrete flush-mounted heating in the enclosure results in local Nusselt numbers that are nearly the same as those reported for a wide flush-mounted heater on a vertical plate. They attributed this to the inherent instability of the problem.

Valencia and Fredrick [26] investigated natural convection of air in square cavities with half-active and half-insulated vertical walls for Rayleigh numbers of 10^3-10^7. Five different relative positions of the active zones were considered. While circulation depended strongly on the total exit length downstream of the active zones, heat transfer depended less on this parameter. Significant conduction effects occurred even at a Rayleigh number of 10^5. Expressions for the average Nusselt number in the five situations and hints on how to generalize heat transfer results to intermediate cases were given.

Neymark et al. [27] conducted an experimental study aimed at determining the effect of internal partitions on the natural convection heat transfer across an enclosure. Experiments were conducted using a representative cubic geometry, differentially heated from the side with an internal partial vertical partition. Two test cells with different working fluids were used- an air and a water cell. Nusselt-Rayleigh aperture-width correlation curves were developed for both the air and the water data using a resistance model.

Mahaney, Incropera and Ramadhyani [28] performed experiments with water and FC-77

to investigate mixed-convection heat transfer from a four-row, in-line array of 12 square heat sources that were flush-mounted to the lower wall of a horizontal, rectangular channel. The experimental data encompassed heat transfer regimes characterized by pure natural convection, mixed convection, laminar forced convection, and the initiation of transition to turbulence. The variation of the row-average Nusselt number with the Reynolds number exhibited a minimum, suggesting that, due to buoyancy-induced flow, heat transfer may be enhanced and pumping power requirements reduced by reducing the flow rate. Additionally, they performed experiments with FC-77 and an array of heat sources with augmented finned surface areas. In contrast to variations for the flush-mounted sources, row-average Nusselt numbers for the finned sources decreased monotonically with a decreasing Reynolds number for rows one through three and were nearly independent of Reynolds number for row four. For both the unfinned and finned arrays, increasing the Rayleigh number enhanced heat transfer and increased the Reynolds number range for which enhancement occurs. Appropriate scaling parameters were introduced for both geometric configurations to characterize mixed-convection heat transfer from an array of discrete sources.

Chadwick, Webb and Heaton [29] performed an experimental and analytical study of natural convection in a vertical cavity with single and multiple flush-mounted, two-dimensional, discrete heat sources. The problem parameters investigated in the study include the Grashof number, heat source locations, and the cavity aspect ratio of single and multiple heater enclosures.

Chen, Keyhani and Pitts [30] conducted an experimental study of convective heat transfer with ten protruding heaters from one vertical wall. The top enclosure wall was maintained at a constant temperature, and all the other surfaces (with the exception of the heater locations) were unheated. Distilled water and ethylene glycol were used as working fluid. The heaters were numbered sequentially from bottom to top. The experimental results indicate that for nearly all cases (with the exception of high Rayleigh number runs), the bottom heater has the highest heat transfer coefficient. The heat transfer coefficient for locations 7, 8 and 9 were found to be the same. The value of the heat transfer coefficient decreases with increasing vertical position up to heater 7. For the high Rayleigh number case, the maximum heat transfer coefficient was observed at location 10. Additionally, the flow visualization experiments indicate the existence of a core flow within the enclosure and recirculating cells in the gaps between heaters.

The dependence of the characteristics of fully developed natural convection flow on the type of imposed thermal boundary conditions was discussed in a paper by Kelkar, Kanchan and Choudhury [31]. The mathematical formulation for periodically fully developed natural convection with thermally active through flow was presented in the context of the flow through an insulated channel with heated blocks mounted on one of the walls. The temperature field was decomposed into a periodic part and a linearly varying part. The solution procedure for the discretization equations that addressed the constraint imposed on the periodic part of the temperature field was described. Computations were carried out for the periodically fully developed natural convection in

the channel geometry considered. The values of the channel length and module heating were varied to illustrate the utility of the proposed formulation in analyzing periodically fully developed natural convection flows encountered in electronics cooling applications.

A numerical study of natural convection heat transfer in enclosed horizontal NxN arrays of heated rods was conducted by Keyhani and Luo [32]. A width to diameter ratio of 20.33 and a pitch to diameter ratio of 1.33 were used. The average Nusselt number of each rod was predicted for a variation in the modified Rayleigh number of 1 to 316, keeping Prandtl number constant at 0.7. Also, pure conduction results were obtained. The conduction Nusselt number of the corner rod was found to decrease with an increase in N from 3 to 7. However, the trend reversed, and an increase in the Nusselt number was observed for N>9. The convection results showed that the bottom row rods experienced the maximum variation in their local Nusselt number. Additionally, it was observed that more than 50% of the total power input was transferred to the top surface, while the bottom surface received less than 2% of the total power.

Keyhani and Dalton [33] conducted an experimental investigation to study natural convection heat transfer in enclosed horizontal N x N arrays (N = 3, 5, and 7) of electrically heated rods with a pitch to diameter ratio of 1.35. Each array was positioned in an isothermal square enclosure with a width-to-diameter ratio of 20.6. Air or helium at high pressure was used as the working fluid. Slight temperature variations were observed for the bottom-row rods, indicating that these rods were relatively insensitive to increases in the array size. But the top row rods demonstrated substantial temperature increases.

Natural convection correlations covering three flow regimes of conduction, transition and convection in the range of $6.45 < Ra_d^* < 3.08x10^5$ were obtained for each rod in each array. These correlations were based on the modified Rayleigh number. Also, a generalized enclosure Nusselt number was correlated as a function of the enclosure modified Rayleigh number and array size. Comparison of the data with previous numerical results indicated that this correlation may be readily used to obtain a conservative estimate of the maximum temperature in the arrays.

Agonafer, Gan and Spalding [34] described a simple method for calculating distances from walls in circumstances of complex geometry. This was then utilized as the basis of a comparative study of conjugate heat transfer, involving previously published low-Reynolds-number turbulence models. It was argued that this model, called LVEL, performs as well as the older Lam-Bremhorst-Yap and Two-Layer- kappa – epsilon models. Since it was computationally less expensive and easily applied to three-dimensional problems, it was recommended for practical use, especially for electronics cooling applications.

2.3.2 Combined Natural Convection and Radiation

Larson and Viskanta [35] considered a transient combined natural convection and radiation problem in a rectangular enclosure. In this paper, they employed an alternating direction, implicit finite difference technique to determine the response of a rectangular enclosure to a high temperature heat source. Their results indicated that thermal radiation

had a significant effect on the convection flow patterns inside the enclosure.

In an experimental study, Elsherbiney et al [36] investigated the effects of thermal boundary conditions on natural convection in vertical and inclined enclosures. Results were obtained for a range in Rayleigh number from 10^3 to 10^8, and a range in orientation from horizontal to vertical. The two-dimensional enclosure was bound by two parallel isothermal flat sidewalls and two end walls of finite thickness made of a low thermal conductivity material. The effect of the emissivity of the walls on the heat transfer process in the enclosure was determined by means of a series of measurements using low and high values of wall emissivity.

Behnia, Reizes and De-Vahl-Davis [37] presented a numerical method for the study of combined natural convection and radiation in a rectangular, two-dimensional cavity containing a non-participating fluid. One wall of the cavity was isothermal, and the opposite wall was partially transparent, permitting radiation exchanges between the cavity and its surroundings and/or the Sun. The latter wall also exchanged heat by convection from its external surface to the surroundings. The other two walls were held adiabatic; convection and radiation were balanced, so that there was no heat transfer through those walls. The equations of motion and energy were solved by finite difference methods. Coupled with these equations were the radiative flux boundary conditions that were used to determine the temperature distribution along the non-isothermal walls.

A numerical study of the combined heat transfer by conduction, natural convection, and

radiation in a sealed electronic package was performed by Smith, Beckermann and Weber [38]. The goal of the study was to investigate the importance of the various heat transfer modes, the effectiveness of different heat transfer paths, and the impact of a number of design changes on the overall thermal performance of a typical electronic package. The package consisted of an enclosure containing three printed circuit boards, on which were mounted various heat-generating electronic components. Heat transfer processes at both small (i.e., inside a component) and large (i.e., the package) scales as well as all heat transfer modes were included simultaneously in the numerical model. Both one and two-dimensional radiations were considered. Results were presented in terms of streamline and isothermal plots, average temperatures and heat transfer rates. Overall, the numerical data showed favorable agreement with available empirical data.

In a paper by Lin and Huang [39], a theoretical analysis on a conjugated problem of transient natural convection combined with radiation in a rectangular enclosure was presented. A two-dimensional rectangular enclosure filled with a radiatively participating fluid medium was considered. The medium was assumed to be emitting, absorbing and isotropically scattering and was initially in thermal equilibrium with boundary walls. A constant heat flux was then imposed onto a vertical wall from outside, while another vertical wall was kept at the initial temperature and both top and bottom surfaces were modeled as insulated surfaces. It was assumed that all walls were diffusely reflecting and that the heated wall had a finite thickness. The effects of radiative and convective parameters on the heat transfer rate and fluid flow, particularly the occurrence and growth of secondary flows, were investigated.

Combined effects of natural convection and radiation on a laminar boundary-layer flow over a semi-infinite horizontal flat plate were studied by Chuang [40]. He showed that increasing the natural convection-radiation interaction in the boundary layer increased the shearing stress on the wall, the boundary-layer thickness, the maximum velocity attainable by fluid, and the buoyancy force in the boundary layer. However, the temperature gradient at the plate decreased with increasing interaction.

Dehghan and Behnia [41] numerically modeled combined natural convection, and radiation heat transfer in an open-top upright cavity containing a discrete heat source was modeled numerically. The surface emissivity was varied, and its effects on the flow and thermal fields were determined for different values of the Rayleigh number. The complex interaction of the three modes of heat transfer was investigated by solving the coupled convection, conduction, and radiation equations. It was noted that including thermal radiation had a significant effect on the flow, resulting in the formation of a recirculation zone within the cavity. Comparison of the local heat transfer coefficients for the conjugate analysis and no radiation case revealed that the inclusion of radiation had a negligible effect on the heat transfer performance of the heat source. Comparison of the numerical results with experimental observations showed that accurate prediction of the flow and thermal fields was strongly dependent on radiative heat transfer in the numerical case.

A three-dimensional investigation of combined conduction, natural convection and radiation in vented enclosures was carried out by Yu and Joshi [42]. An electronic

component was simulated using a discrete flush type heat source mounted on a vertical substrate. Combined natural convection in the air; conduction in the heat source, the substrate and the enclosure walls; and surface radiation, were solved for Rayleigh numbers of 2.6×10^6 and 2.0×10^7. Radiation was incorporated based on the radiosity-irradiation approach. The resulting flow and temperature patterns were discussed, focusing on radiation and three-dimensional effects. The relative contributions of natural convection and radiation were investigated for different emissivities of the internal surface of the substrate. Heat transfer rates from the substrate and other internal walls were presented to illustrate conjugate heat transfer due to combined modes. Reasonably good agreement with the experimental data was achieved by the numerical solutions.

2.3.3 Cooling of Electronic Equipment

References [43] through [45] consist of papers dealing with flow through screens and perforated plates. This information could be useful in modeling flows through openings in enclosure surfaces. In the following paragraphs, a survey of literature on natural convection heat transfer in electronic equipment is presented. Some of these papers include problems in partial enclosures.

There are a number of papers published on the development of natural convection between two vertical flat plates. This configuration occurs in electronic equipment such as printed circuit boards. Aung in [46] studied the situation in which both walls were heated with prescribed heat fluxes equally distributed. He also studied the asymmetric

heat flux case in reference [47].

A numerical study of the interacting natural convection flows, which are generated by isolated heat sources located on an adiabatic vertical wall, was performed by Jaluria [48]. In his paper, he considered two-dimensional flow (without making the boundary-layer assumptions) and solved the full elliptic governing equations numerically using finite difference techniques.

Torok [49] applied the finite element method to two problems involving natural convection in electronic equipment. In the first problem, he considered a rectangular box enclosing a tilted heat plate. In the second problem, he found numerical results for the case of a tilted, open-ended enclosure heated from below.

Oosthuizen [50] studied the free convective flow through an open-ended plane duct with the lower portion of the walls heated to a uniform temperature and the upper portion of the walls insulated. He employed a forward marching finite element scheme to investigate the effect of the addition of the insulated section (the "chimney" effect).

Coyne [51] presents a thermal analysis of a piece of electronic equipment with horizontal and vertical variations in heat dissipation. In his paper, he first considered a symmetrically heated air channel between printed circuit boards. In the second part of his analysis, he investigated the radiative and convective heat transfer across the gap between the dissipating PCB's. In the third part, he considered the frame as a whole. The

results of parts one and two were checked against known experimental data.

In order to clarify the dependence of heat transfer performance on heater size, Park and Bergles [52] ran a number of experiments using simulated microelectronic circuits. They achieved the simulation through the use of foil heaters and obtained heat transfer coefficients for various heater heights and widths. In this paper data was obtained for in-line and staggered arrays of heaters with varying distances between them.

Lejannou et al [53] developed a numerical method, based on the finite volume technique, to predict the airflow and temperature field in electronic switching systems. This model allowed for inflow or outflow of air through the vent holes. The results of the numerical scheme were checked using a series of experiments with different geometrical configurations and thermal power dissipations.

Ishizuka et al [54] presented a simplified formula for thermal design of natural air-cooled electronic equipment casings with a standard arrangement of circuit boards and power supplies. Some important factors such as the stack effect, airflow resistance, and natural convective heat transfer were implemented by the formula, making it suitable for most practical air-cooling systems. The formula was applied to predict the temperature rise in three cases. The first two cases used electronic equipment cabinets with standard equipment arrangements, and the third case was a casing model. In all cases, the predicted temperature rise was within ten percent of the actual values based upon the experimental results.

Shen, Prasad and Keyhani [55] conducted a numerical study of natural convection in a discretely heated vertical cavity by three uniform flux heat sources to examine the effects of aspect ratio and the heater size. They observed that the flow structure and temperature field are strongly influenced by the Rayleigh number, the aspect ratio and the heater size. For tall cavities, it was observed that the effect of the aspect ratio on maximum temperature and Nusselt number was minimal. However, it was shown that the heat transfer coefficient for various heating elements depends strongly on the length of the adiabatic sections separating the heat sources. It was concluded that discrete heating can achieve a much higher rate of heat transfer compared to flat heating. Several generalized heat transfer correlations are presented in this paper.

In a paper by Carmona and Keyhani [56], the effect of cavity width on natural convection heat transfer due to discrete flush-heated sections of equal height in an enclosure cooled from the top was experimentally investigated. One vertical wall contained five heated sections (with equal heights for heated and unheated sections); the other vertical wall and the bottom were kept insulated. A number of experiments were conducted for six cavity width values resulting in aspect ratios ranging from 3.67 to 12.22. Ethylene glycol and FC-75 were used as convective media. The flow visualization results with ethylene glycol showed a fairly inactive core for low power input and small cavity width. Higher power input and cavity width transforms a rather well-structured core flow into a time-dependent one. For a given width, it was shown that the heat transfer result for all heaters can be expressed using a single correlation using the height from the cavity

bottom to heater center as the local height. A comparison between ethylene glycol and FC-75 revealed no appreciable Prandtl number effects.

Agonafer and Chu [57] introduced a methodology for numerical simulation of the heat transport behavior of card-on-board packages using a commercial finite-control-volume program called PHOENICS. Model preparation was done using the EASYFLOW interface. Two electronic cooling examples were presented. The examples simulated card-on-board package with and without flow turbulators. The problem was assumed laminar; both the conductive and convective heat transfer (conjugate heat transfer) were computed simultaneously.

Rhee and Moffat [58] conducted a study to outline considerations in the joint design of numerical and experimental research of electronics cooling situations. The authors discussed implementations of velocity and temperature boundary conditions that can be unambiguously and accurately applied using both methods. They noted examples of measurement biases due to the finite time constant, size and conductivity of certain instruments. They concluded that these instrumental limitations cannot be eliminated and must be simulated in the interpretation of numerical work through the appropriate averaging schemes.

In the paper by Linton and Agonafer [59], some of the issues that need to be considered in defining a "benchmark problem" for electronic cooling packages were discussed. They focused their efforts in the numerical modeling of complete boxes (system level

modeling). The example proposed as a benchmark in this study is comprised of an electronic box complete with covers, floppy drive, hard disk drive, power supply, fans, feature cards and Single In-line Memory Modules (SIMM's). The ultimate goal of the effort was to assist new users who want to consider CFD codes for electronic cooling applications at the system level as well as vendors who want to include practical problems in their list of benchmark problems.

Lee, Moran and Yovanovich [60] developed an analytical approximate solution for predicting the thermal resistance of bolted joints between two square plates of the same material but different thicknesses. The plates were assumed to have perfectly flat and smooth surfaces, and they were joined by a bolted connection at the center of the square, forming a concentric annular contact region at the interface. The entire surface area of the plates was assumed insulated, except for the surfaces where the heat source/sink was applied and where the interfacial contact was formed.

A novel Virtual Prototyping Environment (VPE) for the multi-scale thermal packaging of electronic systems was described in a paper by Przekwas, Lai and Agonafer [61]. All scales of thermal packaging, chip, board, and system scales were integrated in a combined model with a reduced need for uncertain boundary conditions. This paper discussed major components of the proposed VPE and presented sample computational simulations for different scales of electronics cooling. Non-traditional computational techniques such as unstructured grids, overset grids with local refinement and parallel execution of module components were identified and demonstrated. The three

dimensional model was applied to the electronics cooling of a card on board package with eighteen components. Recommendations for future developments of electronic cooling design tools were provided.

Habchi and Przekwas [62] presented the results of a computational study on a proposed benchmark computer box. Their numerical analysis accounted for the effects of the cooling fan through the use of a novel fan model validated against experimental data. All the elements of the computer box were accounted for, including feature cards, SIMM's, floppy drive, power supply and other elements. This paper provided the results of the air flow and heat transfer calculations along with a discussion and recommendations for future efforts.

In a paper by Landon, Campo and Johnson [63], arbitrary shape deformation software tools were coupled with design optimization software and CFD and heat transfer software to perform shape optimization of natural convective cavity cross-sections for use in the study of electronics cooling. A two-step optimization process was performed, first to minimize the area (volume) of the cavity, and second to minimize the maximum temperature, thus maximizing the system heat transfer. The first optimization problem resulted in a significant reduction in area (volume) while raising the maximum temperature a small amount. The second optimization resulted in a remarkable reduction of the maximum temperature with a small increase in area (volume) as compared to the results of the first optimization.

Yu and Joshi [64] conducted experimental flow visualizations and temperature measurements to investigate the passive air-cooling of electronic components in partially open horizontal enclosures. A discrete flush type heat source, centrally mounted on a horizontal substrate was placed in a compact enclosure (127 mm x 127 mm x 41.3 mm). Effects of power levels, opening sizes, enclosure aspect ratios and opening configurations on the thermal performance of the discrete component and their interactions were found using Design of Experiments Methodology. Convective heat transfer coefficients were obtained.

A review of the applications of thermoelectric devices to cooling electronics and prospects for the future was presented in a paper by Chu and Simons [65]. The need to accommodate increased module heat flux and reduce chip-operating temperatures was discussed, along with the cooling technology developed within IBM to do this. A brief background discussion of thermoelectric cooling and a survey of heat flux capability of commercially available modules was provided. Examples were given of early applications of thermoelectric cooling technology within IBM. The paper focused on the desire to use thermoelectric devices as a means to either augment heat removal from electronic modules or achieve lower operating temperatures. An example considering the augmentation of high performance multi-chip module cooling with thermoelectrics was presented. The analysis was discussed and summarized in terms of the relevant equations and calculation results.

The modeling methodologies and the results of the numerical investigation on a laminar forced convection in a heated microchannel were documented in a paper by Tso et al [66]. A conjugate heat transfer model was set up using commercial software, STAR-CD, to investigate the localized flow and heat transfer in a microchannel. The model was then solved using typical flow, heat transfer and dimensional parameters. The temperature distributions in both the solid and fluid region and the flow field in terms of velocity and pressures were shown and discussed with the help of the numerical simulation.

Narasimhan and Mira [67] modeled heat sinks for natural convection scenarios in vertical configurations. First, the compact modeling technique was applied to both extruded and pin fin heat sinks to validate the methodology in laminar natural convection scenarios. Following validation, the methodology was applied to a system level model consisting of a set of pin fin heat sinks placed on a row of components. The compact heat sink technique resulted in a significant savings in mesh size and computing time and also gave good accuracy when compared with the results from the detailed heat sink models.

Zero thickness conducting plates are CFD objects that may be used to model three-dimensional conduction in thin objects used in electronic cooling applications. The use of zero thickness conducting plates, when applicable can result in significant reduction in finite volume element count. The validity of using these thin conducting plates for CFD modeling of certain objects frequently used in electronic systems was studied by Karimanal and Nair [68] using commercially available CFD software for electronics cooling application.

In a study by Stiver and Shidore [69] a simple technique to extract a two-resistor/two-capacitor (2RC) model from a detailed model using analytical and computational techniques was proposed. The ability of the 2RC model to predict the junction and case temperature responses to a step power excitation was investigated by applying the technique to a common package, the Plastic Ball Grid Array (PBGA). The resultant 2RC networks were implemented in a commercial CFD tool, and appropriate conclusions were drawn from the results.

Phelan et al [70] conducted a study to examine current and future miniature refrigeration cooling technologies for high power microelectronics. The authors argue that utilizing refrigeration may provide the only means by which future high-performance electronic chips can be maintained below predicted maximum temperature limits. Their review of existing micro scale refrigeration systems revealed that thermoelectric coolers (TECs) were commercially available in small sizes. However, the then existing TECs were limited by their maximum cooling power and low efficiencies. A simple model was constructed to analyze the performance of both existing and predicted future TECs in an electronic packaging environment.

A thermal architecture concept for analysis of thermal problems and solutions existing in electronics systems was presented by Batty et al [71]. In this paper, the thermal problems were categorized into a total of seven levels from chip to system. Advanced thermal technologies for addressing the thermal problems at all seven levels were discussed. They

concluded that integrating the thermal architecture with the electronic architecture could significantly improve the effectiveness of the thermal management.

2.3.4 Coupled Thermal-Electrical Analysis

Krabbenborg et al [72] performed coupled thermal and electrical simulations to obtain physical insight into the process that leads to permanent damage in protection devices due to electrostatic discharge (ESD) pulses. Locations with considerable temperature rise that eventually led to damage were extracted from the calculated temperature distributions.

Moussali and Vullierme [73] conducted a numerical study of steady state heat transfer in an anisotropic composite material made up of many cross directional layers of epoxy carbon fibers and epoxy glass fibers with an electric current passing through the material. To understand this phenomenon, the transfers of heat and electricity were coupled. A mathematical model of a de-icer on a helicopter rotor blade was developed and employed to determine the dispersed electric power distribution. This information was then used to calculate the temperature distribution. It was shown that the temperature distribution is strongly linked to the dissipated electric power.

Lai and Majumdar [74] developed a simple coupled electrical and thermal model of sub-micron MOSFETs (metal-oxide-semiconductor field-effect transistor). Based on the

external voltage, electron transport properties and device size, an electron Reynolds number was proposed and used to simplify the electron momentum equation.

In a paper by Krabbenborg et al. [75], a method was proposed for the extraction of coupled networks from layout information for the simulation of electrothermal device behavior. The networks represented a three-dimensional device structure with circuit elements. The electrical and thermal characteristics of this circuit representation were calculated with a circuit simulator. Spatial potential distributions, current flows, and temperature distributions in the device structure were calculated on the spatial coordinates. This method of simulation was implemented in a circuit simulator and was demonstrated for simulation of the self-heating of a bipolar power transistor.
A novel methodology for analyzing the performance of AMTEC (alkali metal thermal-to-electric conversion) cells was presented by Schock, Noravian and Or [76]. The methodology consists of an iterative procedure for the coupled solution of the interdependent thermal, electrical, and fluid flow differential and integral equations, which govern the performance of AMTEC cells and generators, taking into proper account the nonlinear axial variations of temperature, pressure, axial current, sodium mass flow rate, and power density. The application of the analytical procedure to latest cell designs and detailed analytical results were illustrated in this paper.

Doerstling [77] presented an approach combining electrical and thermal analyses to predict the thermal performance of electrical centers and junction blocks. In this paper,

on the component level, procedures were outlined for developing electrical and thermal models of electro-mechanical and circuit protection devices contained in bussed electrical centers (BEC's). Additionally, a method for creating a system level steady state model of a BEC was demonstrated. Several BEC designs were modeled using a largely automated process, and the predicted temperatures agreed well with the test results.

In a paper by Zhu, Vafai and Xu [78], a numerical thermal-electrical model was developed for a typical power metal-oxide semiconductor field effect transistor (MOSFET) device. The temperature and heat-generation distributions within the device were obtained and their effects on the device I-V characteristics were examined.

A comprehensive analysis procedure was developed by Sun and Dong [79] to perform the incrementally coupled thermal-electrical-mechanical analysis in order to simulate the resistance spot welding process of aluminum alloys. Due to aluminum's high thermal conductivity, low melting temperature and low yield strength, deformation resulting from resistance spot welding was expected to be more severe than for steel. This paper took into account the incremental changes in sheet-deformed shape, contact area and current density profile as well as large deformation effects. The analysis procedures considered electrical contact resistivities to be not only functions of contact temperature but also functions of pressure. Joule heating at the contact surfaces was computed using an equivalent surface heat generation concept, a procedure suitable for analyzing many important parameters such as contact area changes, electrode movement and dynamic resistance, as well as other factors that contribute to weld quality. It can also be used to

study nugget development and analyze the mechanisms of electrode wear and weld cracking.

A new approach to transient thermal characterization of widely used flip-chip structures was presented in a paper by Fedasyuk; Levus and Petrov [80]. The thermal model was based on the formalization of the conjugate problem of heat exchange in the dye and the substrate. The utilization of the mathematical model was illustrated by using an example of thermal simulation in the test structure and validated by comparisons with the results obtained by thermal-electrical techniques.

The coupling of current, temperature and stress was studied in a "metal thin plate with crack" at the moment of switching of the pulse current in a paper by Zheng et al. [81]. This finite element analysis utilized the coupling that exists in thermal-electrical and thermal-mechanical processes. The temperature field and stress fields obtained from the numerical simulation compared favorably with the theoretical results.

Chapter Three

III. GOVERNING EQUATIONS

The numerical solution of a heat transfer and fluid-flow problem begins with the differential equations expressing the laws governing these processes. Each governing differential equation expresses a unique conservation principal. It employs a certain physical quantity as its dependent variable and implies that there exists a balance among various factors influencing this variable. The dependent variables are generally specific quantities (i.e., velocity, specific enthalpy), and each term in these equations denotes a certain influence per unit volume.

The governing equations for the flow of a Newtonian fluid are presented below in their most general form. These equations, along with an appropriate set of boundary and initial conditions, form a mathematically well-posed problem that can be solved to obtain values of the dependent variable throughout the domain of interest.

3.1 Conservation of Mass (Continuity Equation)

The principle of conservation of mass simply states that the rate of creation of mass is zero. The term creation has the connotation of outflow minus inflow plus increase of storage. This equation in vector notation is given by:

$$\frac{D\rho}{Dt} + \nabla.\vec{V} = 0 \qquad (3.1)$$

Where:

$\vec{V}$ is the velocity vector with components (u,v,w),

$\frac{D}{Dt}$ represents the material derivative $\frac{D}{Dt} = \frac{\partial}{\partial t} + u\frac{\partial}{\partial x} + v\frac{\partial}{\partial y} + w\frac{\partial}{\partial z}$,

∇ is the gradient operator $\nabla = i.\frac{\partial}{\partial x} + j.\frac{\partial}{\partial y} + k.\frac{\partial}{\partial z}$

In Cartesian coordinate system the continuity equation is expressed as:

$$\frac{\partial \rho}{\partial t} + \frac{\partial(\rho u)}{\partial x} + \frac{\partial(\rho v)}{\partial y} + \frac{\partial(\rho w)}{\partial z} = 0 \qquad (3.2)$$

3.1.1 Continuity Equation for Incompressible Fluids

For the majority of the problems encountered in electronics applications, temporal and spatial variations in density are negligible compared to the variations in velocity. For these problems, the continuity equation can be further simplified to:

$$\nabla.\vec{V} = 0 \qquad \text{(in vector notation)} \qquad (3.3)$$

$$\frac{\partial u}{\partial x}+\frac{\partial v}{\partial y}+\frac{\partial w}{\partial z}=0 \qquad \text{(in Cartesian coordinates)} \qquad (3.4)$$

3.2 Momentum Equation (Newton's Second Law of Motion)

The momentum equation in x-direction states that the rate of increase of x-direction momentum per unit volume equals the rate of net inflow of x-direction momentum per unit volume plus total x-direction force per unit volume.

$$\rho\frac{Du}{Dt}=\frac{\partial \sigma_x}{\partial x}+\frac{\partial \tau_{xy}}{\partial y}+\frac{\partial \tau_{xz}}{\partial z}+F_x \qquad (3.5)$$

3.2.1 The Navier-Stokes Equations

The stress terms in the momentum equation can be related to the local velocity using the constitutive relationships:

$$\sigma_x=-P+\lambda\left(\frac{\partial u}{\partial x}+\frac{\partial v}{\partial y}+\frac{\partial w}{\partial z}\right)+2\mu\frac{\partial u}{\partial x} \qquad (3.6)$$

$$\tau_{xy}=\mu\left(\frac{\partial v}{\partial x}+\frac{\partial u}{\partial y}\right) \qquad (3.7)$$

$$\tau_{xz}=\mu\left(\frac{\partial w}{\partial x}+\frac{\partial u}{\partial z}\right) \qquad (3.8)$$

Note that the "bulk viscosity", λ, is related to the "dynamic viscosity coefficient" through:

$$\lambda=-\frac{2}{3}\mu \qquad (3.9)$$

The x-direction Navier-Stokes equation is obtained by replacing the stress terms in the momentum equation with Equation (3.6) through (3.8).

$$\rho\frac{Du}{Dt}=-\frac{\partial P}{\partial x}+\frac{\partial}{\partial x}\mu\left(2\frac{\partial u}{\partial x}-\frac{2}{3}\left(\frac{\partial u}{\partial x}+\frac{\partial v}{\partial y}+\frac{\partial w}{\partial z}\right)\right)+\frac{\partial}{\partial y}\left(\mu\left(\frac{\partial u}{\partial y}+\frac{\partial v}{\partial x}\right)\right)+\frac{\partial}{\partial z}\left(\mu\left(\frac{\partial u}{\partial z}+\frac{\partial w}{\partial x}\right)\right)+F_x \tag{3.10}$$

If the flow is considered to be incompressible and the variation in viscosity, μ, is negligibly small, a considerable simpler formulation may be obtained:

$$\rho\frac{Du}{Dt}=-\frac{\partial P}{\partial x}+\mu\left(\frac{\partial^2 u}{\partial x^2}+\frac{\partial^2 u}{\partial y^2}+\frac{\partial^2 u}{\partial z^2}\right)+F_x \tag{3.11}$$

Equation (3.11) is the appropriate form of the momentum equation for the majority of the electronics thermal management problems. This equation can be easily rewritten for the y- and z-directions:

$$\rho\frac{Dv}{Dt}=-\frac{\partial P}{\partial y}+\mu\left(\frac{\partial^2 v}{\partial x^2}+\frac{\partial^2 v}{\partial y^2}+\frac{\partial^2 v}{\partial z^2}\right)+F_y \tag{3.12}$$

$$\rho\frac{Dw}{Dt}=-\frac{\partial P}{\partial z}+\mu\left(\frac{\partial^2 w}{\partial x^2}+\frac{\partial^2 w}{\partial y^2}+\frac{\partial^2 w}{\partial z^2}\right)+F_z \tag{3.13}$$

Alternatively, the Navier-Stokes equations with constant properties can be represented in vector notation by:

$$\rho\frac{D\vec{V}}{Dt}=-\nabla P+\mu\nabla^2\vec{V}+\vec{F} \tag{3.14}$$

The body force term, $\vec{F}$, is given by:

$$\vec{F} = \rho \vec{g} \tag{3.15}$$

Natural convection flows are driven by the buoyancy effect due to density variations and the presence of the gravitational field. Mathematically, these flows are coupled with the temperature field (governed by the energy equation), since variations in temperature induce variations in fluid density. This is the reason natural convection flows are also called "buoyancy induced" flows.

3.2.2 Fluid Motion Pressure

The "motion pressure" (P_d) at a point in the fluid is defined as the difference between the actual (static) pressure, (P) and the hydrostatic pressure (P_a) at the point.

$$P = P_a + P_d \tag{3.16}$$

For a gravitational field, the hydrostatic pressure is obtained from:

$$\nabla P_a = \rho_a \vec{g}, \tag{3.17}$$

where ρ_a denotes the density of the ambient fluid, which in general may not be constant because the ambient fluid may be thermally stratified.

Equation (3.14) can be rewritten in terms of the motion pressure by grouping the pressure force and body force terms.

$$\vec{F} - \nabla P = \vec{F} - \nabla P_a - \nabla P_d = (\rho - \rho_a)\vec{g} - \nabla P_d \tag{3.18}$$

Substituting in Equation (3.14), yields:

$$\rho\frac{D\vec{V}}{Dt}=-\nabla P_d+\mu\nabla^2\vec{V}+(\rho-\rho_a)\vec{g} \tag{3.19}$$

3.2.3 Boussinesq Approximation

In its simplest form, the Boussinesq approximation states that all the fluid properties with the exception of density as it appears in the body force term of the Newton's 2nd law are constant. This leads to the following expression relating the change in densities to the change in temperatures:

$$(\rho_a-\rho)=\rho\beta(T-T_a) \tag{3.20}$$

Where β is the coefficient of thermal volumetric expansion and is given by:

$$\beta=-\left(\frac{1}{\rho}\right)\left(\frac{\partial\rho}{\partial T}\right)_p \tag{3.21}$$

For an ideal gas, β can be expressed in terms of the absolute temperature as:

$$\beta=\frac{1}{T} \tag{3.22}$$

Note that for the Boussinesq approximation to hold, the temperature difference in the flow must be small compared to the value of the absolute temperature. In other words, the following inequality must hold:

$$\beta(T-T_a)\ll 1;\quad \textit{or for ideal gas}\ \Rightarrow\frac{(T-T_a)}{T}\ll 1 \tag{3.23}$$

The Newton' 2nd law with Boussinesq approximation is now obtained by substituting the density variation term in Equation (3.19) using Equation (3.20).

$$\rho\frac{D\vec{V}}{Dt}=-\nabla P_d+\mu\nabla^2\vec{V}+\beta\vec{g}\rho(T-T_a) \tag{3.24}$$

3.3 Conservation of Energy (First Law of Thermodynamics)

This law states that the rate of increase of stored energy plus the net rate of outflow of energy by advection equals the net rate of inflow of energy by heat conduction plus the rate of work done by surface stresses plus the rate of heat sources. The differential equation for conservation of energy in its most general case is given by:

$$\rho\frac{Di}{Dt}=\nabla\cdot(k\nabla T)+\frac{DP}{Dt}+\mu\Phi+q''' \tag{3.25}$$

Φ is the viscous dissipation function, given by:

$$\Phi=\left\{2\left[\left(\frac{\partial u}{\partial x}\right)^2+\left(\frac{\partial v}{\partial y}\right)^2+\left(\frac{\partial w}{\partial z}\right)^2\right]+\left(\frac{\partial u}{\partial y}+\frac{\partial v}{\partial x}\right)^2+\left(\frac{\partial v}{\partial z}+\frac{\partial w}{\partial y}\right)^2+\left(\frac{\partial w}{\partial x}+\frac{\partial u}{\partial z}\right)^2-\frac{2}{3}\left(\frac{\partial u}{\partial x}+\frac{\partial v}{\partial y}+\frac{\partial w}{\partial z}\right)^2\right\} \tag{3.26}$$

This term is only significant in flows with high velocity and/or high Prandtl number. In order to express the energy equation in terms of temperature, the changes in specific enthalpy are related to changes to temperature and pressure. The left hand side of the Equation (3.15) is given by:

$$\rho\frac{Di}{Dt}=\rho c_P\frac{DT}{Dt}+(1-\beta T)\frac{DP}{Dt} \tag{3.27}$$

Therefore, the conservation of energy can be written in terms of temperature as:

$$\rho c_p \frac{DT}{Dt} = \nabla \bullet (k \nabla T) + \beta T \frac{DP}{Dt} + \mu \Phi + q''' \tag{3.28}$$

3.3.1 Simplifying Assumptions for Energy Equation

This equation is further simplified by realizing that in electronics applications (with flow velocity in the low to moderate range), the viscous dissipation ($\mu\Phi$) and compressibility effects ($\beta T \frac{DP}{Dt}$) are negligible. The resulting equation is:

$$\rho c_p \frac{DT}{Dt} = \nabla . (k \nabla T) + q''' \tag{3.29}$$

This is the formulation of the conservation of energy most applicable to electronics cooling applications. In the Cartesian coordinate system this equation is written as:

$$\rho C_p \left(\frac{\partial T}{\partial t} + u \frac{\partial T}{\partial x} + v \frac{\partial T}{\partial y} + w \frac{\partial T}{\partial z} \right) = \left\{ \frac{\partial}{\partial x} \left(k \frac{\partial T}{\partial x} \right) + \frac{\partial}{\partial y} \left(k \frac{\partial T}{\partial y} \right) + \frac{\partial}{\partial z} \left(k \frac{\partial T}{\partial z} \right) \right\} + q''' \tag{3.30}$$

Note that q''' is the heat generation term, which is zero in fluid regions and has a non-zero value in current carrying conductors and inside of electronic components.

3.4 Voltage Field Equation

The voltage field, ϕ, satisfies the following partial differential equation:

$$\frac{\partial}{\partial x} \left(\mathrm{K} \frac{\partial \phi}{\partial x} \right) + \frac{\partial}{\partial y} \left(\mathrm{K} \frac{\partial \phi}{\partial y} \right) + \frac{\partial}{\partial z} \left(\mathrm{K} \frac{\partial \phi}{\partial z} \right) = 0 \tag{3.31}$$

Here, the electrical conductivity is defined as $K = \frac{1}{\rho_e}$, where ρ_e is the electrical resistivity of the conductor, which is related to temperature by:

$$\rho_e = \rho_0 \left[1 + \alpha (T - T_0) + \beta (T - T_0)^2 \right]$$

Where:

ρ_0 ≡ Resistivity at Reference Temperature (T_0)

α, β ≡ Resistance Temperature Coefficients

3.5 Thermal Radiation

Thermal radiation often plays an important role in electronics cooling. It is easy to underestimate the role of thermal radiation as a significant contributor to electronics cooling in environments without forced air flow. Neglecting radiation leads to over-prediction of components' junction temperature, which will result in a conservative thermal design.

3.5.1 Surface-to-surface radiation

The surface-to-surface radiation heat transfer approach employed in this study is based on enclosure theory. An enclosure is an envelope of solid or open areas which completely surround a system. Thus an enclosure accounts for all directions surrounding the volume. The participating surfaces may be "black", "gray-diffuse" or perfectly transparent. The

word "gray" signifies that emissivity (ε) and absorptivity (α) of the surface do not depend on wavelength, but can depend on temperature. The word "diffuse" signifies that emissivity and absorptivity do not depend on direction. For a gray-diffuse surface $\varepsilon=\alpha$ and $\varepsilon+\rho_r=1$. Note that a black body surface has unit emissivity ($\varepsilon=1$).

Consider an enclosure consisting of N gray-diffuse surfaces with ε_k as the emissivity of the kth surface. Suppose that the fluid enveloped by this enclosure is non-participating and that the view factor matrix is given by the tensor F_{k-j}. The heat exchange relationship between the kth surface and all other radiating boundaries is given by:

$$\sum_{j=1}^{N}\left[\delta_{k,j}-(1-\varepsilon_k)F_{k-j}\right]\cdot q_r^j=\varepsilon_k\cdot\sigma\cdot T_k^4 \qquad (3.32)$$

Here, q_r^j is the radiative heat flux and T_k is the temperature of the k^{th} surface.

Chapter Four

IV. NUMERICAL PROCEDURE

As mentioned earlier, there are no exact solutions available for the set of governing equations, and one must resort to numerical solutions using methods of computational fluid dynamics. The present study employs the "Finite Volume" techniques for its CFD formulation. This method is discussed in great detail by Patankar [8] and Ferziger and Peric [10]. Some of the important features relating to this dissertation are presented in this chapter.

4.1 General Differential Balance Equation

In a flowing fluid, any scalar specific property, ϕ, is transported by two mechanisms, diffusion and advection. Consider the balance of ϕ over an arbitrary control volume shown in Figure 4.1.

Rate of accumulation of ϕ inside surface s = $\frac{\partial}{\partial t}\int_{v}\rho\phi dV$ (4.1)

Net rate of outflow of ϕ by advection = $\int_{s}\left(\rho\vec{U}\phi\right)\bullet\vec{n}ds$ (4.2)

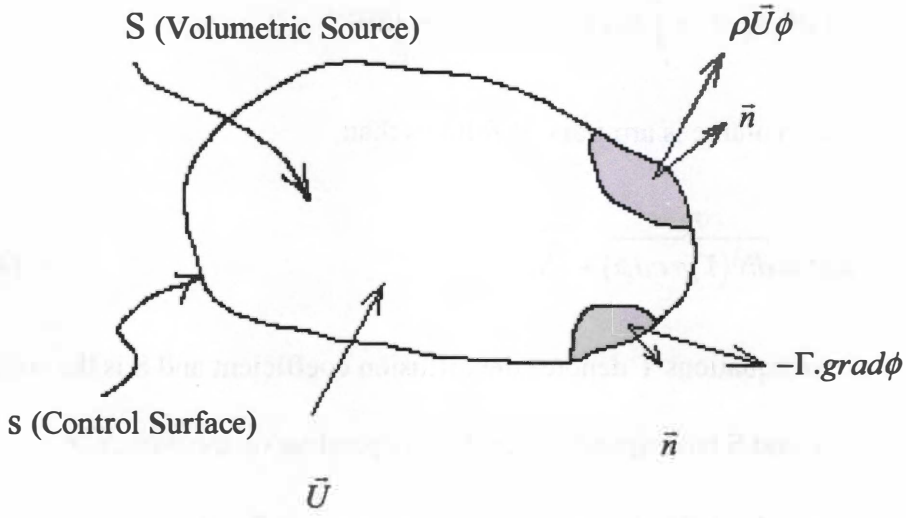


Figure 4.1: Arbitrary Control Volume with Fluxes

Net rate of outflow of ϕ by diffusion = $\int_s (-\Gamma grad\phi)\bullet\vec{n}ds$ (4.3)

Rate of production of ϕ inside surface s = $\int_V SdV$ (4.4)

Establishing a balance among the above quantities requires:

$$\frac{\partial}{\partial t}\int_V \rho\phi dV = -\int_s \left(\rho\vec{U}\phi\right)\bullet\vec{n}ds - \int_s (-\Gamma grad\phi)\bullet\vec{n}ds + \int_V SdV \tag{4.5}$$

Transforming the two surface integrals into volume integrals using the divergence theorem (discussed in Appendix A) yields:

$$\frac{\partial}{\partial t}\int_V \rho\phi dV = -\int_V div\left(\rho\vec{U}\phi\right)dV + \int_V div\left(\Gamma grad\phi\right)dV + \int_V SdV \tag{4.6}$$

And, since the control volume is arbitrary, it follows that:

$$\overbrace{\frac{\partial}{\partial t}(\rho\phi)}^{Accumulation} + \overbrace{div(\rho u\phi)}^{Advection} = \overbrace{div(\Gamma grad\phi)}^{Diffusion} + \overbrace{S}^{Source} \tag{4.7}$$

Note that in the above equations Γ denotes the diffusion coefficient and S is the source term. Variables ϕ, Γ and S have specific meanings depending on the particular conservation equation. Also, "div" represents the divergence of a vector:

$$div(A) \equiv \nabla\bullet A = \frac{\partial A_x}{\partial x} + \frac{\partial A_y}{\partial y} + \frac{\partial A_z}{\partial z} \tag{4.8}$$

and, "grad" represents the gradient of a scalar quantity:

$$grad(\phi) \equiv \nabla\phi = \hat{i}.\frac{\partial\phi}{\partial x} + \hat{j}.\frac{\partial\phi}{\partial y} + \hat{k}.\frac{\partial\phi}{\partial z} \tag{4.9}$$

4.2 Discretization

As we have seen in the previous section, the partial differential equations governing the transfer of heat, mass and momentum can be written in the form of Equation (4.7). These equations have to be solved over a computational domain, subject to certain initial and boundary conditions.

In general, any numerical procedure involves the approximation of the original partial differential equation by a system of algebraic equations. This approximation is accomplished by "discretizing" the computational domain. If the calculation domain is rectangular, it is convenient to discretize it using a network of orthogonal lines. In general, the discretization need not involve uniform spatial increments between successive grid lines, nor need the lines be orthogonal. An algebraic approximation is then obtained at each grid point. The approximation may be obtained through any of the number of different available techniques, including:

- Classical finite difference approach
- Method of weighted residuals
- Variational approach
- Control volume method.

Typically, each algebraic equation involves a computational cluster of nodes and represents a linear relationship among the nodal values, as shown in Figure 4.2.

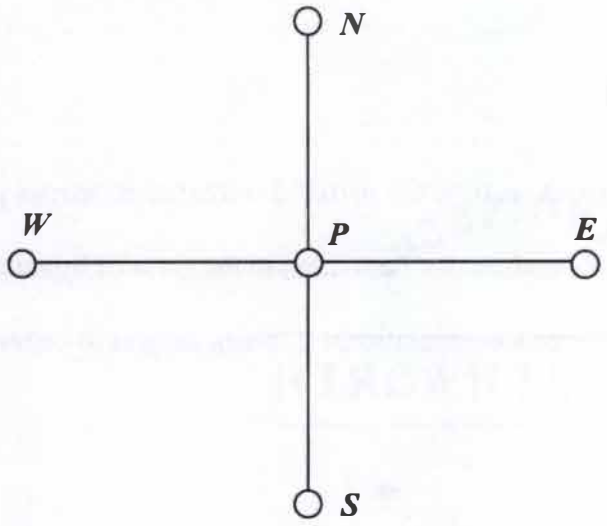


Figure 4.2: Cluster of Nodes Surrounding Center Node, P

$$a_P\phi_P = a_E\phi_E + a_W\phi_W + a_N\phi_N + a_S\phi_S + b \tag{4.10}$$

The a's appearing in Equation 4.10 are constants that may be viewed as influence coefficients, while b is a constant related to the source term. A common requirement of any successful numerical method is that all influence coefficients be positive. This comes from the fact that in most situations the value of the dependent variable at a grid-point is influenced by the values at the neighboring points only by the processes of advection and diffusion. Therefore, an increase in the value at one grid-point should lead to an increase in the value at its neighbors, given all other factors remain unchanged. Note that in each computational cluster, the central node value is related to the values at the restricted set of its neighboring points.

4.3 Control Volume Formulation

This is the most popular and successful formulation for CFD applications, and it is the chosen discretization approach for this study. This formulation is very intuitive and easy to follow. The computation domain is divided into a number of non-overlapping control volumes with a grid point located at its center. Each control volume has a number of neighboring control volumes surrounding it and separated from it by control surfaces. To obtain the discretization equations, the governing differential equation is integrated over each control volume, and the control surface fluxes are evaluated by assuming piecewise profiles for the variation of the dependent variable.

The most attractive feature of this formulation is that it offers the advantage of a direct physical interpretation – it establishes an energy balance over the control volume. Moreover, since this energy balance is exactly enforced over each individual control volume, the solution will exactly satisfy a global energy balance, regardless of the number of control volumes involved. In other words, even the solution obtained using a coarse mesh will exhibit exact integral balances.

We now examine the simplest case, the one-dimensional steady-state heat conduction equation, which will serve as a vehicle in studying the method of derivation of algebraic approximations.

4.3.1 One-Dimensional Steady-State Heat Conduction

Consider the differential equation governing one-dimensional steady-state heat conduction:

$$\frac{d}{dx}\left(k\frac{dT}{dx}\right)+S=0 \tag{4.11}$$

The Upwind Scheme

This scheme recognizes the fact that the difficulties associated with the central difference scheme come from the assumption that ϕ varies linearly between the nods, and it tries to overcome it by assigning the nodal value of ϕ to the control surface downstream to the node. Using this scheme the coefficients are always positive, and physically unrealistic solutions are precluded. The weak point of this scheme is that since the diffusion terms are always approximated by using linear profiles between the nodes, it tends to overestimate the diffusion flux at high flow rates.

The Exponential Scheme

This scheme is based on the exact solution for the one-dimensional, steady-state, convection/diffusion equation with a constant diffusion coefficient. The discretization equation is obtained using this exponential profile. Therefore, this represents the most accurate of all of the schemes considered here. However, this method is unattractive in practical problems because of relatively large computational effort associated with evaluating the coefficients.

The Hybrid Scheme

This method recognizes the strengths and weaknesses of the central difference and the upwind schemes. This scheme is equivalent to the central difference scheme for $-2 \le P_{\delta x} \le 2$ and it is equivalent to the upwind scheme, with the diffusion coefficient set to zero, for the grid Peclet number outside this range.

The Power-Law Scheme

The error in the hybrid scheme becomes appreciable around $|P_{\delta x}| \simeq 2$. The power-law scheme, developed by Patankar, provides a far better approximation of the exact exponential solution, without the associated heavy computational cost. This is by far the most accurate and preferred scheme, and it is the scheme used in this dissertation.

4.3.2 A General Convection-Diffusion Formulation

In order to present a general framework for obtaining the discretization equations for problems involving convection and diffusion, we re-examine the control surface fluxes and take a closer look at the coefficients involved along with their properties. Figure 4.3 shows a control surface between two grid-points i and i + 1, separated by a distance δ. The total flux (J) crossing the interface is given by:

$$J_f = \overbrace{\rho u \phi|_f}^{Convection} - \overbrace{\Gamma \frac{\partial \phi}{\partial x}\Big|_f}^{Diffusion} \qquad (4.23)$$

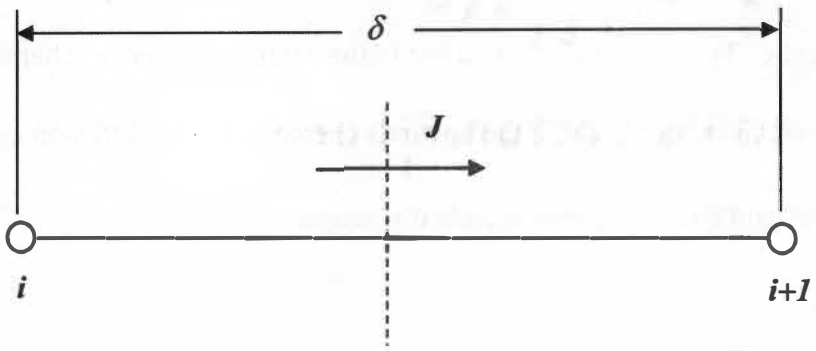


Figure 4.3: Total Flux on Interface Between Two Grid Points

Or, in non-dimensional form:

$$J_f^* = \frac{J_f \delta}{\Gamma} = \overbrace{P_\delta \phi|_f}^{Convection} - \overbrace{\left.\frac{d\phi}{d\left(\frac{x}{\delta}\right)}\right|_f}^{Diffusion} \qquad (4.24)$$

It is desirable to come up with expressions for ϕ and its derivative at the interface. We propose that, at the interface, the value of ϕ will be some weighted average of the values at the two grid-points surrounding it. For example, with the central difference scheme, the interface value will be the arithmetic mean of the values at the surrounding nodes. This can be expressed as:

$$\phi_f = \alpha\phi_i + (1-\alpha)\phi_{i+1} \qquad 0 \le \alpha \le 1 \qquad (4.25)$$

Similarly, we propose that the derivative at the face will be some multiple of $(\phi_{i+1} - \phi_i)$.

$$\Gamma \frac{\partial \phi}{\partial\left(\frac{x}{\delta}\right)}\bigg|_f = \beta(\phi_{i+1} - \phi_i) \qquad (\beta \text{ is a dimensionless multiplier.}) \tag{4.27}$$

Therefore, Equation (4.24) can be written as:

$$J_f^* = P_\delta\left[\alpha\phi_i + (1-\alpha)\phi_{i+1}\right] - \beta(\phi_{i+1} - \phi_i) = B\phi_i - A\phi_{i+1} \quad , \tag{4.28}$$

where A and B are dimensionless functions of the Peclet number.

Properties of A and B

Consider a case where $\phi_i = \phi_{i+1}$, implying zero diffusion flux. For this case we have:

$$J_f^* = P_\delta \phi_i$$

Substituting for J_f^* from Equation (4.28), we have:

$$P_\delta \phi_i = B\phi_i - A\phi_{i+1} \tag{4.29}$$

Since $\phi_i = \phi_{i+1}$, they can be cancelled out, leading to the following property:

$$B - A = P_\delta \tag{4.30}$$

To obtain a second important property of A and B, consider the case where the flow direction is reversed. Then A and B interchange their places and the Peclet number will appear as $-P_\delta$. Or,

$$A(-P_\delta) = B(P_\delta) \tag{4.31}$$

$$B(-P_\delta) = A(P_\delta) \tag{4.32}$$

Note that once the function A is known for positive values of the Peclet number, both functions for all values of the Peclet number can be completely determined.

$$A(P_\delta) = A(|P_\delta|) + \|-P_\delta, 0\| \tag{4.33}$$

$$B(P_\delta) = A(|P_\delta|) + \|P_\delta, 0\| \ , \tag{4.34}$$

where $\|A, B\|$ means the maximum of A,B.

4.3.3 General Expressions for ϕ on Control Volume Faces

Consider the cluster of nodes shown in Figure (4.4). The following two expression can be written for fluxes J_e and J_w:

$$J_e^* = B_e\phi_P - A_e\phi_E \tag{4.35}$$

Substitute for B_e:

$$J_e^* = (A_e + P_e)\phi_P - A_e\phi_E = P_e\phi_P + A_e(\phi_P - \phi_E) \tag{4.36}$$

Recall that $J = D_e J_e^*$ and $F_e = D_e P_e$. The control surface flux is obtained from:

$$J_e = F_e\phi_P + A_e D_e(\phi_P - \phi_E) \tag{4.37}$$

Similar expressions can be written for the flux on the west surface.

$$J_w^* = B_w\phi_W - A_w\phi_P \tag{4.38}$$

Substitute for A_w:

$$J_w^* = B_w\phi_W - (B_w - P_w)\phi_P = P_w\phi_P + B_w(\phi_W - \phi_P) \tag{4.39}$$

Again, recall that $J_w = D_w J_w^*$ and $F_w = D_w P_w$. The control surface flux is obtained from:

$$J_w = F_w\phi_P + B_w D_W(\phi_W - \phi_P) \tag{4.40}$$

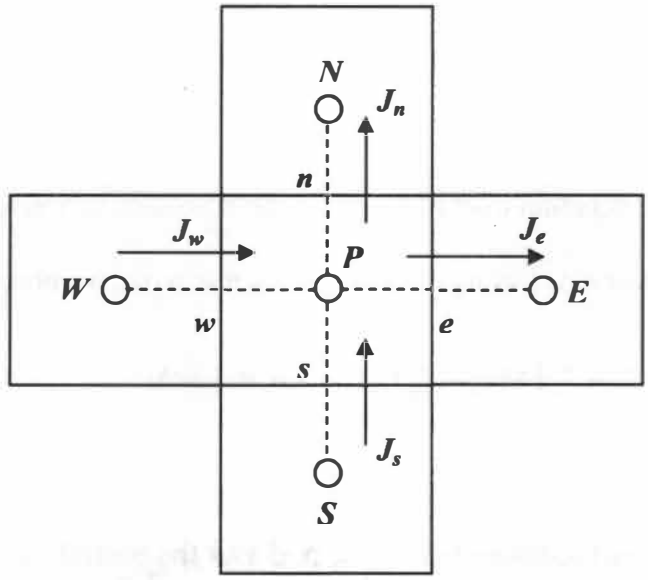


Figure 4.4: Two-Dimensional Control Volume

4.3.4 Discretization Equation for Convection-Diffusion

At this point, we have the tools necessary for writing the discretization equation corresponding to a general differential equation involving convection and diffusion. The procedure is illustrated for a two-dimensional situation; however, it can easily be applied to a three-dimensional case.

The governing equation for a general differential equation in two dimensions is:

$$\frac{\partial}{\partial t}(\rho\phi)+\frac{\partial}{\partial x}\overbrace{\left(\rho u\phi-\Gamma\frac{\partial\phi}{\partial x}\right)}^{J_x}+\frac{\partial}{\partial y}\overbrace{\left(\rho v\phi-\Gamma\frac{\partial\phi}{\partial y}\right)}^{J_y}=S \tag{4.41}$$

Integration of the above equation over space (the control volume surrounding the point P) and time (from time t to $t+\Delta t$) using the fully-implicit scheme, we obtain:

$$\left(\rho_P\phi_P-\rho_P^o\phi_P^o\right)\frac{\Delta x\Delta y}{\Delta t}+\left(J_e-J_w\right)+\left(J_n-J_s\right)=\left(S_C+S_P\phi_P\right)\Delta x\Delta y\,. \tag{4.42}$$

Note that J_e, J_w, J_n, J_s are the integrated total fluxes over the control volume surfaces. In other words, J_e represents $\int_e J_x dy$.

Now, consider the continuity equation:

$$\frac{\partial\rho}{\partial t}+\frac{\partial}{\partial x}(\rho u)+\frac{\partial}{\partial y}(\rho v)=0 \tag{4.43}$$

Integration of this equation over the same intervals leads to:

$$\left(\rho_P - \rho_P^o\right)\frac{\Delta x\Delta y}{\Delta t} + \left(F_e - F_w\right) + \left(F_n - F_s\right) = 0 \quad , \tag{4.44}$$

where ***F***'s represent the mass flow rates through control surfaces of the control volume.

To obtain the discretization equation, Equation (4.44) is subtracted from Equation (4.42):

$$\begin{aligned}\left(\phi_P - \phi_P^o\right)\frac{\Delta x\Delta y}{\Delta t} + \left(J_e - F_e\phi_P\right) - \left(J_w - F_w\phi_P\right) + \\ \left(J_n - F_n\phi_P\right) - \left(J_s - F_s\phi_P\right) = \left(S_C + S_P\phi_P\right)\Delta x\Delta y\end{aligned} \tag{4.45}$$

Now, substitute for the interface fluxes from the expression derived in the previous section:

$$\begin{aligned}\left(\phi_P - \phi_P^o\right)\frac{\rho_o\Delta x\Delta y}{\Delta t} &+ \left(F_e\phi_P + A_eD_e\left(\phi_P - \phi_E\right) - F_e\phi_P\right) \\ &- \left(F_w\phi_P + B_wD_W\left(\phi_W - \phi_P\right) - F_w\phi_P\right) \\ &+ \left(F_n\phi_P + A_nD_n\left(\phi_P - \phi_N\right) - F_n\phi_P\right) \\ &- \left(F_s\phi_P + B_sD_s\left(\phi_S - \phi_P\right) - F_s\phi_P\right) = \left(S_C + S_P\phi_P\right)\Delta x\Delta y\end{aligned} \tag{4.46}$$

Canceling out terms and collecting the coefficients of ϕ's will result in the discretization equation:

$$\begin{aligned}&\overbrace{\left(A_eD_e + B_wD_W + A_nD_nB_sD_s + \frac{\rho_o\Delta x\Delta y}{\Delta t} - S_P\Delta x\Delta y\right)}^{a_P}\phi_P = \\ &\underbrace{A_eD_e}_{a_E}\phi_E + \underbrace{B_wD_w}_{a_W}\phi_W + \underbrace{A_nD_n}_{a_N}\phi_N + \underbrace{B_sD_s}_{a_S}\phi_S + \overbrace{\frac{\rho_o\Delta x\Delta y}{\Delta t}\phi_P^o + S_C\Delta x\Delta y}^{b}\end{aligned} \tag{4.47}$$

The final form of the discretization equation is obtained by expressing functions A and B using their general form given by Equations (4.33) and (4.34).

$$
\begin{aligned}
a_P\phi_P &= a_E\phi_E + a_W\phi_W + a_N\phi_N + a_S\phi_S + b \\
a_E &= D_e A_e\left(|P_e|\right) + \|-F_e, 0\| \\
a_W &= D_w A_w\left(|P_w|\right) + \|F_w, 0\| \\
a_N &= D_n A_n\left(|P_n|\right) + \|-F_n, 0\| \\
a_S &= D_s A_s\left(|P_s|\right) + \|F_s, 0\| \\
a_P &= a_E + a_W + a_N + a_S + a_P^o - S_P\Delta x\Delta y \\
b &= S_C\Delta x\Delta y + a_P^o\phi_P^o
\end{aligned}
\tag{4.48}
$$

$$
a_P^o = \frac{a_P^o\Delta x\Delta y}{\Delta t} \tag{4.49}
$$

Recall that F, D and P represent mass flow rate, diffusion term and the Peclet number, respectively. For control surface located at "e", these are shown below:

$$
F_e = (\rho u)\Delta y; \quad D_e = \frac{\Gamma_e}{(\Delta x)_e}\Delta y; \quad P_e = \frac{F_e}{D_e} \tag{4.50}
$$

Obviously, this derivation can be extended to three dimensions in a straightforward manner.

Table 4.1 provides a listing of expressions of the function A for various schemes.

4.3.5 Solution of the Flow Field

In previous sections, a procedure was presented to solve the general differential equation of a dependent variable, ϕ, in presence of a given velocity field. In general, ϕ can stand for any scalar variable, including each of the velocity components. However, ϕ cannot stand for pressure – the pressure field does not obey such a conservation equation.

Table 4.1: Function $A(|P|)$ Expressions for Various Schemes

Scheme	$A(\|P\|)$
Central Difference	$1-0.5\|P\|$
Upwind	1
Hybrid	$\|0,(1-0.5\|P\|)\|$
Power-Law	$\|0,(1-0.1\|P\|)^5\|$
Exponential	$\frac{\|P\|}{\left[\exp(\|P\|)-1\right]}$

When ϕ stands for a velocity component, the problem becomes nonlinear, requiring an iterative solution starting with a guessed velocity field. For a two-dimensional situation, the governing equations are shown below:

$$\frac{\partial \rho}{\partial t}+\frac{\partial(\rho u)}{\partial x}+\frac{\partial(\rho v)}{\partial y}=0 \tag{4.51}$$

$$\frac{\partial}{\partial t}(\rho u)+\frac{\partial}{\partial x}\left(\rho uu-\mu\frac{\partial u}{\partial x}\right)+\frac{\partial}{\partial y}\left(\rho vu-\mu\frac{\partial u}{\partial y}\right)=-\frac{\partial p}{\partial x}+B_x \tag{4.52}$$

$$\frac{\partial}{\partial t}(\rho v)+\frac{\partial}{\partial x}\left(\rho uv-\mu\frac{\partial v}{\partial x}\right)+\frac{\partial}{\partial y}\left(\rho vv-\mu\frac{\partial v}{\partial y}\right)=-\frac{\partial p}{\partial y}+B_y \tag{4.53}$$

Note that in the above coupled and nonlinear equations the pressure field appears as a source term in the form of $\frac{\partial p}{\partial x}$ and $\frac{\partial p}{\partial y}$. The main difficulty comes from the fact that there does not seem to be an equation that allows us to solve explicitly for pressure. We may try guessing the pressure field, but if the guess is incorrect, the resulting velocity field will not satisfy the continuity equation. The correct procedure is one that involves the continuity equation indirectly – the correct pressure field is one which yields a velocity field that satisfies the continuity equation.

Difficulties Associated with First Derivatives

In attempting to develop a method to solve the momentum and continuity equations, we encounter an additional difficulty – a way to handle the first derivatives (i.e., $\frac{\partial p}{\partial x}$, $\frac{\partial u}{\partial x}$ ...). The discretization of first derivatives leads to terms such as "$\phi_e - \phi_w$" which must be expressed in terms of grid-point values. Consider a grid structure with faces e and w midway between the main grid-points and assuming a piecewise linear variation for ϕ, we have:

$$\phi_e - \phi_w = \frac{\phi_P + \phi_E}{2} - \frac{\phi_W + \phi_P}{2} = \frac{\phi_E - \phi_W}{2} \tag{4.54}$$

Note that the expression contains that value of ϕ at alternate grid-points. This implies that the term is evaluated from a coarser grid, which can lead to inaccuracies in the solution. Another implication is that a "checker-board" pattern variation would be seen as a uniform distribution.

One way to get around this difficulty is to realize that we do not have to use the same grid location for every dependent variable. In fact, if we employ an alternative grid for the distribution of the velocity components, these difficulties will disappear. The grid used for the velocity component is called the "staggered-grid" – for each velocity component it is displaced by half of a control volume in that direction. Note that the staggered grid is used only for the velocity components. All other variables (temperature, pressure...) are evaluated by the main grid-points.

Figure (4.5) shows an example of staggered grid locations. The advantages of employing this grid structure are obvious from this figure. For the x-momentum control volume surrounding node u_e, the term P_p-P_E can be used directly to calculate the pressure force on this element. Similarly, u_e-u_w is used for expressing $\frac{\partial u}{\partial x}$ at point P.

Discretization of the Momentum Equations

The procedure developed for the discretization of the general differential equation applies directly to the momentum equation. The only difference is the appearance of an additional source term in the form of the pressure gradient. However, since pressure appears as an unknown in the momentum equations, it is advantageous to treat the pressure source term separately. Consider the general form of the x-momentum equation:

$$\frac{\partial}{\partial t}(\rho u) + div(\rho \vec{U} u - \mu \nabla u) = S_u - \frac{\partial p}{\partial x} \tag{4.55}$$

There are two main differences between this equation and the general equation considered earlier: 1) the velocity field $\vec{U}$ itself depends on u, and 2) the pressure field is unknown. We start by using a guessed velocity field and integrate the equation over a staggered control volume shown in Figure 4.5

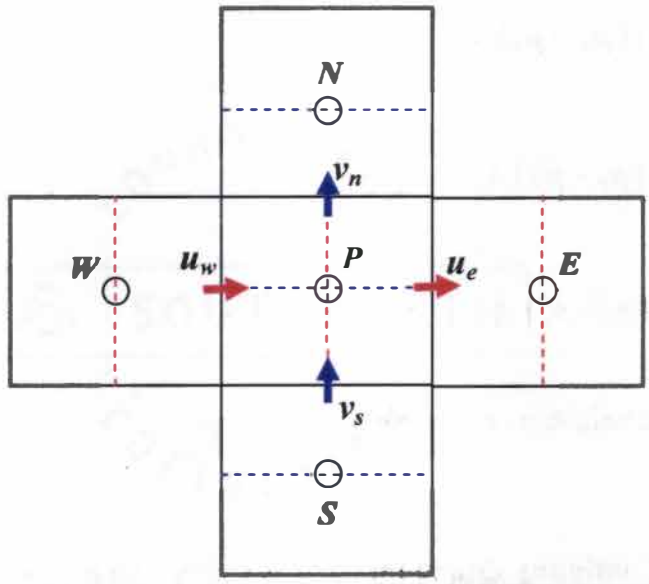


Figure 4.5: Staggered Grid Locations for u and v

Using the techniques described earlier, the discretized momentum equation for the nodes surrounding the point P is obtained.

$$a_e u_e = \left(\sum_i a_i u_i \right)_e + b_e + (p_P - p_E) A_e \tag{4.56}$$

$$a_w u_w = \left(\sum_i a_i u_i \right)_w + b_w + (p_W - p_P) A_w \tag{4.57}$$

$$a_n v_n = \left(\sum_i a_i v_i \right)_n + b_n + (p_P - p_N) A_n \tag{4.58}$$

$$a_s v_s = \left(\sum_i a_i v_i \right)_s + b_s + (p_S - p_P) A_s \quad , \tag{4.59}$$

where the i's denote the neighbors of the point.

Discretization of the Continuity Equation

In addition to the momentum equations, the velocity components appear in the continuity equation, given by:

$$\frac{\partial \rho}{\partial t} + div(\rho \vec{U}) = 0 \tag{4.60}$$

We have already noted that if the correct pressure filed is used, the momentum equation would result in the velocity component that will satisfy the continuity. Therefore, in the solution procedure, the pressure will serve as a link between the continuity and momentum equations.

Integration of the continuity equation over the main grid control volume using the fully implicit scheme yields:

$$\frac{\rho_P - \rho_P^o}{\Delta t}\Delta x\Delta y + (\rho_e u_e - \rho_w u_w)\Delta y + (\rho_n u_n - \rho_s u_s)\Delta x = 0$$

4.3.6 The SIMPLER Algorithm

The following procedure is called the SIMPLER algorithm, which stands for Semi-Implicit Method for Pressure Linked Equations – Revised. It involved re-writing the continuity equation to obtain two additional equations necessary for solving the flow field. The first equation is the Pressure Equation and the second one is an equation used for correcting the velocity field obtained by the momentum equations so that it will satisfy the continuity equation.

The Pressure Equation

Recall the discretized x-momentum equation:

$$u_e = \frac{1}{a_e}\left\{\left(\sum_i a_i u_i\right)_e + b_e\right\} + \underbrace{\frac{A_e}{a_e}}_{d_e}(p_P - p_E) \tag{4.61}$$

Now, the first term on the right hand side is defined as pseudo-velocity:

$$\hat{u}_e = \frac{1}{a_e}\left\{\left(\sum_i a_i u_i\right)_e + b_e\right\} \tag{4.62}$$

Therefore, the velocity at point e can be represented by:

$$u_e = \hat{u}_e + d_e(p_P - p_E) \tag{4.63}$$

Similarly, we can express the velocity component in the y direction in terms of the pseudo-velocity component.

$$v_n = \hat{v}_n + d_n\left(p_P - p_N\right) \tag{4.64}$$

The pressure discretization equation can now be obtained by substituting the velocity components in the discretized continuity equation by expression given in Equations (4.63) and (4.64). The resulting equation after the collection of terms is:

$$a_P p_P = a_E p_E + a_W p_W + a_N p_N + a_S p_S + b \tag{4.65a}$$

$$a_E = \rho_e d_e \Delta y \tag{4.65b}$$

$$a_W = \rho_w d_w \Delta y \tag{4.65c}$$

$$a_N = \rho_n d_n \Delta x \tag{4.65d}$$

$$a_S = \rho_n d_n \Delta x \tag{4.65e}$$

$$a_P = a_E + a_W + a_N + a_S \tag{4.65f}$$

$$b = \frac{\left(\rho_P^o - \rho_P\right)}{\Delta t}\Delta x \Delta y + \left[\left(\rho\hat{u}\right)_w - \left(\rho\hat{u}\right)_e\right]\Delta y + \left[\left(\rho\hat{v}\right)_s - \left(\rho\hat{v}\right)_n\right]\Delta x \tag{4.65g}$$

Velocity Correction

In general, the velocity field obtained by solving the momentum equation with an imperfect pressure field will not satisfy the continuity equation. To remedy this, the following procedure is proposed.

Let p and u denote the true pressure and velocity components, and p^* and u^* be the current imperfect pressure and velocity component. Also, we define a pressure correction and velocity correction terms as

$$p' = p - p^* \tag{4.66}$$

$$u' = u - u^* \tag{4.67}$$

Now, the discretized momentum equation is written for the true and imperfect velocity fields:

$$a_e u_e = \left(\sum_i a_i u_i \right)_e + b_e + (p_P - p_E) A_e \tag{4.68}$$

$$a_e u_e^* = \left(\sum_i a_i u_i^* \right)_e + b_e + (p_P^* - p_E^*) A_e \tag{4.69}$$

Subtract Equation (4.69) from Equation (4.68) to get an expression for the velocity correction.

$$u_e' = \frac{1}{a_e} \left(\sum_i a_i u_i' \right)_e + (p_P' - p_E') \frac{\overbrace{A_e}^{d_e}}{a_e} \tag{4.70}$$

The final form of the velocity correction is obtained after ignoring $\sum_i a_i u_i'$:

$$u_e' = d_e (p_P' - p_E') \tag{4.71}$$

Therefore, the true velocity components can be expressed in terms of the imperfect velocity field as:

$$u_e = u_e^* + \overbrace{d_e (p_P' - p_E')}^{u_e'} \tag{4.72}$$

$$v_n = v_n^* + \overbrace{d_n\left(p'_P - p'_N\right)}^{v'_n} \tag{4.73}$$

A discretization equation can now be obtained for p' by substituting the velocity components in the discretized continuity equation by expression given in Equations (4.72) and (4.73). The resulting equation after collecting terms is:

$$a_P p'_P = a_E p'_E + a_W p'_W + a_N p'_N + a_S p'_S + b \tag{4.75a}$$

$$a_E = \rho_e d_e \Delta y \tag{4.75b}$$

$$a_W = \rho_w d_w \Delta y \tag{4.75c}$$

$$a_N = \rho_n d_n \Delta x \tag{4.75d}$$

$$a_S = \rho_n d_n \Delta x \tag{4.75e}$$

$$a_P = a_E + a_W + a_N + a_S \tag{4.75f}$$

$$b = \frac{\left(\rho_P^o - \rho_P\right)}{\Delta t}\Delta x \Delta y + \left[\left(\rho u^*\right)_w - \left(\rho u^*\right)_e\right]\Delta y + \left[\left(\rho v^*\right)_s - \left(\rho v^*\right)_n\right]\Delta x \tag{4.75g}$$

Note that the constant term, *b*, may be viewed as a mass source or sink in the control volume. This term will serve as an indicator for convergence to a correct flow field – the correct velocity components, as obtained from the solution of the momentum equation will result in a negligibly small value of *b*.

Sequence of Operations

a) Transient Flow Problems

1. Initialize the velocity field.
2. Compute the coefficients of the discretized momentum equations using the initial velocities.
3. Calculate the pseudovelocities.
4. Setup and solve the pressure equation.
5. Using this pressure field, solve the momentum equations to obtain the velocity components.
6. Calculate the mass source.
7. Setup and solve p' equation.
8. Correct the velocity components.
9. Solve the energy and other equations and update material properties and sources.
10. Increment the time by Δt.
11. Return to step 2

Note that this procedure can be improved by using a predictor-corrector approach, in which the time is incremented after a corrector passes through steps 2 – 9.

b) Iterative Steady-State Approach

The SIMPLER algorithm may also be used iteratively to directly solve for a steady-state velocity field. To make the iterations converge, it is usually necessary to under-relax the momentum equations. The procedure is illustrated in Figure 4.6.

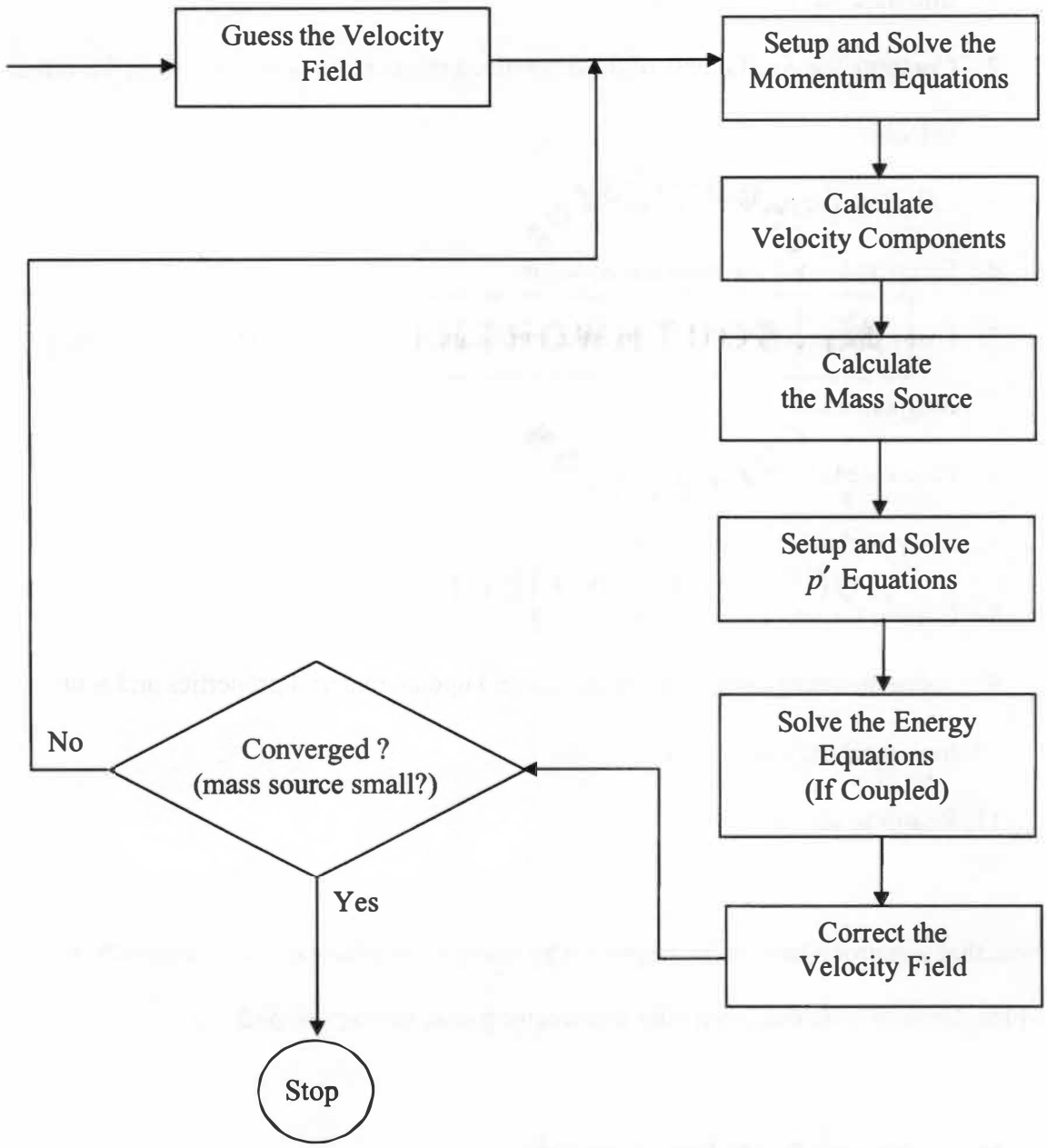


Figure 4.6: Flow Diagram for SIMPLER Algorithm Steady-State

4.4 Coupled Thermal / Electrical Analysis

In these types of applications, the heat dissipation distribution is not known prior to the solution and must be evaluated by simultaneously solving the electrical field. This is accomplished through a "coupled electrical/thermal solution" scheme, where the voltage field is solved throughout the region knowing electrical loads and boundary conditions (in addition to thermal and flow fields) during each iteration. The most recent temperature field is then used to update the electrical resistivity of the conductors in the model. Next the Joulian power dissipation is calculated for all elements. The procedure, along with the related equations, is presented below.

The current density, $\vec{J}$, is related to the electrical field, $\vec{E}$, by ohm's law. For an isotropic conductivity medium with electrical conductivity, σ, this takes the form:

$$\vec{J}(\vec{x}) = \sigma(\vec{x}).\vec{E}(\vec{x}) \tag{4.76}$$

The electrical field can be expressed as the gradient of a scalar potential function, ϕ, or voltage:

$$\vec{E}(\vec{x}) = -\nabla\phi(\vec{x}) \tag{4.77}$$

The total rate of work done in an element with volume V is:

$$P = \int_V \vec{J}.\vec{E}dV = \int_V \sigma\nabla\phi.\nabla\phi dV \tag{4.78}$$

Therefore, the power dissipation in one element is given by:

$$P_{Element} = \sigma V_{Element} \nabla\phi.\nabla\phi = \frac{V_{Element}}{\rho} \nabla\phi.\nabla\phi \tag{4.79}$$

where, ρ denotes electrical resistivity.

For an element in a Cartesian coordinate system Equation (5.79) can be simplified to:

$$P_{Element} = \frac{\left(\Delta\phi_x\right)^2}{R_x} + \frac{\left(\Delta\phi_y\right)^2}{R_y} + \frac{\left(\Delta\phi_z\right)^2}{R_z} \tag{4.80}$$

A complete and thorough discussion of the above is presented in the book by J. D. Jackson [11].

4.5 Boundary Conditions

Evaluation of fluxes through control volume faces coinciding with the domain boundary requires special treatment. They must be either known, or be expressed in terms of interior values and boundary data. Moreover, since boundary conditions do not result in additional equations, they must not introduce additional unknowns. Typically, convective fluxes are assumed

- known at inflow boundaries (with the exception of pressure which is extrapolated from interior data),

- zero at impermeable walls and symmetry planes, and
- independent of the coordinate normal to an outflow boundary (again, pressure is the exception; it is set to external ambient pressure at all outflow boundaries).

Diffusive fluxes are either specified at a wall (given heat flux or adiabatic surface) or calculated using the prescribed boundary variables using one-sided approximations for normal gradients.

4.6 The Computational Details

The important operations for the solution of transient coupled Thermal – Electrical – CFD problem are described below, in the order of their execution:

1. **Initialization:**

   All relevant parameters that define the problem are read by the program and loaded into the computer memory. This includes geometrical parameters, thermal, CFD and electrical loads and boundary conditions, thermal and electrical properties for all solids in the model.

2. **Solve for the initial voltage field:**

Using the values for the electrical resistivity (evaluated at the initial temperature), the voltage differential Equation (Eq. 6) is solved in all electrically conducting regions in the model subject to current and voltage boundary conditions.

3. **Obtain the initial Joulian heat dissipation distribution:**

Knowing the values of the voltage at all electrically conductive elements, the Joulian heat dissipation is calculated from Eq. 11 and added to the element "source term".

4. **Solve for temperature and flow fields for the initial time level:**

Next, the differential equations for energy and flow are solved throughout the domain of interest to yield values for the temperature, velocity components and pressure for all elements in the model. This requires knowledge of:

- The initial temperature and flow distribution.
- Thermo-physical properties for all solids and fluid regions.
- Thermal and flow boundary conditions.
- The values of heat sources at all conductors obtained from the previous step.

The SIMPLER algorithm is used to couple the continuity and momentum equations. The reader should refer to reference [8] for details of this algorithm.

5. **Update Material Properties:**

   All material properties (including the electrical resistivity) are updated to correspond to the current temperature field.

6. **Solve the electrical field:**

   Using the updated values for the electrical resistivity, solve for the voltage field. Update heat sources to account for changes in the Joulian heat dissipation resulting from the changed electrical field.

7. **Solve for temperature and flow:**

   Using the updated material properties and the current temperature and flow fields, increment the time and solve the governing differential equations to obtain temperature and flow for the current time iteration.

8. **Iterate:**

   Return to step 5 and repeat the entire procedure until the end time is reached.

Chapter Five

V. Description of the Analysis Package

5.1 General Description

ElectroFlo (EFlo) is a software developed based on the principles and procedures described in the previous chapters. The software is specially designed for engineers concerned with electronics cooling. It uses the methods of computational fluid dynamics to solve for the temperature and flow field characteristics (i.e., velocity, pressure, etc.) for problems involving natural or forced convection and may be used for component, board, or system level calculations.

EFlo has been designed for ease of use. It uses a menu structure, which guides the user through modeling procedure and includes on-line help for quick reference. In addition, there are several features of the code that ease the burden of problem setup. For example, the user has the ability to define a component and store this definition in a library. Placing additional components of the same type on a board is then a simple matter of referencing the component library and providing the new location on the board.

5.2 Model Creation

ElectroFlo is accessed through a windows-driven menu system. The user will generally proceed from left to right and from top to bottom along any given form to complete the information required in each step of the model building process. In this way, the user is able to proceed in a systematic way through building a model, submitting an analysis and looking at results.

In the following sections, the user will be introduced to the menu structure and modeling procedures used in creating an Eflo model and will then be taken step by step through the model creation process. The user should first understand the "philosophy" and the basic building constructs of an Eflo model.

Figure 5.1 shows the GUI along with Treeview and Listview tools. The basic building blocks of a model consist of components, PCBs (or boards), walls and enclosures. All models may contain any or all of these basic constructs (and may contain more than one of each type). Further, there are relationships between the different building block types. For instance, a component has a parent board and the component's location is specified relative to this board (e.g., 5 cm up and 10 cm over from the corner of the board). In this way, it is very easy to modify an existing model. For example, changing the orientation of a board in an enclosure only requires the user to modify the position of the board. Once this is done, all of the components on that board are repositioned automatically since their locations were specified relative to the board.



Figure 5.1: EFlo Interface with Treeview and Listview Tools

As geometry is created, its volume is "installed" (i.e., reserved) in the calculation domain. Once the geometry installation is completed, any portion of the calculation domain not reserved as a solid is automatically assumed to be the working fluid (air properties will be used by default; to specify a fluid other than air the user simply defines new material properties). Installing the geometry also results in the definition of key planes, which are used in mesh creation. A key plane is formed along the solid boundaries of the geometry. It should be noted that this version of Eflo requires a structured mesh. One result of this is that irregular boundaries must be approximated in a "stair-stepped" fashion. To aid the user in handling this type of geometry, a secondary object may be created. These entities can be created to the shape of the (irregular) geometry to be modeled. No key planes are created for these entities, but the meshing algorithm will use the existing mesh to represent the irregular boundary as closely as possible. This allows the user to easily specify material properties and boundary conditions for these regions as well.

Meshing is performed through the use of an automated utility and, optionally, by manually specifying the mesh density in local regions. The meshing utility will automatically bias the mesh close to solid walls where high gradients generally exist to aid the user in obtaining accurate results. The user may manually override the automatically produced mesh in local regions using any of the three different methods to produce the desired mesh density. This results in an easy-to-use and highly flexible method of creating the mesh for analysis. In addition to the standard meshing capabilities, the user may define "point-to-point" resistances. For example, rather than modeling the component to board connections in detail, the user may opt to define a

resistance between the component and PCB. Similarly, the user may define a resistance between a PCB and an enclosure to simulate the thermal path between them.

The next step in creating the model is to define the material properties. Note that during the creation of the geometry the user may specify the material to be used for each component, PCB, wall and/or enclosure. This duplication of functionality exists between many of the menu picks in Eflo and allows the user more flexibility and efficiency in producing the model to be analyzed. A library of material properties for commonly used materials has been included with Eflo. Rather than try to provide a comprehensive list of material properties (which are very often not used in favor of a customer's "officially approved" material properties), we have chosen to make this library user extensible. It is intended that the user add and update this library as needed for easy and permanent access to the desired material properties.

After creation of the geometry, mesh and material properties, the user may specify the boundary conditions to be used. Here again, some duplication of functionality has been provided as the user has the option of providing temperature and power input during the geometry creation phase. The user may specify temperature, heat input (absolute and per unit area, or per unit volume), convection coefficient (to be used either on boundaries where no CFD solution is run or for runs where no CFD calculations are performed), velocity, and flow rate, as well as define radiation surfaces. The radiation capability includes automatic viewfactor calculation (with obstruction checking). For most of the boundary condition types, the user is allowed a "quick" application of constant or tabular

data. In addition, the user may specify a very general variation of space, time and/or temperature.

In areas of the model where the fluid velocities are not solved (or when a non-CFD run has been chosen), the user may apply convection as a boundary condition. Several options have been provided to allow the user to handle this easily. The user may supply a constant value for the convection coefficient (h). For cases where the h may change, a convection correlation library has been provided; the user simply indicates the correlation to be used on a given surface and the convection coefficient is automatically calculated during the analysis (again, this is provided for areas and/or runs where no CFD calculations are performed). Similarly, the user may choose to apply convection coefficients calculated from a previous CFD run for further "what-if" studies where CFD calculations are disabled.

At this stage, the model is ready for analysis (see Chapter 4). Chapter 3 covers more detail on the various aspects of modeling covered in this overview. In summary, model creation is performed as follows:

1. Geometry is specified. The basic building blocks consist of components, PCB's, walls, and enclosures. "Irregular" geometry may be modeled using secondary objects. Key planes are defined automatically by EFlo as geometry is created.

2. Mesh is created. A mesh will automatically be produced based on the key plane definitions. This mesh includes automatic biasing toward all solid surfaces. The mesh may be manually modified in local regions at the user's discretion. In addition to the "standard" meshing options, the user may specify point-to-point resistances to allow a thermal path between objects.

3. Material Properties are specified. The user specifies the material name of entities as they are created. The material may exist in the user-extensible material library, in which case no further action is required on the part of the user. If the material name entered does not exist in the library, the user will be prompted for property input in the material properties form. Material properties may be constant or a function of temperature and may be homogeneous or orthotropic (e.g., the thermal conductivity may be different in the x direction than in the y direction).

4. Boundary Conditions are defined. The user may specify temperature, heat input, convection coefficients (for non-CFD calculations), velocity, and flow rate, and may define radiation surfaces. A convection correlation library is provided. The radiation capabilities of the code include automatic viewfactor calculation with the ability to control the complexity of the radiosity network generated.

5.3 Meshing

Once the geometry has been defined, the user proceeds with creating the finite volume mesh. Obviously, this procedure is extremely critical to the solution process as the quality of the mesh will be directly reflected in the quality of the results obtained. Considerable effort has been expended in an attempt to make this a relatively automated process; however, it is inevitable that user interaction will be necessary to produce an acceptable mesh for complex problems. As usual, a little common sense goes a long way in producing a mesh that balances acceptable solution accuracy with acceptable computational time. Obeying general rules of thumb, such as refining the mesh in regions where high gradients are expected (e.g., in the portion of the fluid next to a solid wall) and coarsening the mesh away from areas of interest, aids considerably in obtaining an acceptable mesh.

Mesh creation is fundamentally tied to the definition of geometry. Geometry installation results in the automatic creation of key planes, which are formed along solid boundaries. To define the mesh used in the analysis, the user specifies the number of elements and element spacing between key planes, initially using the global parameters and then using the local refinement parameters. Note that the global parameters include enough flexibility to automatically pack the mesh in the fluid near a solid/fluid interface, specify element spacing on the solid side of the solid/fluid interface, provide a maximum element size and the mesh grade (which determines how quickly elements change size away from a solid boundary). This provides the ability to very quickly obtain a mesh with the

desired qualities of being refined near solid boundaries and coarsened in regions where high gradients are not expected.

After the initial mesh has been formulated, the user may decide to refine the mesh in local regions. This is accomplished by selecting a pair of key planes (to define the local region) and specifying, by one of three methods, the mesh spacing between them. This is repeated for individual regions until the desired mesh is obtained.

5.4 Material Properties

At any time after creation of geometry, the user may proceed to define the materials referenced in the model that were not contained in the material library (the association of a material with specific entities is performed during the creation of the geometry. Note that if all materials used in a model are contained in the material library file, the user may skip the materials menu altogether.

Material properties may be defined as constant or as a function of temperature. In addition, the material may be designated as homogeneous or orthotropic. An orthotropic material designation allows separate input of the thermal conductivity along the (global) x, y and z axes.

5.5 Boundary Conditions

Following the creation of geometry, discretization (i.e., meshing), and assignment of material properties, the numerical representation of the problem is completed by specifying the boundary conditions. The boundary conditions available in EFlo include temperature, heat flux, heated volume, convection (for regions or analyses where no fluid velocities are being calculated), radiation to ambient (viewfactor is specified), surface-to-surface radiation (viewfactors are calculated), point source, velocity, thermal resistance, voltage, current and heat exchanger.

All of these boundary condition types may be constant or may be general functions of time, temperature and/or spatial coordinates. Variable boundary conditions are created by first defining a "Variation". The Variation (function or table) simply defines an independent variable (x,y,z,time, and/or temp) and how the dependent variable (e.g., heat input or temperature) varies as the independent variable changes value. Figure 5.2 shows the input for an exponential function variation. Once a Variation is defined, it may be referenced by any number of boundary conditions. If multiple Variations are specified for a single boundary condition, the values of each Variation are computed and multiplied together to give the final boundary condition value (note: this calculation is done during the solution of the problem). Various boundary condition types are discussed in the following sections.

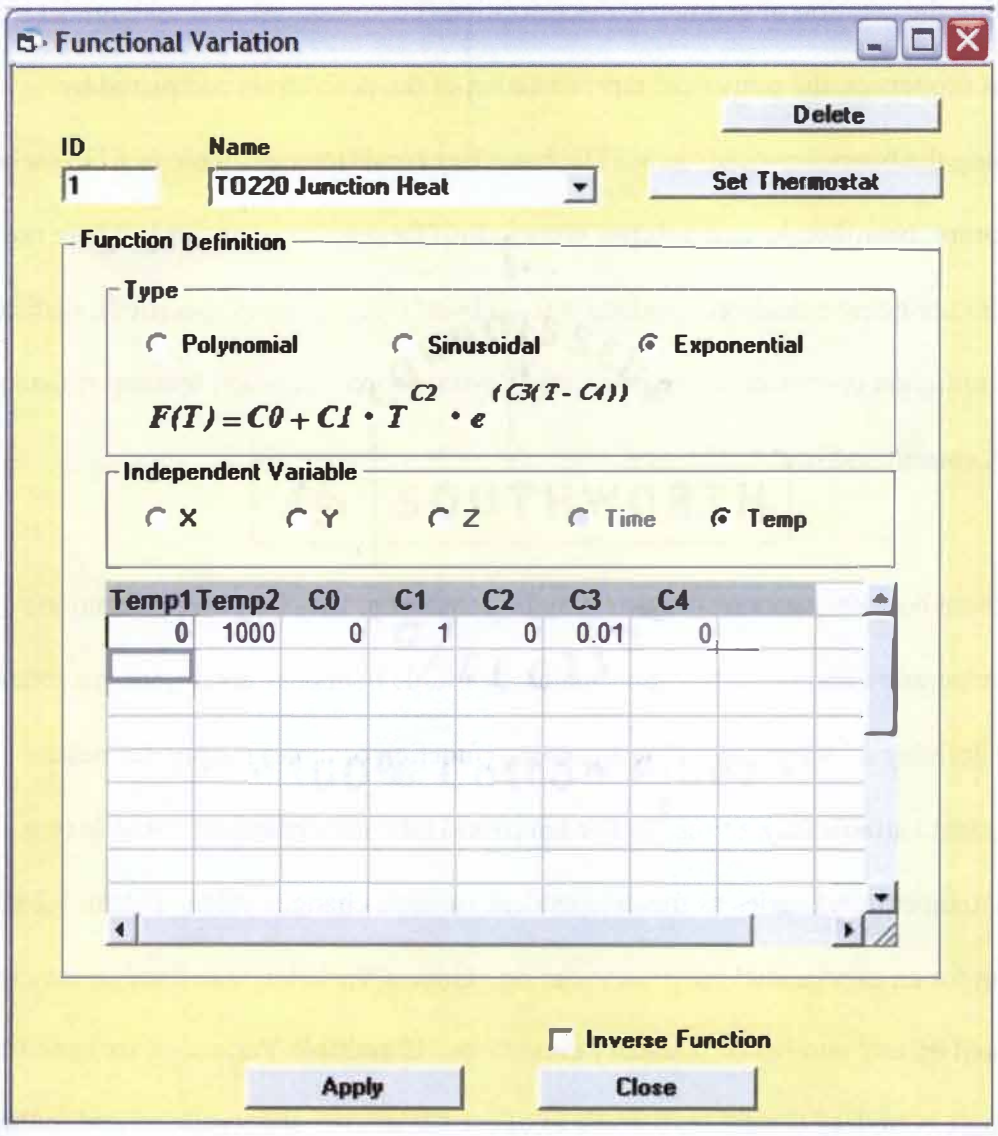


Figure 5.2: Definition Form for Functional Variati

5.5.1 Temperature

This boundary condition type is used to specify a constant or variable temperature to a plane application region.

5.5.2 Heat Flux

This boundary condition type is used to specify a constant or variable heat flux to a plane application region.

5.5.3 Heated Volume

This boundary condition type is used to specify a constant or heat generation (total or volumetric) to a volume.

5.5.4 Convection

For portions of the computational domain in which the fluid equations are not solved (e.g., if the model domain only extends to the edge of an enclosure), convective heat transfer from a solid surface to the ambient may be handled by applying a convective boundary condition. Two methods are available to define convective boundary conditions: "*Define BC*" and "*Auto Gen*". The "*Define BC*" method is one in which the user specifies the plane from which convection occurs, the convection coefficient (either directly or by reference to a correlation), and all other data necessary to define the convective loading. In the "*Auto Gen*" method, EFlo determines all of the surfaces

within the user-specified volume, and automatically applies the user-specified convection coefficient. For either method, the ambient temperature may be specified or may be calculated at solution time.

5.5.5 Radiation

EFlo allows for the definition of two different types of radiation boundary conditions: Radiation to Ambient and Surface-To-Surface Radiation ("Radiation Network").

5.5.5.1 Radiation to Ambient

This boundary condition type is used to apply thermal radiation to a single surface. The user specifies the ambient temperature, surface emissivity and the viewfactor to be applied.

5.5.5.2 Radiation Network

The radiation capabilities in EFlo include the ability to automatically perform viewfactor calculations and generate a radiosity network. Radiosity networks can become quite complex and for larger models may represent significant computational overhead. Very often, however, the radiosity network may be simplified considerably while maintaining an acceptable level of accuracy. EFlo provides the user with full control over the complexity of the radiosity network generated. This is accomplished by manipulating radiation surfaces (which may contain one or more element faces). These surfaces really

represent a separate mesh, which is used for the radiation solution (and coupled to the overall solution sequence).

The radiation problem is solved by calculating an effective radiation surface temperature based on the elemental temperatures of all elements contained in the surface. This temperature is used in the radiation solution, which, in turn, allows a radiative flux to be mapped back to the individual elements (again, split based on elemental temperatures). As long as the viewfactors to other surfaces do not change significantly over the radiation surface and the temperature gradients are not "large", the resulting solution accuracy is very good.

The radiation surfaces are automatically generated in EFlo based on user specified tolerances. Once the surfaces have been initialized, the user may edit the default surfaces, if needed, to obtain the desired level of detail. Note that since radiation is a nonlinear process, it is advantageous to use the smallest possible radiosity network (i.e., the largest possible radiation surfaces) that still maintains an acceptable level of accuracy.

Emissivities may be defined by material (from the Radiation form) or may be individually assigned to radiation surfaces. It should be noted that the default emissivity for every material type is 0. This is done so that if a user does not wish to include radiation everywhere in the enclosure, emissivities may be assigned only to those few surfaces (e.g., a few key components) that the user wishes to include in the analysis.

Once the user is satisfied with the radiation surfaces, viewfactors can be calculated by clicking on the Calculate Viewfactors command button. This results in the display of a window showing solution progress. At the conclusion of viewfactor calculations, the file "*View.Dat*" is created in the current directory. This file is necessary for EFlo execution and must be present along with EFlo Solver input.

This is all that is required to include radiation in the model. Once the model has been completed and the job submitted for analysis, everything else is automatically handled by EFlo. In most cases, including radiation is simply a matter of defining surface tolerances and initializing the BC surfaces and calculating viewfactors.

The inclusion of radiation in the model may be specified when the model is first created from the File-New menu pick. Selecting this File-New will result in the display of the Model Parameters form. The user may select the Switch-For-Radiation option box to include radiation. In addition, at any time during the modeling process the user may opt to include radiation by entering the Model Parameters menu and again selecting the Switch-For-Radiation option box. Once this switch has been activated, the radiation surface tolerance boxes will appear. The user specifies both a minimum and maximum surface tolerance. No surface will be created smaller than the minimum surface size nor larger than the maximum surface size specified. Additionally, no surface will be generated smaller than an element nor larger than the geometry surface size. Thus, to include radiation on all elements, the user may simply specify zero tolerance sizes for both the min and max surface sizes. Similarly, to generate the largest possible surfaces

the user may specify a maximum surface tolerance larger than any geometric dimension in the problem (e.g., 999 meters). Note that the minimum surface size may be used to suppress radiation from small surfaces (e.g., sides of components); the user simply indicates an appropriate geometric tolerance. No surface will be generated for any geometric surface with dimensions smaller than the tolerance.

To change radiation surface tolerance, the user may return to the Model Parameters form, specify a new tolerance and select the Initialize Surfaces menu pick again. This will erase any previous radiation surface definitions and a new surface network will be generated according to the new tolerances.

5.5.6 Point Source

The Point Source boundary condition is used to fix a temperature, heat input, electrical current or voltage for a single point (applied to the centroid of the element).

5.5.7 Velocity

This feature is used to specify velocity on a plane. Note that the "Fan" feature can also be used to define a flow through a plane. The user must specify a value for each velocity component. Additionally, the incoming temperature may be specified.

5.5.8 Plane Resistance

This feature allows the user to define a thermal or electrical resistance across a surface (resistance is assumed normal to the surface). The *Thermal Resistance* BC is very useful for modeling contact resistances or including a thermal resistance due to parts not modeled in detail (e.g., gasket material, etc.) but whose presence may not be thermally insignificant. The *Electrical Resistance* BC may be used to separate adjoining electrical conductors.

5.5.9 Voltage

The Voltage boundary condition is used to specify a constant voltage on a face of an electrical conductor. This boundary condition is only available when *Electrical Solver* is activated.

5.5.10 Current

The Current boundary condition is used to specify a constant current on a face of an electrical conductor. This boundary condition is also available when *Electrical Solver* is activated.

5.5.11 Heat Exchanger

The Heat Exchanger boundary condition employs a flow network for simplified modeling of compact heat exchanger. Flow Network Modeling (FNM) represents an alternative

approach for quick prediction of the flow field in a variety of applications and is the primary solution methodology for several electronics cooling packages in the market. This approach, not nearly as complex and time-intensive as CFD, involves representation of a flow system as a network of "components" and "flow-paths", which leads to the prediction of system-wide flow rates and temperatures.

5.6 Analysis Options

Upon completion of the model, a job may be submitted for analysis. Prior to choosing the analysis option, the user must decide whether to activate the *Electrical Solver* and/or *Network Radiation Solver*. There are three solution options available: *Full CFD*, *Frozen CF*" and *Non-CFD*. The *Full CFD* option is the default solution procedure that employs SIMPLER algorithm for the coupled solution of conservation of mass, momentum and energy equations. For the *Frozen CFD*, the program takes whatever airflow results have been calculated up to that point and then completes the solution by solving the energy equation. This allows the user to get more accurate results in a short time span for problems that are mainly conduction driven. If the *Non-CFD* option is picked, the program only solves the energy equation in solid regions – all fluid regions will be neglected. In this option, convection coefficients are used to include the effect of fluid flow at the solid boundaries.

Chapter Six

VI. Validation Using IPC Design Rules and Limitations to IPC-2221

In this chapter, the procedure developed earlier is applied to a simple three-dimensional model of a board and a trace, and the results are compared to experimental data reported in IPC 2221.

6.1 IPC-2221 Background

The ability of an etched or printed conductor to safely carry the electrical current necessary for a particular application (referred to as "current carrying capacity") is an important property. In the majority of cases, the printed circuits are capable of carrying more electrical current than they ever encounter. However, there are a significant number of applications (some were discussed in chapter one), for which the designer must know with a reasonable degree of certainty whether a particular conductor can fulfill its requirements. To address this issue, in 1955, the National Bureau of Standards (NBS) was commissioned to establish a set of guidelines for sizing electrical traces on circuit boards. In 1956, the NBS team conducted a variety of experiments to provide

guidelines for determining the trace width as a function of trace thickness, the electrical current and the maximum permissible temperature rise. At the conclusion of the initial phase of this study, NBS researchers noticed a wide scatter of data points. They concluded that their results had many variables that required further investigation. Due to lack of funding, however, the effort was terminated prematurely, and the results were published as tentative guidelines for trace sizing (as shown in Figure 6.1).

These graphs represent the upper limit of the data points [82]. The lower limit is in better agreement with the so-called "Design-News" correlations presented by Brooks [83]. Brooks suggests the following two fits for the two correlations, where I is in amps, ΔT is in °C, and A is in square mils for in both correlations:

$$I = 0.065 * \Delta T^{0.43} * A^{0.68} \qquad \text{IPC Data} \qquad (6.1)$$

$$I = 0.040 * \Delta T^{0.45} * A^{0.69} \qquad \text{DN Data} \qquad (6.2)$$

In reference [82] it is shown that these equations provide reasonable predictions for the Euro-format PCB (100mm x 160 mm x 1.6 mm) of bare epoxy with a single 1 oz (0.035 mm) copper trace. Equation (6.2) is used for PCB's with no additional copper plane, while Equation (6.1) is suggested for use in applications with a 1-oz copper back plane. In both cases, it is assumed that the board and the trace are oriented vertically in the ambient air at 20 °C. In the next section a numerical model representing the above problem is presented.

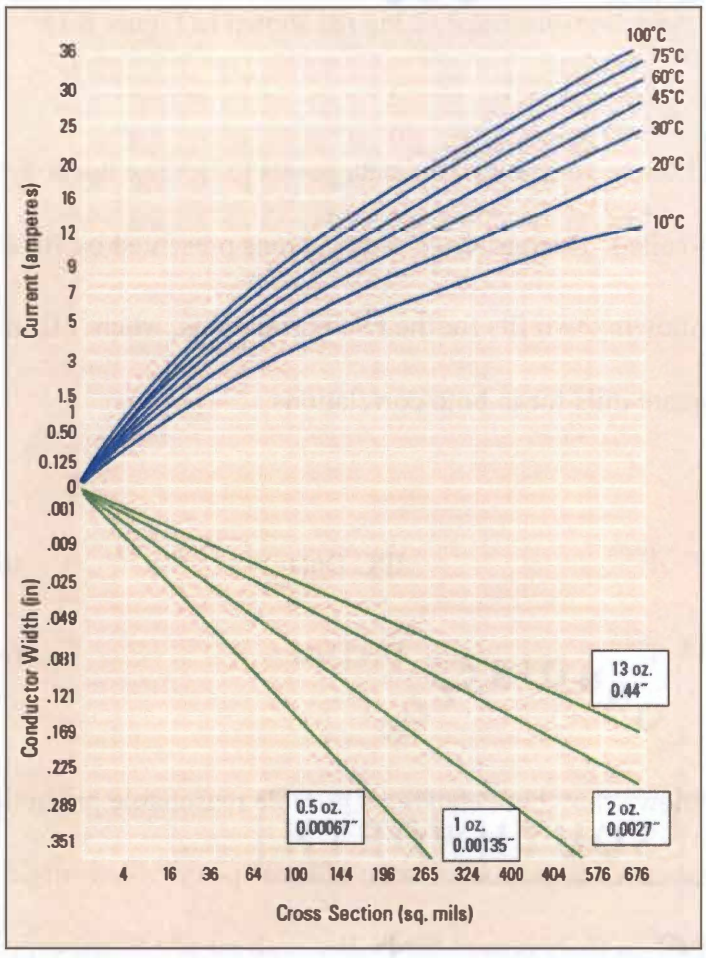


Figure 6.1: Conductor Sizing Guidelines Based on NBS Testing

6.2 Single Board with a Trace

Consider a printed circuit board, made of pure FR4, oriented vertically in quiescent ambient air at 20 C, as shown in Figure 6.2. The board is assumed to be 100 mm wide, 160 mm long and 1.6 mm thick and made of pure FR4. A single copper trace, 100 mm long, 8 mm wide and 0.035 mm thick (i.e., 1-oz copper), is etched on one side of the board. It is assumed that 10 amps of electrical current is flowing through the trace.

6.2.1 Cases Analyzed

Numerical simulations were performed for two cases. In Case 1 the model with geometry exactly as described above was simulated. In Case 2, a copper back plane (0.035 mm thick) was included in the model. The results of Case 1 are used for comparison with "Design News" data, whereas Case 2 results are used for comparison with "IPC" data.

6.2.2 Material Properties

The following material properties were used in the two models.

Board:	FR4	$k = 0.3 \frac{W}{m-K}$
Traces and Backplane:	Copper	$k = 395 \frac{W}{m-K}$

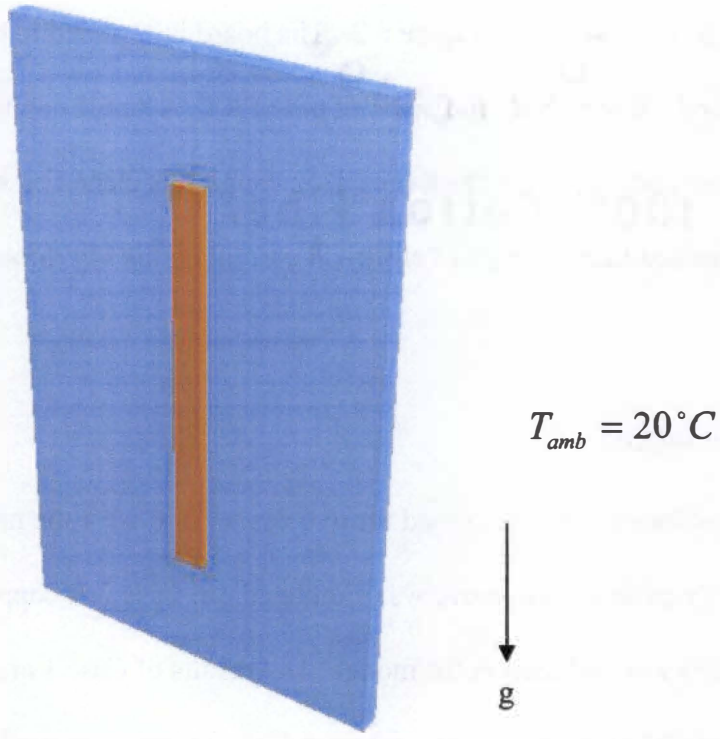


Figure 6.2: Vertical Board with a Single Trace

The electrical resistivity for copper is calculated from:

$$\rho_e = \rho_0\left[1+\alpha(T-T_0)\right]$$

T_0 ≡ Reference Temperature = 20 °C

ρ_0 ≡ Resistivity at T_0 = 0.0175e-06 $\Omega.m$

α ≡ Resistance Temperature Coefficients = 0.0039 $°C^{-1}$

6.2.3 Model Details and Boundary Conditions

The computational domain consisted of the board and an air region (extended by 24 mm on each side) surrounding the board. Approximately 48,000 non-uniform elements were used for discretization of this model. A much finer mesh was used near the solid surfaces as required by the steep gradients near the walls. Figure 6.3 illustrates the non-uniform mesh used for discretization of this problem

The only boundary conditions required for this model were two *Current BC's* to specify 10 amps of electrical current passing through the trace. It should be noted that no boundary conditions are necessary to specify air inflow and outflow regions. The program recognizes the "open" boundaries at the edges of the computational domain and applies inflow and outflow boundaries as needed based on the local pressure gradient.

Figures 6.4 and 6.5 illustrate the temperature and velocity fields for Case 1 and Case 2 respectively.

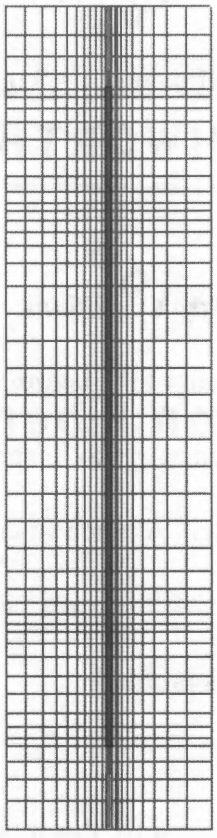
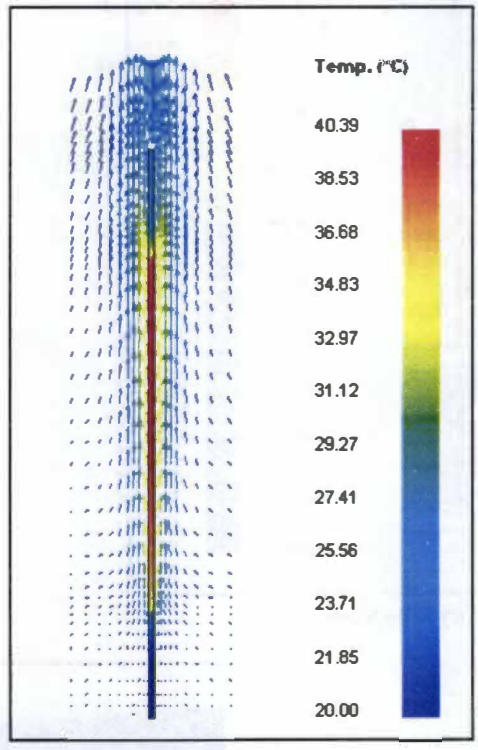
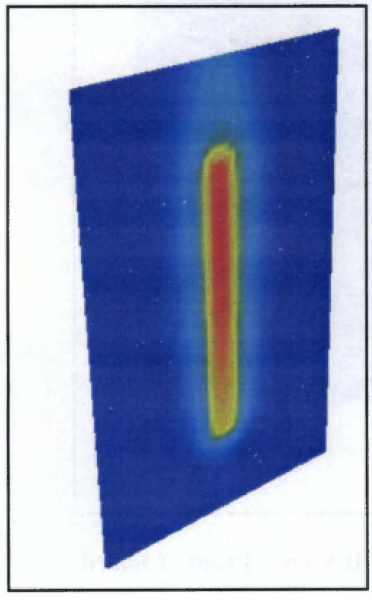


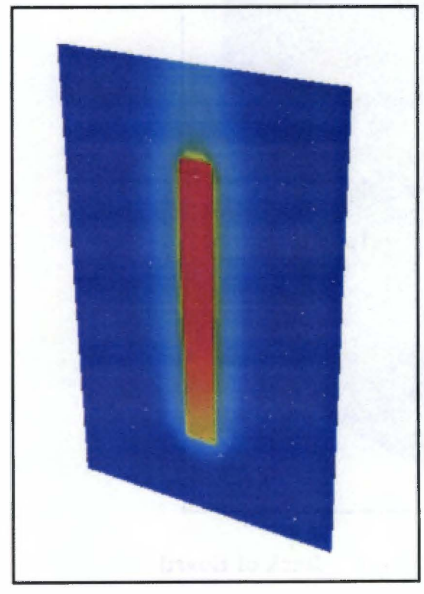
Figure 6.3: Mesh Used for Vertical Board with a Single Trace



a) Side View

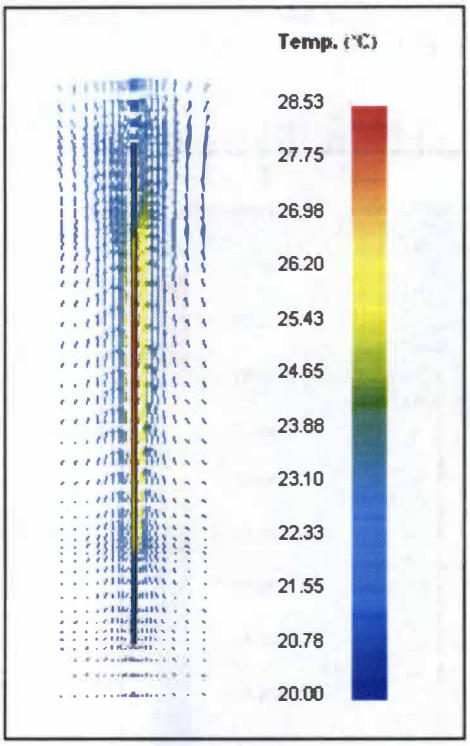


b) 3D View – Back of Board

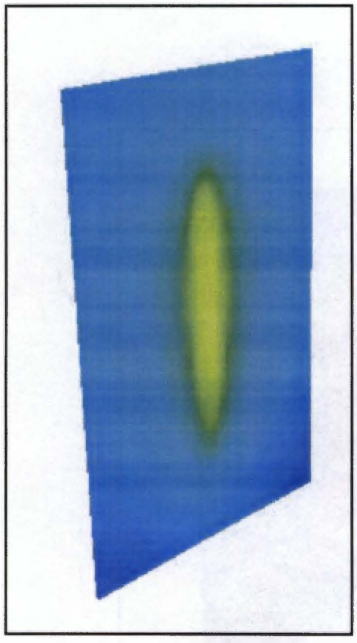


c) 3D View – Front of Board

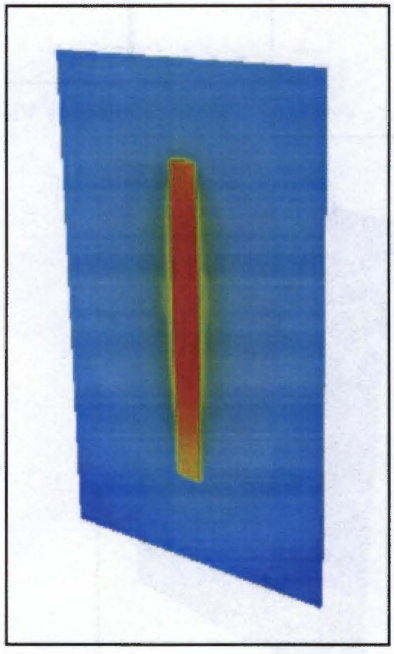
Figure 6.4: Temperature and Velocity Field – Vertical Board w/ No Back Plane



a) Side View



b) 3D View – Back of Board



c) 3D View – Front of Board

Figure 6.5: Temperature and Velocity Field – Vertical Board - with Back Plane

6.2.4 Comparison with Test Data

Equation (6.2) and (6.1) can be used to obtain the predicted average temperature rise using DN and IPC test data (corresponding to Case 1 and Case 2 numerical models).

DN Comparison:

$I = 0.040 * \Delta T^{0.45} * A^{0.69}$ with I=10 amps, and A=434 mil^2

$$\Rightarrow \quad \Delta T_{DN} = 19.257^{\circ}C$$

$$\%\Delta = \frac{|\Delta T_{DN} - \Delta T_{Sim}|}{\Delta T_{DN}} \times 100 = \frac{|19.257 - 19.244|}{19.257} \times 100 = 0.0675\%$$

IPC Comparison:

$I = 0.065 * \Delta T^{0.43} * A^{0.68}$ with I=10 amps, and A=434 mil^2

$$\Rightarrow \Delta T_{IPC} = 8.23^{\circ}C$$

$$\%\Delta = \frac{|\Delta T_{IPC} - \Delta T_{Sim}|}{\Delta T_{IPC}} \times 100 = \frac{|8.23 - 8.04|}{8.23} \times 100 = 2.308\%$$

Figure 6.6 shows these results in the form of a bar chart. As it is evident from these results, there is excellent agreement between numerical and experimental results.

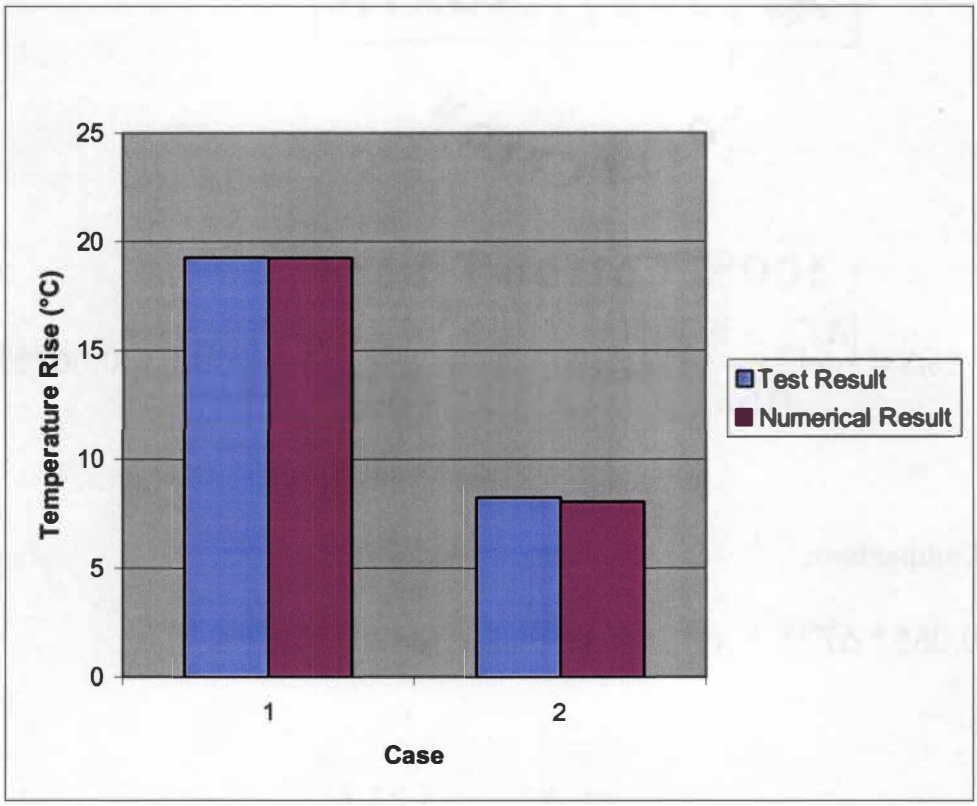


Figure 6.6: Comparison between Numerical and Experimental Results

6.3 Problems with IPC Design Rules

As previously mentioned, traditionally, trace sizing has been performed using the IPC charts which are based on tentative results relating electrical current, cross-sectional area and temperature rise. Soon after these results were published, they were adapted by the military and were included in MIL-STD-275. Over the years, the electronic packaging industry has turned to these charts for guidance, not paying close attention to what the information in the chart actually means. This lack of understanding of what the charts represent and how to work with them has generated significant confusion, leading to many flawed thermal designs.

Some of the factors to consider are presented in the following paragraphs:

- The tests were performed using only external traces, since back in 1955 there were no multi-layer boards with internal traces. There are, however, charts in use today that are used for internal traces. These charts were generated using the original charts for external traces but assuming half of the current, a very questionable assumption, indeed.

- The tests were performed using single and double sided phenolic and epoxy boards of varying thickness – some boards had a full copper plane on the backside, and some did not. Originally, the idea was to gain a better understanding of factors affecting the temperature rise in traces. But, since the research was stopped prematurely due to lack of funding, the NBS researchers

compiled all these results to produce the IPC charts. This implies that the charts represent an average with respect to variable in the test samples.

- The user of the chart must keep in mind that the predictions are for a specific board configuration with a single copper trace, suspended in air. A great majority of today's designs fall outside these conditions.

In the next section, we will examine the effect of enclosing the board on the trace temperature, and in the following section we will look at the effect of additional boards.

6.4 Single Board inside Enclosure

In the earlier examples, we considered cases involving a board with a single trace with no flow restrictions. In the next two sections, we will investigate the effect of placing the board inside an enclosure, and also, possible effects of other boards in close proximity on the trace temperature rise. The goal here is to check the accuracy of IPC predictions for realistic cases, and to determine whether they can be extrapolated beyond test conditions.

The board studied earlier is modeled inside an enclosure in a natural convection environment at 20 °C. The enclosure is 0.168 m long, 0.108 m wide and 0.07 m high and made out of plastic with thermal conductivity of 0.5 (W/m-K). The board is assumed to exist inside the enclosure (1.22 cm from the bottom wall) with no contacts between the enclosure walls and the board and a 2 mm gap between the enclosure walls and the edges of the board. Figure 6.7 shows the enclosure with the board.

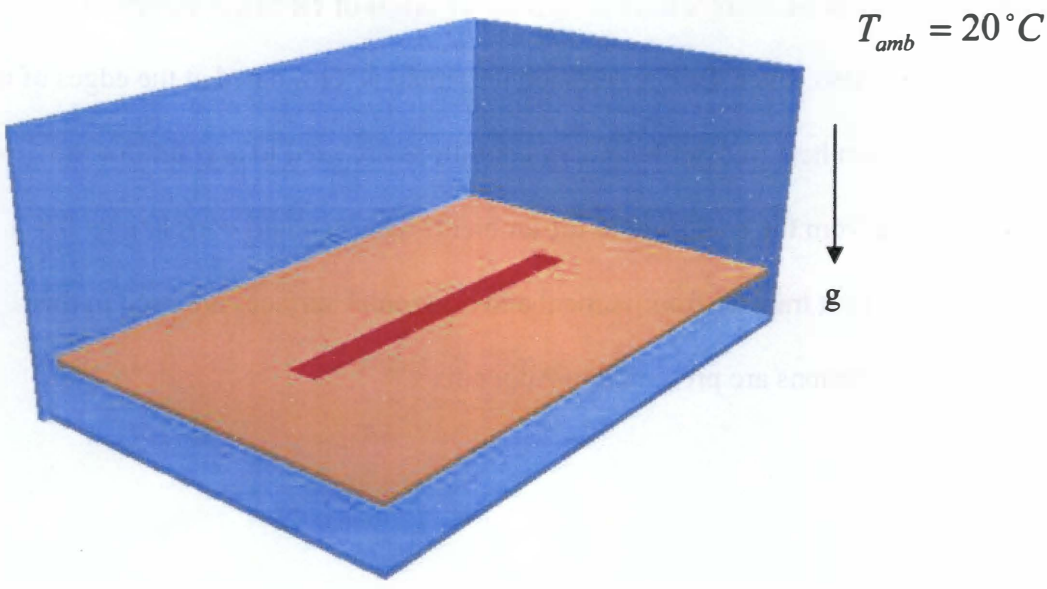


Figure 6.7: Enclosure and Board Geometry

6.4.1 Model Details

For this model, the computational domain was extended to the edges of the enclosure. Approximately 43,000 non-uniform elements were used for discretization of this model (Figure 6.8).

6.4.1 Boundary Conditions

As before, the *Current BC's* were used to specify 10 amps of electrical current passing through the trace. Also, since the computational domain is terminated at the edges of the enclosure, convection heat transfer boundary conditions are used to account for the transfer of the heat from the enclosure to the ambient. The standard correlations for natural convective heat transfer from vertical and horizontal surfaces are used in this model. These correlations are presented in Appendix C.

6.4.2 Analysis

The numerical simulations for the steady-state solution were performed using EFlo software, using *Full-CFD* options with electrical and radiation solvers enabled.

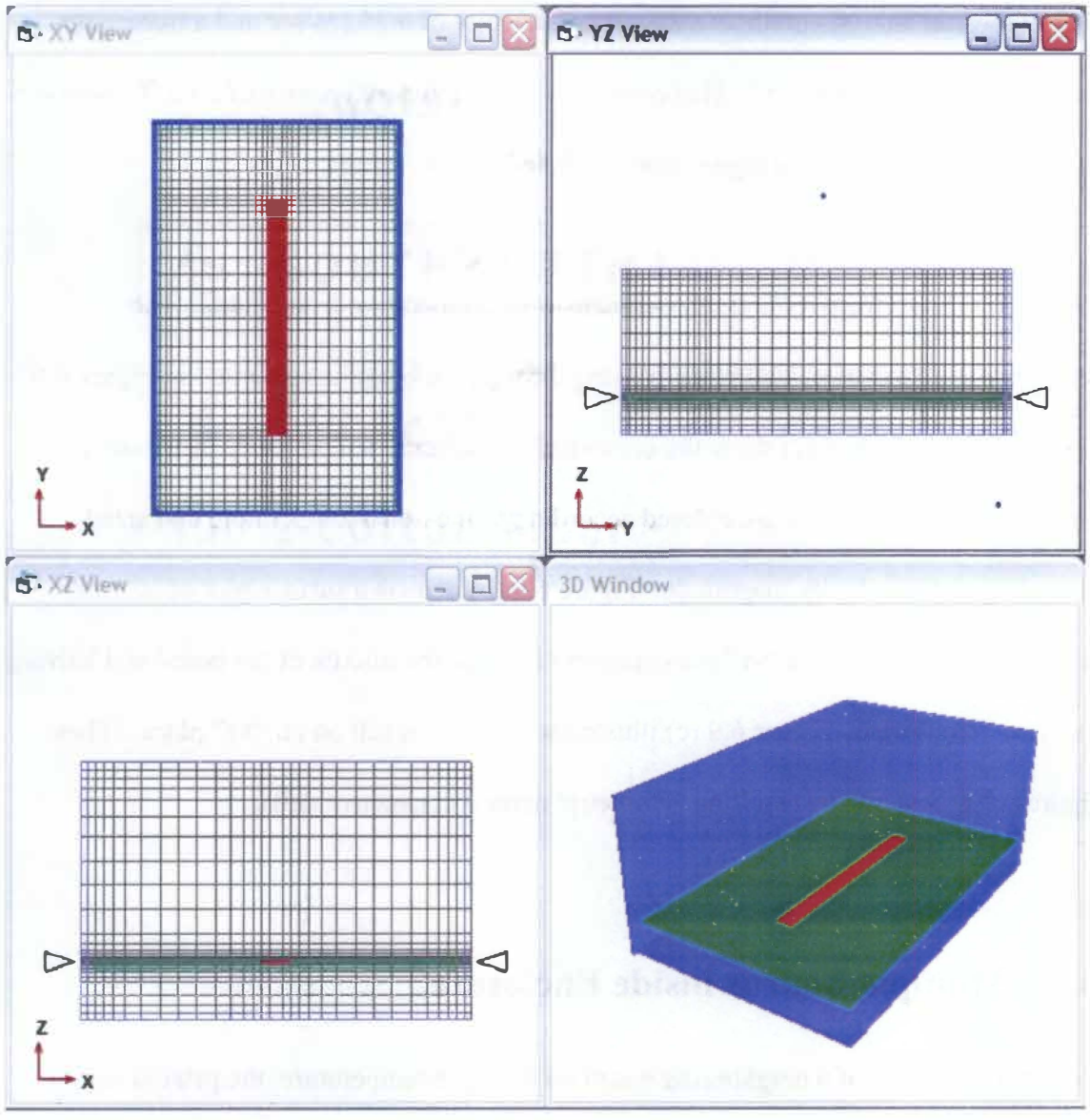


Figure 6.8: Finite Volume Mesh

6.4.3 Results

The numerical analysis predicts a maximum velocity of 9.75 cm/sec and a maximum trace temperature of 49.9 °C. This corresponds to a temperature rise of 29.9 °C, which is 10 degrees (roughly 50 %) higher than predicted by IPC results.

Figure 6.9 shows the two- and three-dimensional temperature fringe plots. The temperature distribution on a plane passing through the board is presented in Figure 6.9 (a). Figure 6.9 (b) and (c) show the combined temperature and velocity distribution. Note that velocity vectors are colored according to the nodal temperature and sized according to the velocity magnitude. Figure 6.9 (b) depicts a surface plot of temperature/velocity on a "yz" plane passing through the middle of the board and halving the trace lengthwise. Figure 6.9 (c) illustrates a similar result on an "xz" plane. These figures clearly show the resulting symmetric natural convective cells.

6.5 Multiple Boards inside Enclosure

To study the effect of a neighboring board on the trace temperature, the printed circuit board in the previous model was copied with 8.4 mm spacing between the two boards, as shown in Figure 6.10. All other parameters remain unchanged.

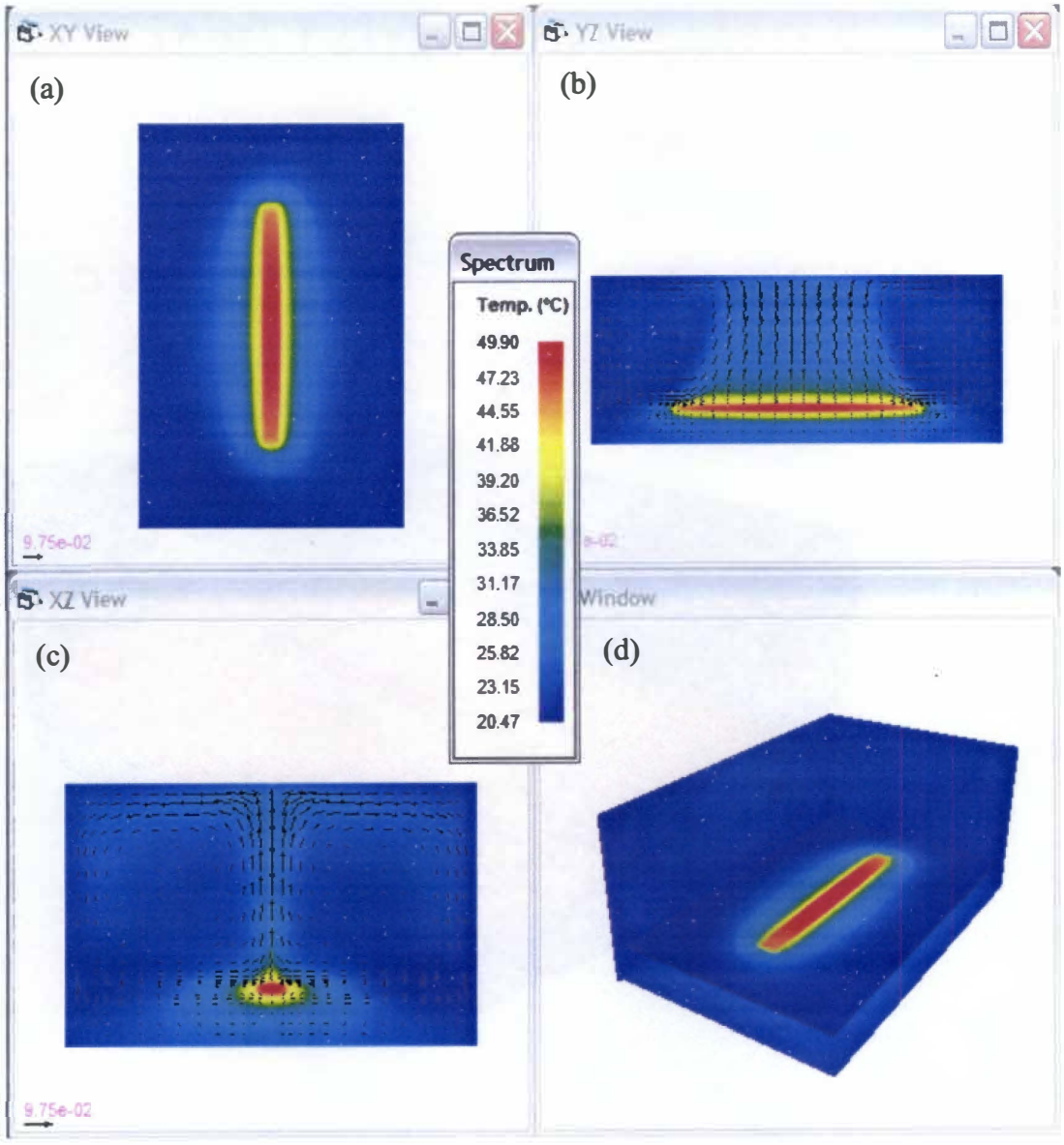


Figure 6.9 : Simulation Results

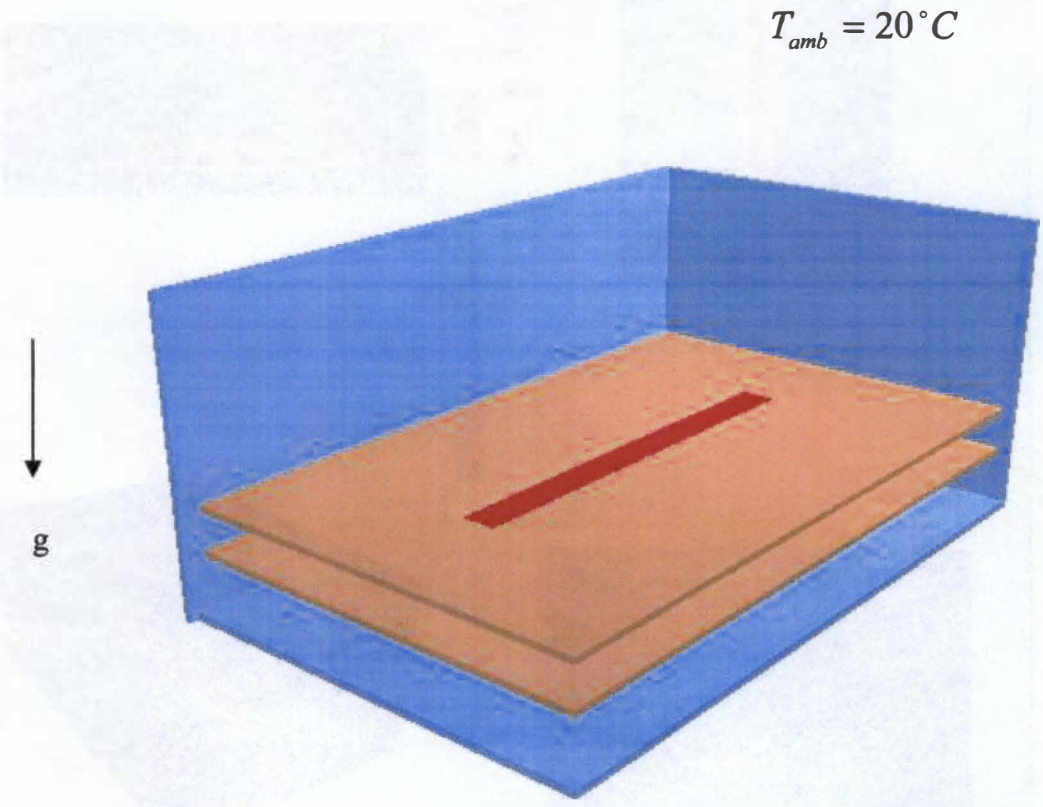


Figure 6.10: Enclosure with Two Boards

6.5.1 Analysis

A numerical model of the enclosure and the two boards were created using 57800 elements. The non-uniform mesh is illustrated in Figure 6.11. Boundary conditions used in this model are identical to those used in the model presented in section 6.5. However, with 10 amps of electrical current flowing through the traces on each board, the total Joulian heat dissipation inside the enclosure is roughly doubled.

The steady-state solution to this problem is obtained using coupled CFD, Thermal and Electrical procedure with surface-to-surface thermal radiation.

6.5.2 Results

The results of the numerical analysis are presented in Figure 6.12. These results indicate that, with the additional board in the enclosure, the maximum trace temperature has increased to 68.11 °C. This corresponds to an increase of 18.2 °C compared to one board in the enclosure and 27.7 °C compared to IPC results. The maximum velocity was found to be 12.6 cm/sec.

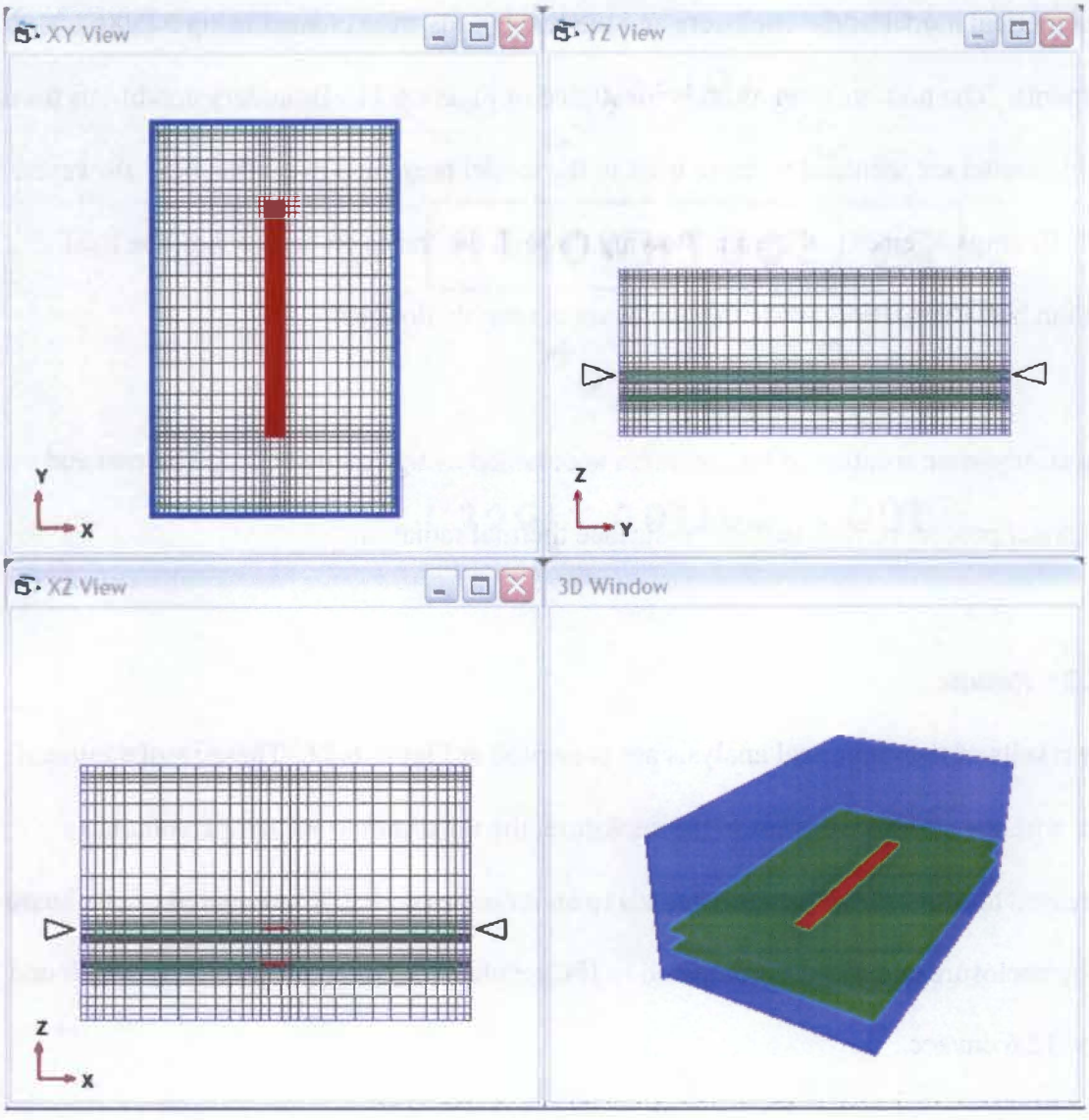


Figure 6.11: Finite Volume Mesh – Two Boards in Enclosure

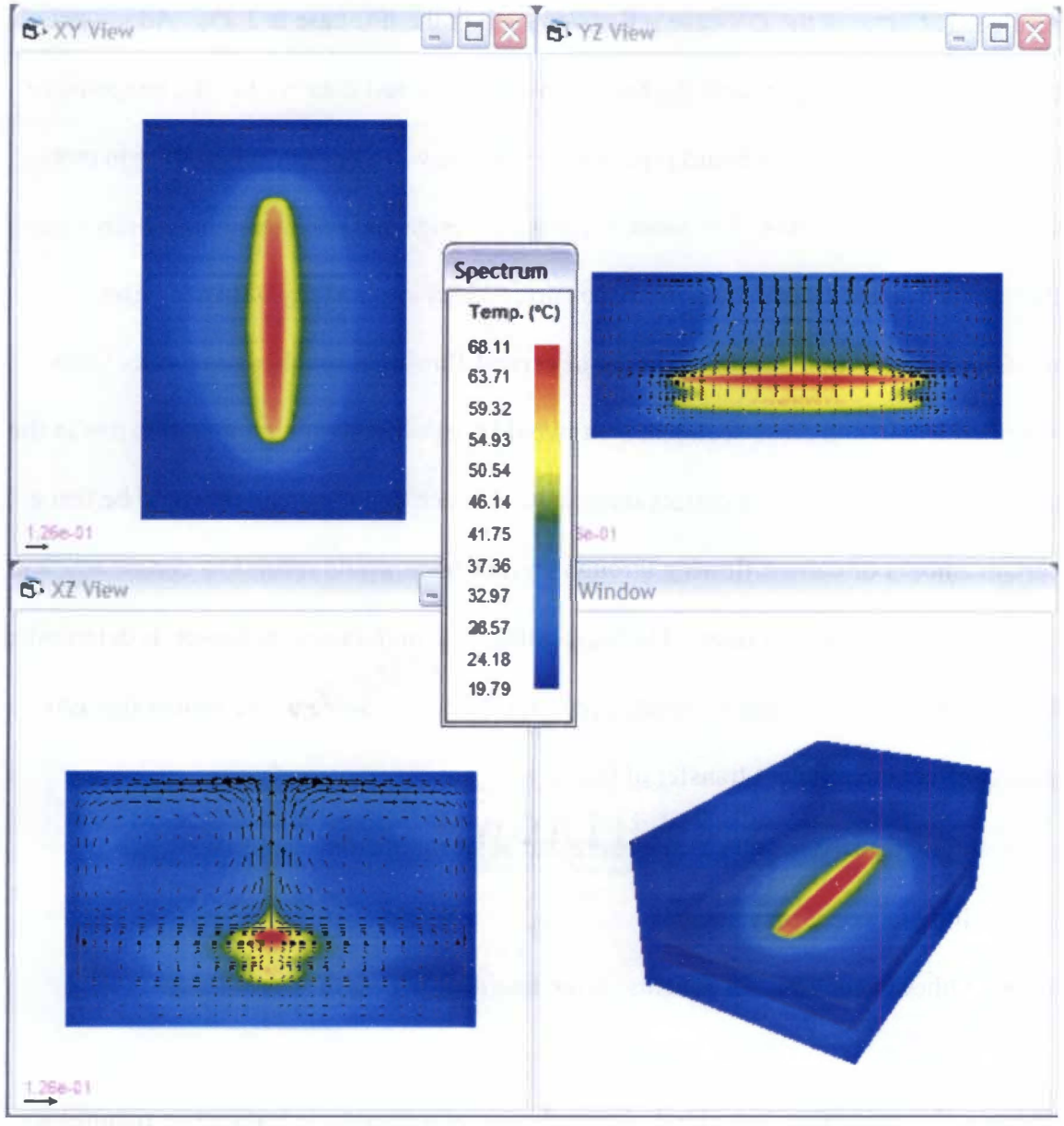


Figure 6.12: Simulation Results – Two Boards in Enclosure

6.6 Closing Remarks

Numerical results are shown to be in excellent agreement with both IPC and DN test results. The error in the DN case is 0.0675% and in the IPC case is 2.3%. Additional analyses, however, underscore the fact that while these test data predict the temperature rise for a single trace on a board remarkably well, they can be very misleading in more complex real world cases. For years, electronics design and packaging have been using the results of these tests to determine the current carrying capacity of traces. The thinking has been that a certain amount of current flowing through a given trace (with specified length and cross-sectional area) would result in a certain temperature rise in the trace. This, in fact, is not a correct statement. A much better statement would be that a certain amount of current flowing through a given trace would result in a certain amount of heat dissipation in that trace. The temperature rise in the trace, however, is determined by how efficiently this heat is transferred to the ambient. Some of the factors that can greatly affect the efficient transfer of heat are:

- Flow restrictions due to enclosure and adjacent boards
- Internal copper layers
- Other traces and components on the board.

This clearly shows that, in general, the prediction of a trace temperature rise requires a thorough heat transfer analysis. In other words, IPC based calculators represent oversimplification of complex problems. In fact, the designers are likely to get a far better estimate of the trace temperature from an educated guess.

Chapter Seven

VII. Transient Coupled Analysis - Six-Layer Board

In the last chapter we examined the simplest type of coupled electrical/thermal analysis consisting of a board and a single active trace. It was shown that IPC design charts can be used to predict the trace temperature rise for this simple configuration in natural convection ambient conditions. Real board designs are far more complex than this. There are many internal copper layers, each containing a complex array of traces and conducting regions. Vias are often used to provide electrical connection between various layers. Vias are vertical connections between layers made by drilling a small hole and filling it with conductive material. They normally consist of three sections:

- Barrel: conductive cylinder filling the drilled hole
- Pad: connects the barrel to components, traces and plane layers
- Antipad: non-conductive clearance between via and a "no-connect" metal layer

In this chapter, a simplified version of a typical aircraft electronics board is studied. The impact of coupling the thermal and electrical solutions for a given circuit board is demonstrated to be important for the accurate prediction of temperature profiles. The significance of this has been demonstrated in numerous real life cases and the coupled

solution has been shown to be a much better representation of the actual observed numbers in every instance. This example presents a numerical investigation of steady-state and transient heat transfer in a multilayered printed wiring board (PWB) where heat is dissipated as a result of the flow of electrical current in various areas in the board. The numerical model consists of a six-layer PWB with ten capacitors on top of the board. Electrical current enters the board through "load" terminal blocks and leaves the board through "return" terminal blocks. The load layers and the return layers are electrically and thermally connected using "vias". The transient solution is performed for two minutes in order to examine a "worst case" condition for the given configuration.

As we have seen in previous chapters, in these types of applications, the heat dissipation distribution is not known prior to the solution and must be evaluated by simultaneously solving the electrical field. This is accomplished through a "coupled electrical/thermal solution" scheme, where the voltage field is solved throughout the region knowing electrical loads and boundary conditions (in addition to thermal and flow fields) during each iteration. The most recent temperature field is used to update the electrical resistivity of the conductors in the model. The power dissipation is then calculated for all elements. For an element in a Cartesian coordinate system, the power dissipation as a result of Joulian heating is given by:

$$P_{Element} = \frac{\left(\Delta\phi_x\right)^2}{R_x} + \frac{\left(\Delta\phi_y\right)^2}{R_y} + \frac{\left(\Delta\phi_z\right)^2}{R_z},$$

where ϕ is Voltage and Rx, R_y and R_z are resistance in the x, y and z directions.

This example shows how numerical simulation can be used to predict transient thermal performance of a circuit board subjected to a "worst case" heating scenario. The main difficulty in this analysis comes from the fact that the majority of the heat is dissipated as a result of the flow of electrical current in various conductors. In order to predict temperatures accurately, the important mechanisms for heat generation and heat transfer must be adequately considered. The issue that complicates matters is that the amount of heat generated by the electric current flowing through the board is itself dependent on temperature, thus requiring an approach that considers the coupling between the electrical and thermal aspects of the model. The current density and resulting power dissipation are calculated with electrical numerical analysis. The coupling with the thermal problem is achieved by specifying the resistivity of the conductor as a function of the calculated temperatures.

The computational procedure shown previously is used to address the main difficulties encountered in practical electronics cooling applications.

7.1 Problem Statement

Figure 7.1 shows a sketch of the system. The region of interest consists of a sealed aluminum enclosure (6.4 in x 3.9 in x 1.4 in) that houses a multilayer printed wiring board (PWB), horizontally oriented in an ambient temperature of 70 °C with no forced flow. The flow of electrical current through various layers in the board is accompanied

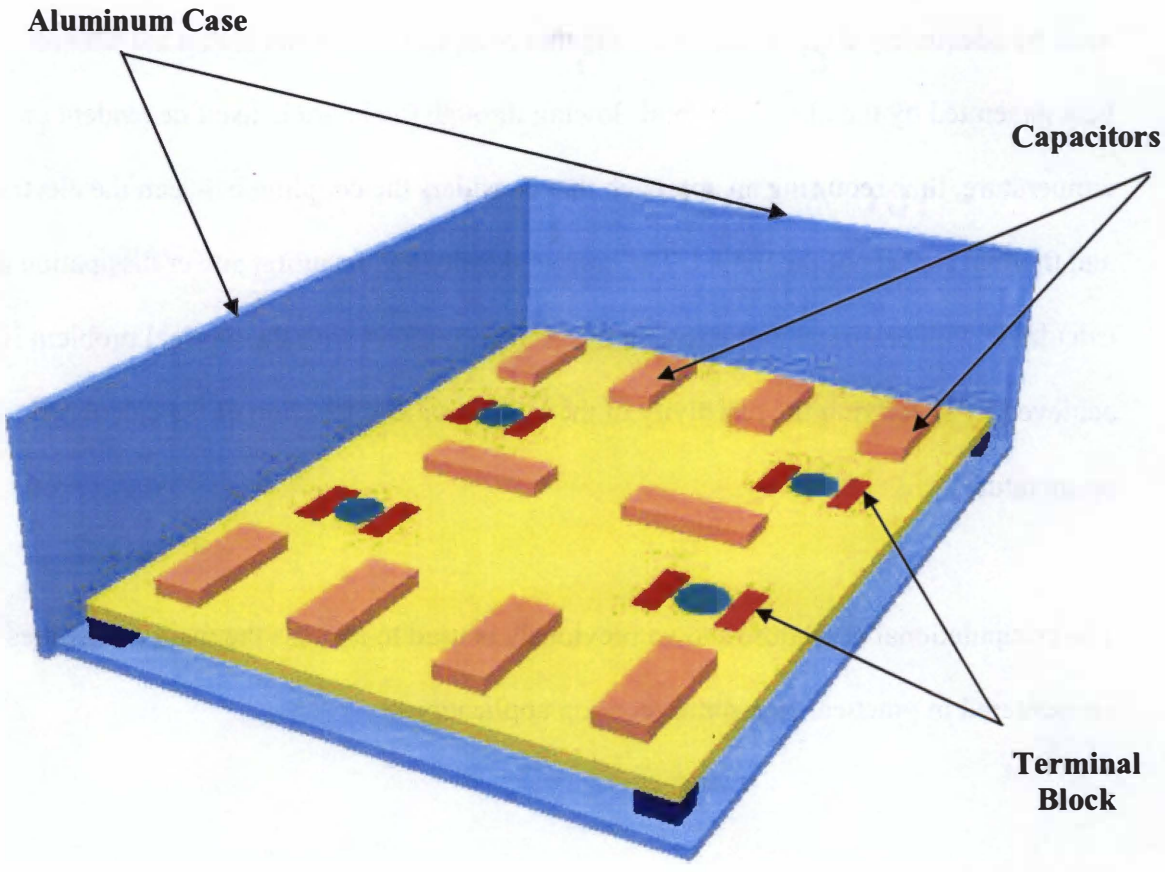


Figure 7.1: Board and Enclosure

with generation of heat in the board. Consequently, the board temperature rises, and unless the heat is transferred to the surroundings efficiently, this temperature will reach critical levels leading to failure of the electronic device. In this study, the resulting transient conduction and natural convection flows are numerically investigated, and the main focus is placed on the effect of the inherent coupling that exists between the electrical and thermal fields.

7.2 Board Geometrical Details

The board is assumed to be 5 inches long, 3.5 inches wide and 0.09 inches thick and contains 6 copper layers, 4 terminal blocks and 10 capacitors. The layers are 0.005 inches thick, and they are geometrically identical. There are 3 load layers providing the electrical current to the capacitors and three return layers to pass the current back to *return* terminal blocks. All load layers and return layers are electrically connected using vias.

Electrical current enters the board through the "load terminal blocks". From there it flows through vias to all *load* layers and to the capacitors. The return current flows back to the *return* terminal blocks, passing through *return* layers and vias. The vias were assumed to have a conducting area of 0.00125 in^2 and a pitch of 0.14 in. Figure 7.2 shows a sketch of the board, traces, vias and terminal blocks.

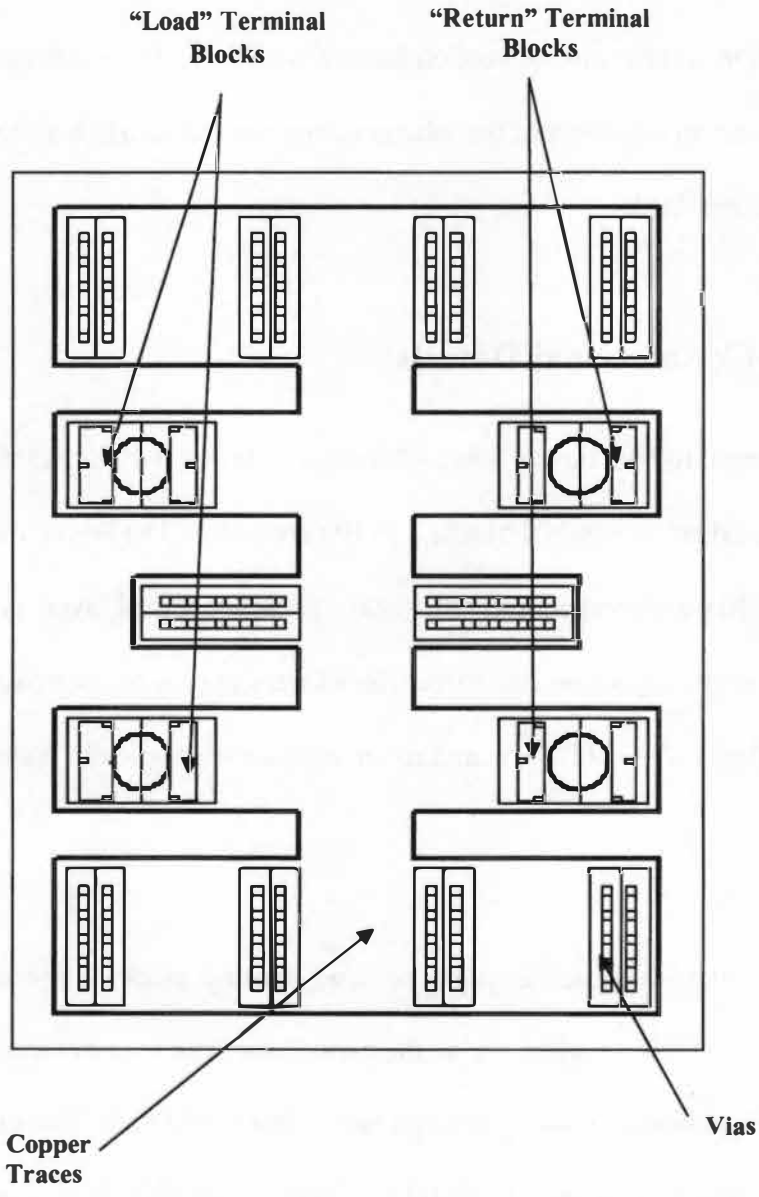


Figure 7.2: Board Details

7.3 Modeling Details

For this model, the computational domain was extended to the edges of the enclosure. Approximately 145,000 non-uniform elements were used for discretization of this model (Figure 7.3).

7.4 Boundary Conditions

As before, the *Current BC's* were used to specify 100 amps of electrical current passing through the load and return traces. Also, since the computational domain is terminated at the edges of the enclosure, convection heat transfer boundary conditions are used to account for the transfer of the heat from the enclosure to the ambient. The standard correlations for natural convective heat transfer from vertical and horizontal surfaces are used in this model. These correlations are presented in Appendix C.

7.5 Material Properties

Table 7.1 provides a listing for all materials used in the model along with their thermo-physical properties. The electrical resistivity for copper is calculated from:

$$\rho_e = \rho_0\left[1+\alpha(T-T_0)\right]$$

$T_0 \equiv$ Reference Temperature $= 20$ °C

$\rho_0 \equiv$ Resistivity at $T_0 = 0.0175\text{e-}06\ \Omega.m$

$\alpha \equiv$ Resistance Temperature Coefficients $= 0.0039\ °C^{-1}$

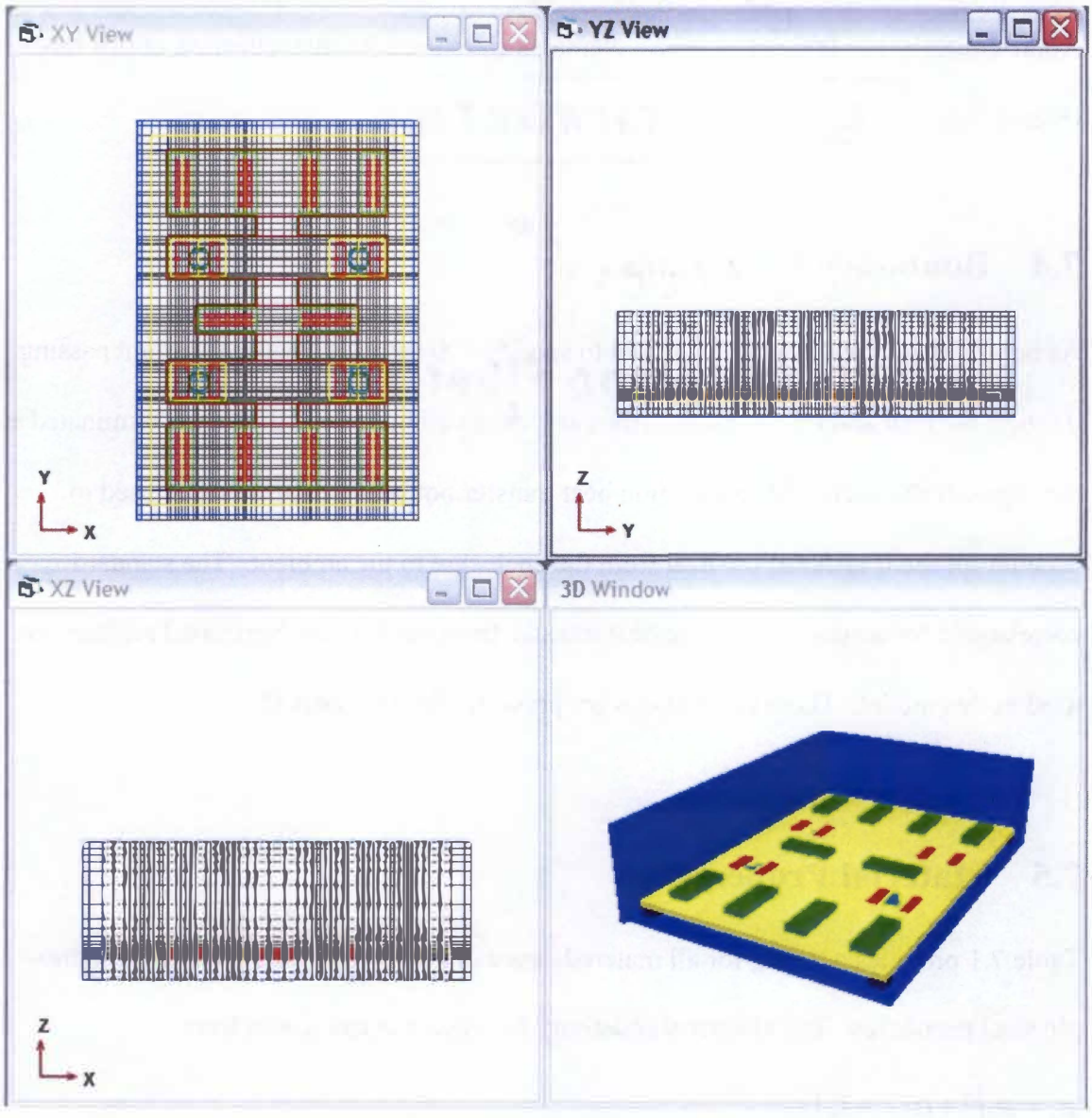


Figure 7.3: Control Volume Mesh

Table 7.1: Material Properties

	Thermal Conductivity (W/m.K)	Specific Heat J/(kg.K)	Density kg/m^3
Epoxy Fiberglass	0.29	1256	1135
Copper	401	385	8933
Aluminum	177	875	2770
Plastic	0.3	1150	1217

7.6 Review of Theory and Governing Equations

In order to predict temperatures within a PWB accurately, the important mechanisms for heat generation and heat transfer must be adequately considered. The issue that complicates matters is that the amount of heat generated by the electric currents flowing through vias and trances is itself dependent on temperature, thus requiring an approach that considers the coupling between the electrical and thermal aspects of the model.

For a system consisting of a printed wiring board inside a sealed enclosure, the governing conservation equations for mass, momentum, energy and voltage are:

$$\frac{\partial u}{\partial x}+\frac{\partial v}{\partial y}+\frac{\partial w}{\partial z}=0 \tag{1}$$

$$\rho\left(\frac{\partial u}{\partial t}+u\frac{\partial u}{\partial x}+v\frac{\partial u}{\partial y}+w\frac{\partial u}{\partial z}\right)=-\frac{\partial p}{\partial x}+\mu\left(\frac{\partial^2 u}{\partial x^2}+\frac{\partial^2 u}{\partial y^2}+\frac{\partial^2 u}{\partial z^2}\right)+F_x \tag{2}$$

$$\rho\left(\frac{\partial v}{\partial t}+u\frac{\partial v}{\partial x}+v\frac{\partial v}{\partial y}+w\frac{\partial v}{\partial z}\right)=-\frac{\partial p}{\partial y}+\mu\left(\frac{\partial^2 v}{\partial x^2}+\frac{\partial^2 v}{\partial y^2}+\frac{\partial^2 v}{\partial z^2}\right)+F_y \tag{3}$$

$$\rho\left(\frac{\partial u}{\partial t}+u\frac{\partial w}{\partial x}+v\frac{\partial w}{\partial y}+w\frac{\partial w}{\partial z}\right)=-\frac{\partial p}{\partial z}+\mu\left(\frac{\partial^2 w}{\partial x^2}+\frac{\partial^2 w}{\partial y^2}+\frac{\partial^2 w}{\partial z^2}\right)+F_z \tag{4}$$

$$\rho C_p\left(\frac{\partial T}{\partial t}+u\frac{\partial T}{\partial x}+v\frac{\partial T}{\partial y}+w\frac{\partial T}{\partial z}\right)=\frac{\partial}{\partial x}\left(k\frac{\partial T}{\partial x}\right)+\frac{\partial}{\partial y}\left(k\frac{\partial T}{\partial y}\right)+\frac{\partial}{\partial z}\left(k\frac{\partial T}{\partial z}\right)+q''' \tag{5}$$

$$\frac{\partial}{\partial x}\left(\mathrm{K}\frac{\partial \phi}{\partial x}\right)+\frac{\partial}{\partial y}\left(\mathrm{K}\frac{\partial \phi}{\partial y}\right)+\frac{\partial}{\partial z}\left(\mathrm{K}\frac{\partial \phi}{\partial z}\right)=0 \tag{6}$$

Recall that the volumetric heat generation term, q‴, represents total heat dissipation in element. This includes the Joulian heat dissipation (as a result of current in conductors), which is not known prior to the solution and must be evaluated by simultaneously solving the equation for the electrical field. This is accomplished through a "coupled electrical/thermal solution" scheme, where the voltage field is solved throughout the region knowing electrical loads and boundary conditions (in addition to thermal and flow fields) during each iteration. The most recent temperature field is used to update the electrical resistivity of the conductors in the model. The power dissipation is then calculated for all elements.

7.7 Results

The goal of this study was to demonstrate the differences in the predicted temperature field for the board after two minutes of high current flow with and without coupling of electrical effects. However, simulations were performed for both steady-state and transient conditions.

7.7.1 Steady-State Results

Figure 7.4 provide the steady-state velocity and temperature fringe plots. The maximum board temperature was 181 °C and the maximum velocity was 14.3 cm/sec.

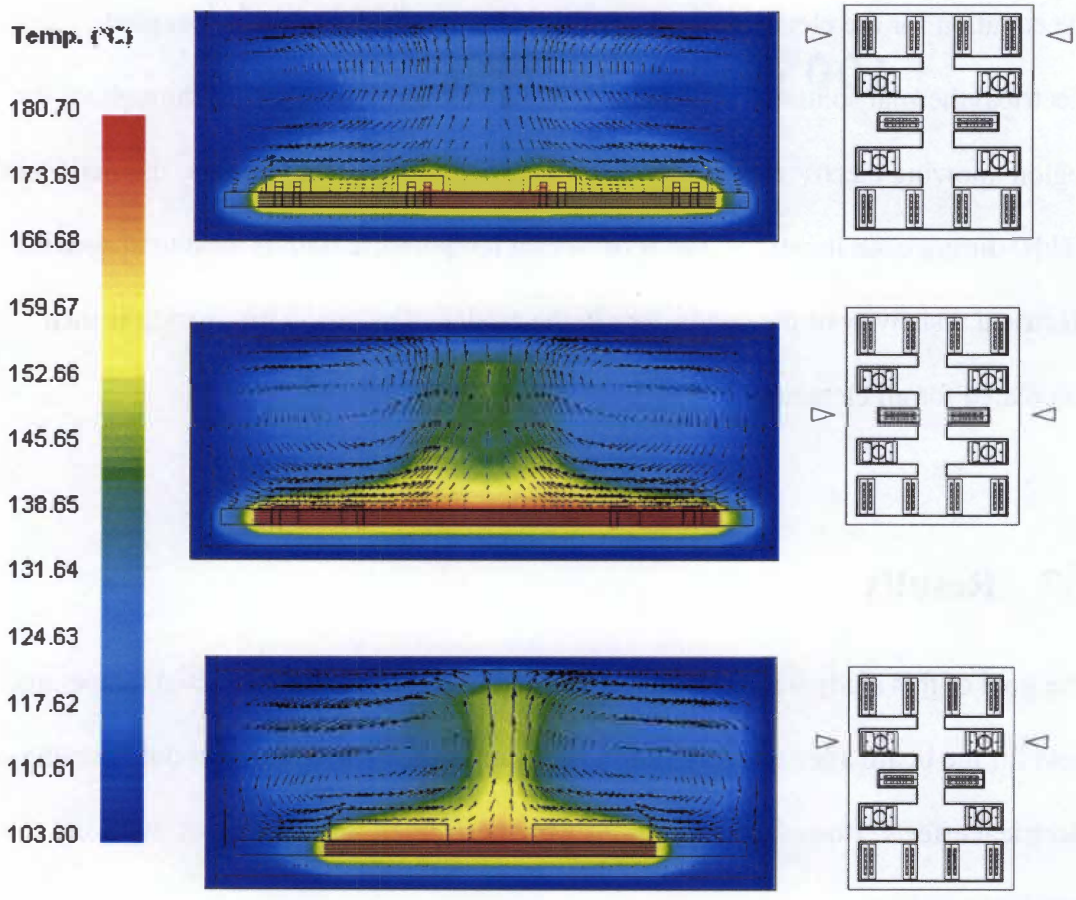


Figure 7.4: Steady-State Temperature and Velocity

7.7.2 Transient Results

The results in Figure 7.5 and Figure 7.6 demonstrate the difference between an analysis done with the thermal and electrical solutions coupled with the electrical solution done first and the thermal analysis done separately, as would be done with most software packages. The more accurate coupled analysis predicts a temperature rise 8 degrees higher than would be obtained with a standard software package after only 2 minutes. Since the maximum allowable temperature in this case is 115 degrees, the coupled technique correctly predicts failure whereas the standard non-coupled technique predicts that there should be no problem. Voltage distribution is shown in Figure 7.7.

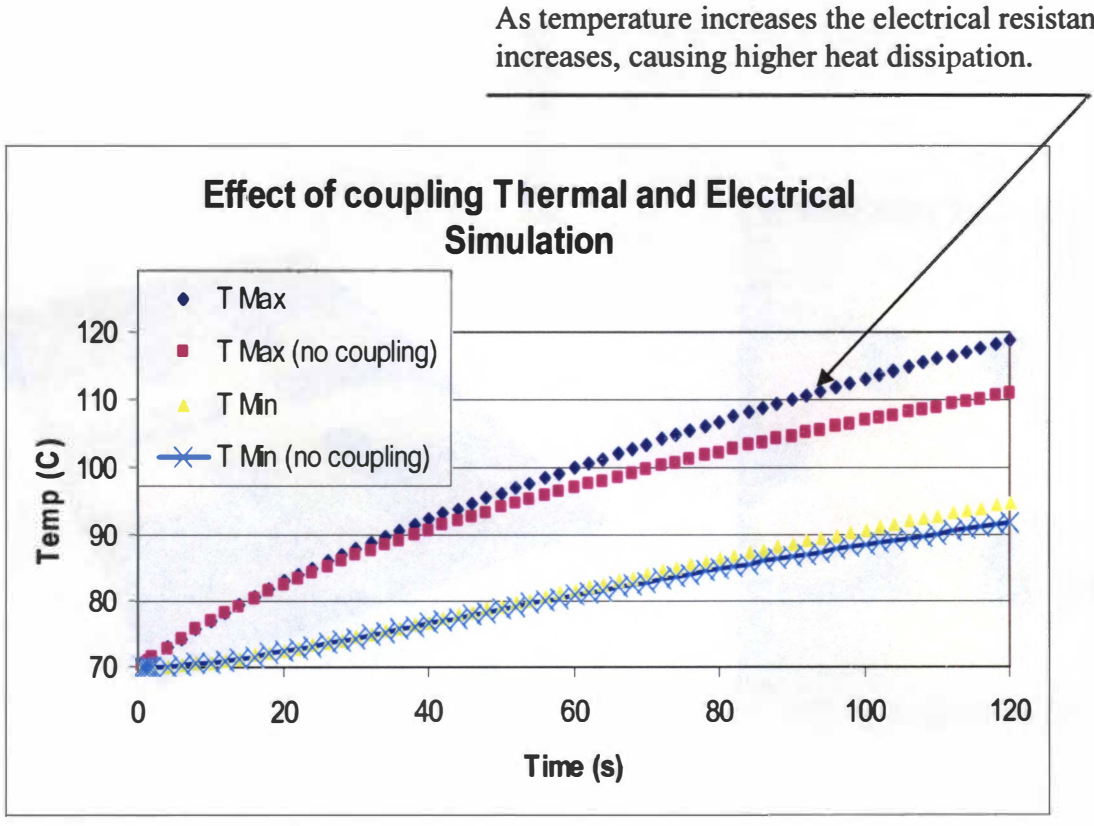


Figure 7.5: Transient Temperature Rise

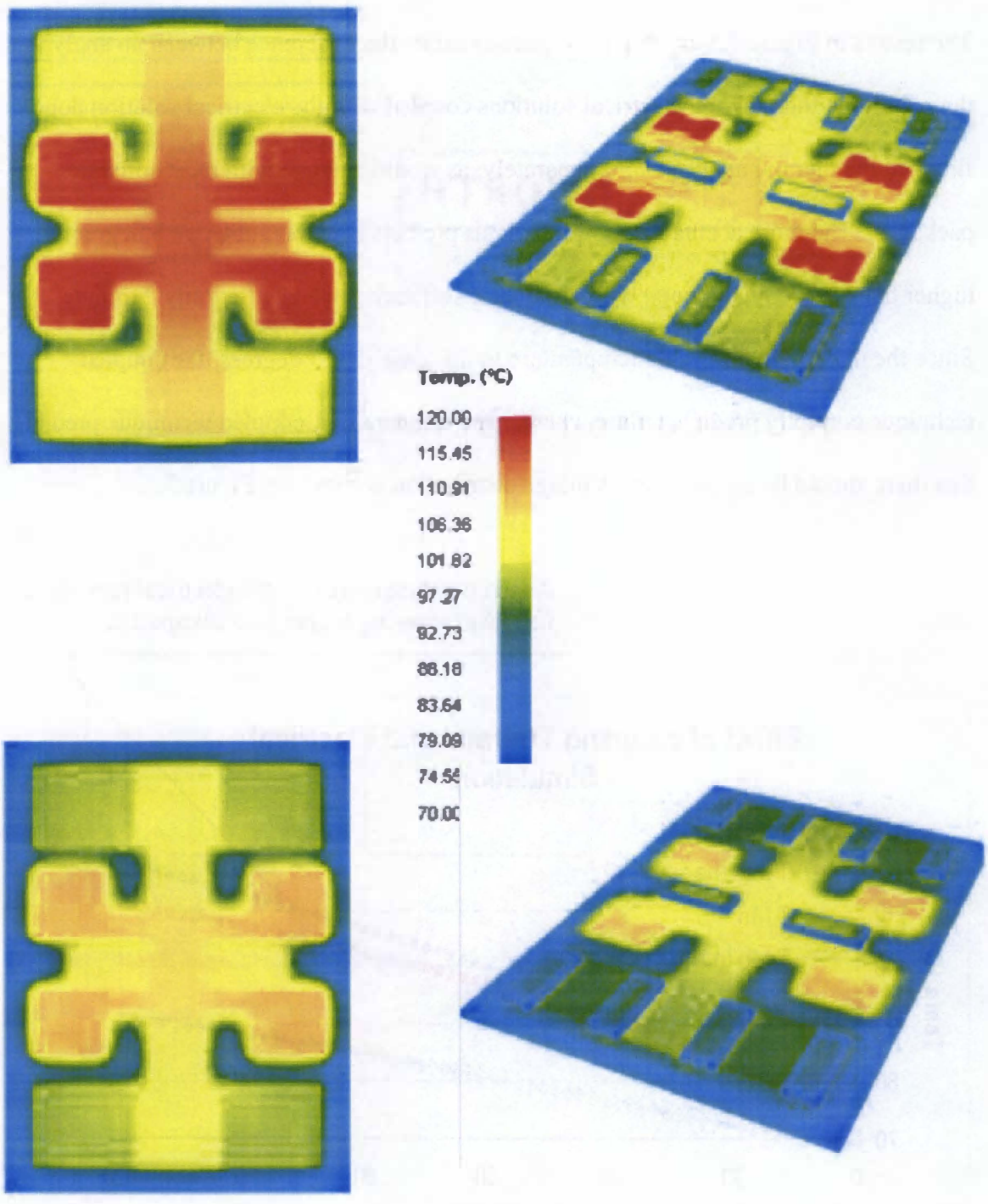


Figure 7.6: Temperature Distribution after 2 Minutes

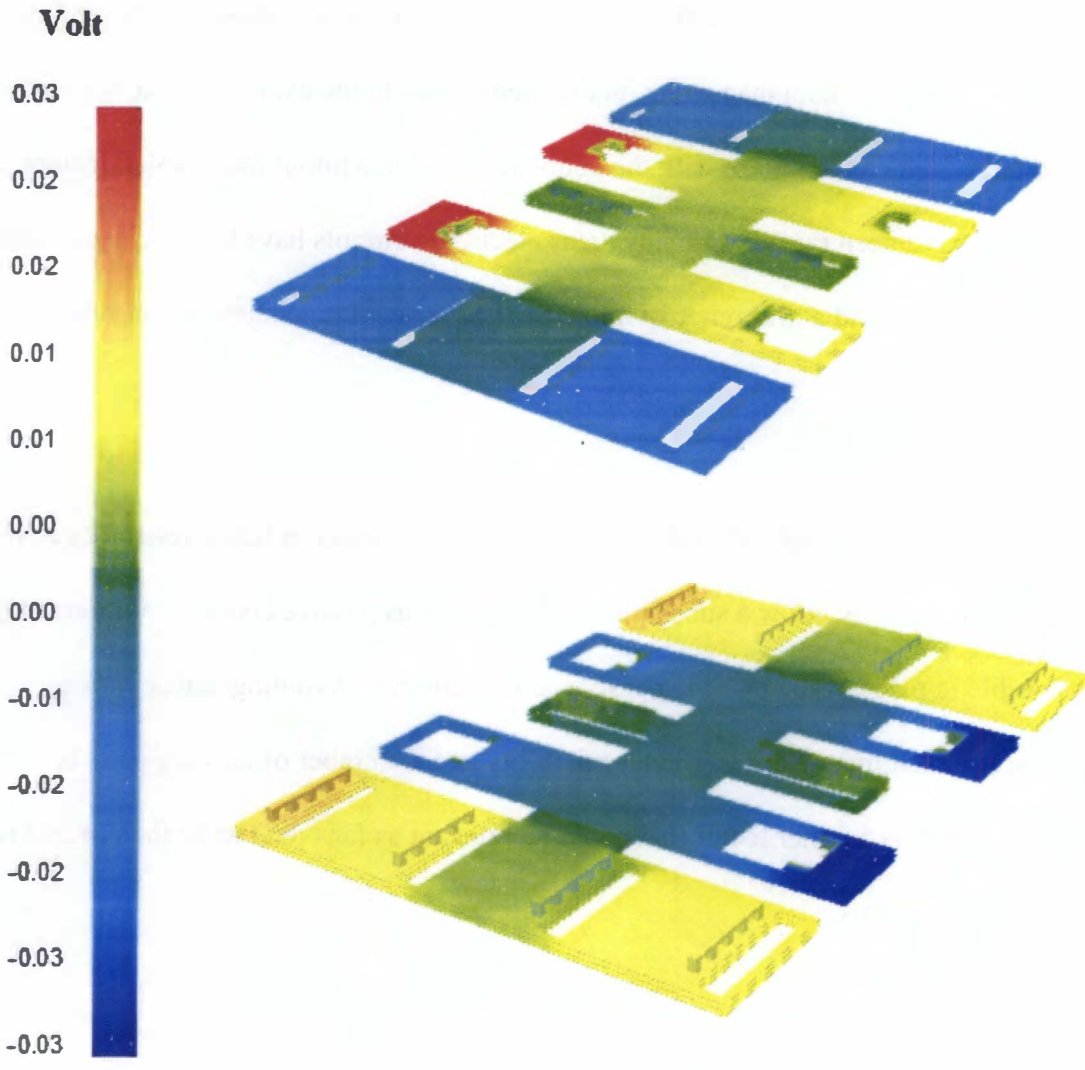


Figure 7.7: Voltage Distribution Load and Return Layers

7.8 Conclusions

The effect of coupling the thermal and electrical solutions was demonstrated. Failure to recognize the effect of the thermal gradients on the electrical properties of the system would have resulted in an inaccurate model prediction. In the example used, the model would have predicted a failure with the coupled, whereas without the coupled feature, no flag would have been raised. In many areas electronic circuits have to run close to their acceptable limits, and a difference of a few degrees in the temperature rise is very significant.

The ability to more closely simulate reality not only can result in better reliability of the circuits, but also may allow a substantial cost savings, as passive cooling solutions may be possible in place of the more expensive active fans etc. Avoiding active cooling solutions in itself may result in greater reliability as the number of moving parts is reduced. Noise is another factor that could be relevant as fans tend to be the noisiest part of electronic systems.

Chapter Eight

VIII. CLOSING REMARKS

This study was aimed at problems in which there is significant heat generation due to the flow of electrical currents in traces and conductors. Its objective was to present a novel approach to the thermal management of electronic systems that focuses on the multi-physics nature of these problems by coupling electrical, thermal and CFD effects.

8.1 Conclusions

A numerical simulator is a valuable tool to the extent that it completely addresses the relevant processes involved. This study points to a large class of electronics applications that require the coupled solution of heat transfer, flow and voltage fields. It was shown that without this coupling, the model would give misleading results. The procedure was demonstrated through the solution of two problems; a simple problem involving a single trace on a board and a relatively complex problem resembling ones often encountered in aircraft electronics applications.

The numerical results for the first application were shown to be in excellent agreement with the available test data (IPC and DN tests). For a typical case (ten amps current

flowing through a 1-oz copper trace) the maximum deviation of 2% was noticed. Additional analyses, however, underscore the fact that while these test data predict the temperature rise for a single trace on a board remarkably well, they can be very misleading in more complex real world cases.

In the second application, analyses were performed with and without coupling of the electrical field. It was shown that failure to recognize the effect of the thermal gradients on the electrical properties of the system would have resulted in an inaccurate model prediction. In the example used, the model would have predicted a failure with the coupled, whereas without the coupled feature, no flag would have been raised. In many areas electronic circuits have to run close to their acceptable limits, and a difference of a few degrees in the temperature rise is very significant.

8.2 Recommendations for Future Work

One of the main sources of inaccuracy in the thermal analysis of an electronics system is the application of the "correct" boundary conditions in order to link the system to its surroundings. The difficulty comes from the fact that electronic systems are occasionally grouped in close quarters in such a way that the temperature field in each system is strongly influenced by the operating temperature of the other electronic packages in the group. Furthermore, there are frequently other heat sources of a "non-electronics" nature that can contribute to this problem. As an example many electronics are used in underhood applications with various heat sources in their environment.

Current Commercial electronics thermal management programs do not address this issue of interconnectivity between various systems. In fact, most commercially available programs offer component level, board level and system level thermal analysis. They rely on the user to provide the necessary boundary conditions – an impossible task in many situations. Consequently, the results represent a relative solution, rather than an absolute one. In other words, they can be used to compare the thermal behavior of various designs – but, in many cases, there are rather large inaccuracies when it comes to predicting absolute component temperatures with any degree of certainty.

With recent advances in computer hardware and software technologies, it is now possible to develop a "next generation" software package for the thermal management of complex electronic systems – one that is capable of simulating several models of various electronic systems at once, all integrated into a global model that is running in parallel. In other words, the boundary conditions for the analysis are automatically provided by the parent model rather than guessed by the user. This represents a totally new approach to electronics thermal management: it enables electronics design engineers to study the thermal performance of a complex electronics module with other electronics packages or other heat sources in close proximity.

LIST OF REFERENCES

1. Baker, H. D., Ryder, E. A., and Baker, N. H., Temperature Measurement in Engineering, Omega Press, Vol. 1 and 2, 1975.

2. Merzkirch, W., Flow Visualization, Academic Press, Inc., New York, 1974.

3. Mallinson, G. D., Graham, A. D., "Experimental Visualization of Three-Dimensional Natural Convection" Aeronautic Research Laboratories, Dec, 1974.

4. Baker, A. J., Finite Element Computational Fluid Dynamics, Hemisphere Publishing Corporation, U.S.A., 1983.

5. Martin, H. C., Carey, G. F., Introduction to Finite Element Analysis, McGraw-Hill Book Company, New York, 1973.

6. Anderson, D. A., Tannehill, J. C., and Pletcher, R. H., Computational Fluid Dynamics and Heat Transfer, Hemisphere Publishing Corporation, U.S.A., 1984.

7. Hornbeck, R. W., Numerical Methods, Quantum Publisher, Inc., New York, 1975.

8. Patankar, S. V., Numerical Heat Transfer and Fluid Flow, Hemisphere Publishing Corporation, Washington, 1980.

9. Patankar, S. V., "A Calculation Procedure for Two-Dimensional Elliptic Situations", Numerical Heat Transfer, Vol. 4, pp. 409-425, 1981.

10. Ferziger, J. H., Peric, M., Computational methods for Fluid Dynamics, Springer, 3rd Edition, 2002.

11. Jackson, J. D., Classical Electrodynamics, 3rd Edition, John Wiley and Sons, Inc., 1998.

Natural Convection In Enclosures:

12. Ostrach, S., "Natural Convection in Enclosures", Adv. Int. Heat Transfer, Vol. 8, pp161-227, 1972.

13. Ostrach, S., "Natural Convection Heat Transfer in Cavities and Cells", Proceedings of the 7th International Heat Transfer Conference, Munich, Vol. 1, pp. 365-379, 1982.

14. Catton, I., "Natural Convection in Enclosures", Proceedings of the 6th International Heat Transfer Conference, Toronto, Vol. 6, pp. 13-43, 1979.

15. Ozoe, H., Sayama, H., Churchill, S. W., "Natural Convection in an Inclined Rectangular Channel", Int. J. Heat Mass Transfer, Vol. 17, pp. 401-406, 1974.

16. Ozoe, H., Sayama, H., Churchill, S. W., "Natural Convection in an Inclined Rectangular Channel at Various Aspect Ratios and Angles – Experimental Measurements", Int. J. Heat Mass Transfer, Vol. 18, pp. 1425-1431, 1975.

17. Arnold, J. N., Catton, I., Edwards, D. K., "Experimental Investigation of Natural Convection in Inclined Rectangular Enclosures of Differing Aspect Ratios", ASME Publication, 75-HT-62, 1975.

18. Ozoe, H., Yamamoto, K., Churchill, S. W. Sayama, H.,, "Three-Dimensional Numerical Analysis of Laminar Natural Convection in a Confined Fluid Heated From Below", Journal of Heat Transfer, pp. 202-207, 1976.

19. Mallinson, G. D., Davis, G. V., Three-Dimensional Natural Convection in a Box: A Numerical Study", Journal of Fluid Mech., Vol. 83, pp. 1-31, 1977.

20. Chao, P., Ozoe, H., Churchill, S. W., "The Effect of Non-Uniform Surface Temperature on Laminar Natural Convection in a Rectangular Enclosure", Chem. Eng. Commun., Vol. 9, pp. 245-254, 1981.

21. Krane, R. J., Jessee, J., "Some Detailed Field Measurements for a Natural Convection Flow in a Vertical Square Enclosure", ASME-JSME Thermal Engineering Joint Conference, Vol.1, pp. 323-329, 1983.

22. Kim, D. M., Viskanta, R., "Effect of Wall Heat Conduction on Natural Convection Heat Transfer in a Square Enclosure" ", Journal of Heat Transfer, Vol. 107, pp. 139-146, 1985.

23. Keyhani, M., Kulacki, F. A., and Christensen, R. N., "Experimental Investigation of Free Convection in a Vertical Rod Bundle - A General Correlation for Nusselt Number", Journal of Heat Transfer, Vol. 107, pp. 611-623, August 1985.

24. Yang, H. Q., Yang, K. T., Lloyd, J. R., "Flow Transition in Laminar Buoyant Flow in a Tree-Dimensional Tilted Rectangular Enclosure", ASME/JSME Thermal Eng. Conf., pp. 1495-1500, Honolulu, 1987.

25. Keyhani, M., Prasad, V. and Cox, R., "An Experimental Study of Natural Convection in a Vertical Cavity with Discrete Heat Sources", J of Heat Transfer. Vol. 110, pp. 616-624, August 1988.

26. Valencia, A., Frederick, R., "Heat Transfer in Square Cavities with Partially Active Vertical Walls", Int. J Heat Mass Transfer. Vol. 32 n 8, pp. 1567-1574, Aug 1989.

27. Neymark, J., Boardman, C. R., Kirkpatrick, A., and, Anderson, R., "High Rayleigh Number Natural Convection in Partially Divided Air and Water Filled Enclosures" Int. J Heat Mass Transfer. Vol. 32 n 8, pp. 1671-1679, Sep 1989.

28. Mahaney, H. V., Incropera, F. P., Ramadhyani, S., "Measurement of Mixed-Convection Heat Transfer from an Array of Discrete Sources in a Horizontal Rectangular Channel with and without Surface Augmentation", Exp. Heat. Transfer, Vol. 3, pp. 215-237, 1990.

29. Chadwick, M. L., Webb, B. W., Heaton, H. S., "Natural Convection from Two-Dimensional Discrete Heat Sources in a Rectangular Enclosure", Int. J Heat Mass Transfer. Vol. 34, pp. 1679-1693, 1991.

30. Chen, L., Keyhani, M., Pitts, D.R., "Convection Heat Transfer Due to Protruded Heat Sources in an Enclosure", J Thermophysics. Vol. 5 n 2, pp. 217-223, April – June 1991.

31. Kelkar, K. M., Choudhury, D., "Numerical Prediction of Periodically Fully Developed Natural Convection in a Vertical Channel with Surface Mounted Heat Generating Blocks", Int. J Heat Mass Transfer. Vol. 36 n, pp. 1133-1145, 1993.

32. Keyhani, M., Luo, L., "A Numerical Study of Convection Heat Transfer within Enclosed Horizontal Rod Bundles", Nuclear Science and Engineering. Vol. 119, pp. 116-127, August 1995.

33. Keyhani, M., Dalton, T., "Natural Convection Heat Transfer in Horizontal Rod-Bundle Enclosures", Journal of Heat Transfer. Vol. 118, pp. 598-605, August 1996.

34. Agonafer, D., Gan, L. L., Spalding, D. B., "LVEL Turbulence Model for Conjugate Heat Transfer at Low Reynolds Numbers", Application of CAE CAD to Electronic Systems, Vol. 18, ASME, New York, pp. 23-26, 1996.

Combined Natural Convection and Radiation:

35. Larson, D. W., Viscanta, R., "Transient Combined Laminar Free Convection and Radiation in a Rectangular Enclosure", J. Fluid Mechanics, Vol. 78, Part 1, pp. 65-85, 1976.

36. EleSherbiney, S. M., Hollans, K. G. T., Raithbi, G. D., "Effect of Boundary Condition in Vertical and Inclined Air Layers", J. Heat Transfer, Vol. 104, pp. 515-520, 1982.

37. Behnia, M., Reizes, J. A., De-Vahl-Davis, G., "Combined Radiation and Natural Convection in a Rectangular Cavity with a Transparent Wall and Containing a Non-Participating Fluid", Int. J. Numerical Methods Fluids, Vol. 10, pp. 305-325, 1990.

38. Smith, T. F.,Beckermann, C., Weber, S. W., "Combined Conduction, Natural Convection, and Radiation Heat Transfer in an Electronic Chassis", J. Electron. Packag, Vol. 113, pp. 382-391, 1991.

39. Lin, J. D., Huang, J.M., "Transient Laminar Natural Convection Combined with Radiation in Conjugated Problem of Rectangular Enclosures",

Conduction, Radiation and Phase Change Second Int. Conf Adv Comp. Method Heat Transfer, pp. 237-256, 1992.

40. Chuang, H., "Natural Convection-Radiation Induced Flows of Air over a Horizontal Plate", Computers in Engineering, ASME, New York, pp. 573-577, 1992.

41. Dehghan, A., Behnia, M., "Combined Natural Convection-Conduction and Radiation Heat Transfer in a Discretely Heated Open Cavity", Journal of Heat Transfer, Transactions of ASME. Vol. 118 , pp. 56-64, 1996.

42. Yu, E., Joshi, Y. K., "Air Cooling of a Vented Enclosure by Combined Conduction, Natural Convection and Radiation", Proceedings of the ASME-Heat Transfer Division ASME, Vol. 333, ASME, New York, pp. 323-330, 1996.

Cooling of Electronic Equipment:

43. Law, E. M., Livesey, J. L., "Flow Through Screens", Ann. Ren. Fluid Mech., Vol. 10, pp. 276-266, 1978.

44. Ishizuka, M., Kiyazaki, Y., Sasaki, T., "Aerodynamic Resistance for Perforated Plates and Wire Nettings in Natural Convection", ASME Publication, 84-WA/HT-87.

45. Idelchik, I. E., Handbook of Hydraulic Resistance, 3rd Edition, Begell House, 1996.

46. Aung, W., "Developing laminar Free Convection Between Vertical Flat Plates with Symmetric Heating", J. Heat Transfer, Vol. 15, 1972.

47. Aung, W., "Heat Transfer in Electronic Systems with Emphasis on Asymmetric Heating", The Bell Systems Technical Journal, Vol. 52, n6, 1973.

48. Jaluria, Y., "Buoyancy-Induced Flow Due to Isolated Thermal Sources in a Vertical Surface", Natural Convection, HTD-Vol. 16, ASME, New York, pp. 25-35, 1981.

49. Torok, D., "Augmenting Experimental Methods for Flow Visualization and Thermal Performance Prediction in Electronic Packaging Using Finite Elements", Fundamentals of Natural Convection / Electronic Equipment Cooling, HTD-Vol. 32, ASME, New York, pp. 49-59, 1984.

50. Oosthuizen, P. H., "A Numerical Study of Laminar Free Convection Flow Through a Vertical Partially-Open Place Heated Duct", Fundamentals of Natural Convection / Electronic Cooling, HTD-Vol. 32, ASME, New York, pp. 41-48, 1984.

51. Coyne, J. C., "An Analysis of Circuit Board Temperatures in Electronic Equipment Frames Cooled by Natural Convection", Fundamentals of Natural Convection / Electronic Cooling, HTD-Vol. 32, ASME, New York, pp. 59-66, 1984.

52. Park, K. A., Bergles, A. E., "Natural Convection Heat Transfer Characteristics of Simulated Microelectronic Chips", Heat Transfer in Electronic Equipment, HTD-Vol. 48, ASME, New York, pp. 29-37, 1985.

53. Lejannou, J. P., Cadre, M., Latrobe, A., Viault, A., "Thermal Field Prediction in Electronic Equipment", Int. Heat Transfer Conference, San Francesco, 1986.

54. Ishizuka, M., Miyazaki, Y., Sasaki, T., Yokono, Y., "A Practical Formula for Thermal Design of Natural-Air-Cooled Electronic Equipment Casings", Proceedings of The International Symposium on Cooling Technologies for Electronic Equipment, Honolulu, Hawaii, pp. 23-30, 1987.

55. Shen, R. Prasad, V. and Keyhani, M., "Effect of Aspect Ratio and Size of Heat Source on Free Convection in a Discretely Heated Vertical Cavity", Numerical Simulation of Convection in Electronic Equipment Cooling. HTD-Vol. 121, ASME, pp. 45-54, 1989.

56. Carmona, R , Keyhani, M., "The Cavity Width Effect on Immersion Cooling of Discrete Flush Heaters on One Vertical Wall of an Enclosure Cooled from the Top", Journal of Electronic Packaging. Vol. 111, pp. 268-276, December 1989.

57. Agonafer, D, Chu, R. C., "Numerical Methodology for Analysis of Card on Board Packages", ASME (Paper), New York, 90-WA/EEP-42. 6p, 1990.

58. Rhee, J., Moffat, R. J., "Considerations in the Numerical Simulation of Experimental Electronics Cooling Studies", Solutions to CFD Benchmark Problems in Electronic Packaging, ASME, Heat Transfer Division, HTD-Vol. 255, ASME, New York, pp. 1-9, 1993.

59. Linton, R. L., Agonafer, D., "Benchmark Problems for System-Level Electronics Cooling", Solutions to CFD Benchmark Problems in Electronic Packaging, ASME, Heat Transfer Division, HTD-Vol. 255, ASME, New York, pp. 37-43, 1993.

60. Lee, S., Song, S., Moran, K.P. and Yovanovich, M. M., "Analytical Modeling of Thermal Resistance in Bolted Joints", Enhanced Cooling Techniques for Electronics Applications , ASME, Heat Transfer Division, HTD-Vol. 263, ASME, New York, pp. 115-122, 1993.

61. Przekwas, A. J., Lai, Y. G., Agonafer, D., "Multi-Scale Thermal Analysis of Electronics Packaging", CAE CAD Application to Electronic Packaging ASME,-EEP-9, ASME, New York, pp. 7-14, 1994.

62. Habchi, S. D., Przekwas, A. J., "Simulation of System Level Electronics Cooling in a Benchmark Computer Box", Heat Transfer in Electronic Systems, ASME, Heat Transfer Division, HTD-Vol. 292, ASME, New York, pp. 71-81, 1994.

63. Landon, M. D., Campo, A., Johnson, A. W., "Optimal Cross-Section of Natural Convective Cavities Arising in Electronics Cooling", American Society of Mechanical Engineers, Heat Transfer Division HTD-Vol. 329 n 7, ASME, New York, pp. 19-26, 1996.

64. Yu, E., Joshi, Y. K., "Natural Convection Air Cooling of Electronic Components in Partially Open Compact Horizontal Enclosures", Thermomechanical Phenomena in Electronic Systems Proceedings of the Intersociety-Conference, IEEE, pp. 51-57, 1998.

65. Chu, R. C., Simons, R. E., "Application of Thermoelectrics to Cooling Electronics: Review and Prospects", International Conference on Thermoelectrics, ICT, Proceedings, IEEE, Pp. 270-279, 1999.

66. Tso, C. P., Wen, Z. M., Choo, K. F., "Numerical Simulation of Flow and Conjugate Heat Transfer in a Microchannel for Electronics Cooling", Journal of Electronics Manufacturing, Vol. 9 n 2, pp. 141-153, 1999.

67. Narasimhan, S., Mira, A., "Characterization of Compact Heat Sink Models in Natural Convection", Thermomechanical Phenomena in Electronic Systems, Proceedings of the Intersociety Conference, Vol. 1, pp. 165-179, 2000.

68. Karimanal, K., Nair, R., "Use of Zero Thickness Conducting Plate Object in Electronics Cooling Applications of CFD", Thermomechanical Phenomena in Electronic Systems, Proceedings of the Intersociety Conference, Vol.1, pp. 308-313, 2000.

69. Stiver, D. W., Shidore, S., "The Extraction of a Two-Resistor/Two-Capacitor Model for Common IC Packages and Their Implementation in CFD", Proceedings of SPIE, The International Society for Optical Engineering, Vol. 4931, pp. 915-920, 2002.

70. Phelan, P. E., Chiriac, V. A., Tom, L/ T. Y., "Current and Future Miniature Refrigeration Cooling Technologies for High Power Microelectronics", IEEE Transactions on Components and Packaging Technologies, 2002.

71. Batty, W., Christoffersen, C. E., Yakovlev, A. B., "Advanced Thermal Architecture for Cooling of High Power Electronics", IEEE Transactions on Microwave Theory and Techniques, 2002.

Coupled Thermal-Electrical Analysis:

72. Krabbenborg, B., Beltman, R., Wolbert, P., Mouthaan, T. "Physics of Electro-Thermal Effects is ESD Protection Devices", J. Electrostatics. Vol. 28 n 3 , pp. 285-299, 1992.

73. Moussali, F. E., Vullierme, J. J., "Coupled Electrical and Thermal Transfers in a Glass-Epoxy Carbon Composite. Application to the Design of a Helicopter Blade De-Icer", Recherché Aerospatiale, n 2, pp. 57-65, 1993.

74. Lai, J., Majumdar, A., "Concurrent Thermal and Electrical Modeling of Sub-Micron Silicon MOSFETs", Micro scale Heat Transfer-ASME, Heat Transfer Division, HTD-Vol. 291, ASME, New York, pp. 17-26, 1994.

75. Krabbenborg, B. H., Bosma, A., de-GraaffH. C., Mouthaan, A. J., "Layout to Circuit Extraction for Three-Dimensional Thermal-Electrical Circuit Simulation of Device Structures", IEEE Transactions on Computer Aided Design of Integrated Circuits and Systems, Vol. 15 n 7, pp. 765-774, 1996.

76. Schock, A., Noravian, H., Or, C., "Coupled Thermal, Electrical, and Fluid Flow Analyses of AMTEC Converters, with Illustrative Application to OSC's Cell Design", Electrochemical Technologies Conversion Technologies-Thermal Management, Proceedings of the Intersociety Energy Conversion Engineering Conference, Vol. 2, IEEE, pp. 1156-1164, 1997.

77. Doerstling, B., "Thermal-Electrical Modeling of Electrical Subsystems", SAE Technical Paper Series, 1998.

78. Zhu, L., Vafai, K., Xu, L., "Device Temperature and Heat Generation in Power Metal-Oxide Semiconductor Field Effect Transistors", Journal of Thermophysics and Heat Transfer, Vol. 13 n 2, pp. 185-194, 1999.

79. Sun, X., Dong, P., "Analysis of Aluminum Resistance Spot Welding Processes Using Coupled Finite Element Procedures", Welding Journal, (Miami,-Fla). Vol. 79 n 8, pp. 215-221, 2000.

80. Fedasyuk, D., Levus, E., Petrov, D., "Flip-Chip Structure Transient Thermal Model", Microelectronics Reliability, Vol.41 n 12, pp. 1965-1970, 2001.

81. Zheng, L., Fu, Y., Bai, X., and Tian, Z., "Numerical Simulation on Electro-Thermal Stress around Crack Tip in Metal Thin Plate with Crack", Jixie Gongcheng Xuebao Chinese Journal of Mechanical Engineering, Vol. 38 n 3, pp. 90-93, 2002.

82. Adam, J., "New Correlations between Electrical Current and Temperature Rise in PCB Traces", 20th IEEE Semi-Term Symposium, 2003.

83. Brooks, D., "Temperature Rise in PCB Traces", Proceedings of the PCB Design Conf., pp. 23-27, 1998.

APPENDICES

Appendix A

Divergence Theorem – Definition and Interpretation

Given a vector field $\vec{A}$ that is continuously differentiable over a regular volume V and its bounding surface s, divergence theorem states the following integral equation:

$$\int_V div\left(\vec{A}\right) dV = \int_s \vec{n}.\vec{A} ds$$

Interpretation of the Divergence

From the above equation, we may write:

$$div\left(\vec{A}\right) = \lim_{V \to 0} \left[\frac{1}{V} \int_s \vec{n}.\vec{A} ds \right]$$

Therefore, the divergence of a vector may be regarded as the net outflow rate per unit volume of the quantity of which $\vec{A}$ measures the flux.

Examples:

When $\vec{A}$ stands for $\rho\vec{U}$ (mass flux), then $div\left(\rho\vec{U}\right)$ is the rate of net outflow of mass per unit volume of an infinitesimal control volume.

When $\vec{A}$ stands for $-k\nabla T$ (conduction heat flux), then $div\left(-k\nabla T\right)$ is the rate of net outflow of energy by conduction per unit volume of an infinitesimal control volume.

Appendix B

Interface conductivity

The conductivity (or in more general sense, the diffusion coefficient) often has spatial variation. For these cases the value of k is generally known at the grid points; but, needed at the control surfaces. This nonuniformity in the conductivity can arise from nonhomogeneous materials (i.e, composites) or from temperature dependence.

To obtain a general expression for the interface conductivity, we focus our attention on the two adjoining control volumes surrounding points P and E and the interface at the location e, as shown in Figure B.1.

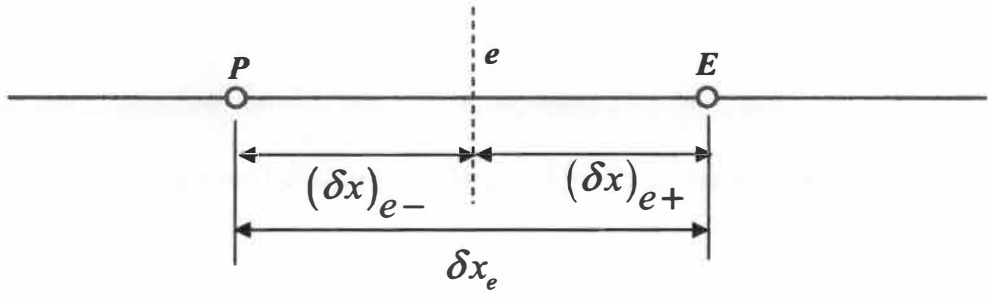


Figure B.1: Adjacent Control Volumes with Associated Distances

The heat flux crossing the control surface, e, can be expressed in two ways, 1) using the interface conductivity, and 2) using grid-point conductivities and treating two adjoining control volumes as a composite slab.

$$q_e = \frac{k_e\left(T_p - T_e\right)}{\left(\delta x\right)_e} \tag{B.1}$$

$$q_e = \frac{\left(T_p - T_e\right)}{\frac{\left(\delta x\right)_{e-}}{k_P} + \frac{\left(\delta x\right)_{e+}}{k_E}} \tag{B.2}$$

Equating Equation (B.1) and (B.2) and solving for k_e yields:

$$k_e = \frac{\left(\delta x\right)_e}{\frac{\left(\delta x\right)_{e-}}{k_P} + \frac{\left(\delta x\right)_{e+}}{k_E}} \tag{B.3}$$

To further simplify, let $f_e = \frac{\left(\delta x\right)_{e+}}{\left(\delta x\right)_e}$

$$k_e = \left[\frac{1-f_e}{k_P} + \frac{f_e}{k_E}\right]^{-1} \tag{B.4}$$

Note that if the control surface is placed midway between the grid-points, the above reduces to the harmonic mean of the two grid-point conductivities:

$$k_e = \frac{2k_P k_E}{k_P + k_E} \qquad \text{if } f_e = 0.5 \tag{B.5}$$

Appendix C

Correlations Used for Natural Convection Boundary Condition

The following correlations were used for various natural convective boundary conditions in Chapters six and seven.

Vertical Walls

The average heat transfer coefficient for a vertical isothermal wall is calculated from the following equation:

$$h = \left(0.68 + \frac{0.670 Ra_L^{1/4}}{\left[1 + \left(\frac{0.492}{\mathrm{Pr}} \right)^{9/16} \right]^{4/9}} \right) \times \left(\frac{k}{L} \right) \qquad \left(0 < Ra_L < 10^9 \right)$$

Top Surface

The convective heat transfer coefficient for the top surface is taken from the correlation for upper surface of horizontal heated plate:

$$h = \left(0.54 Ra_L^{1/4} \right) \times \left(\frac{k}{L} \right) \qquad \left(10^4 \le Ra_L \le 10^7 \right)$$

$$h = \left(0.15 Ra_L^{1/3} \right) \times \left(\frac{k}{L} \right) \qquad \left(10^7 \le Ra_L \le 10^{11} \right)$$

Bottom Surface

For the bottom surface the correlation for the lower surface of a heated plate can be used::

$$h = \left(0.27 Ra_L^{1/4}\right) \times \left(\frac{k}{L}\right) \qquad \left(10^5 \le Ra_L \le 10^{10}\right)$$

Where:

h	=	Heat transfer coefficient
Ra	=	Rayleigh number
Pr	=	Prandtl number
L	=	Characteristic length

The Rayleigh number, Prandtl number and characteristic length are defined as follows:

$$Ra_L = \frac{g\beta\left(T_s - T_\infty\right)L^3}{\nu\alpha}$$

$$\mathrm{Pr} = \frac{\nu}{\alpha}$$

L = Plate height for vertical plate

= Surface area divided by the perimeter for horizontal plate

VITA

Mr. Bahram (Ben) Zandi completed his early schooling in Tehran, Iran. In September of 1979, he started his undergraduate studies at the University of Tennessee. He received his B.S. degree in Mechanical Engineering with "High Honors" in 1983. Mr. Zandi began his graduate studies in Fall term of 1983 and he maintained a GPA of 3.99/4.00 through the Masters and Ph.D. programs. In summer 1992, Mr. Zandi put the pursuit of his Ph.D. on hold (at the time, the numerical problem was too complex for the available computers) and accepted a job at e3 Engineering in Southfield, Michigan, as a thermal specialist. In August 1994, Mr. Zandi founded Thermal Engineering Services, Inc, a Michigan corporation providing software and services to automotive and aircraft electronics industries. Mr. Zandi obtained his Ph.D. degree in May 2005. He is currently Founder, Chairman and Chief Technology Officer at TES International, a software and services company serving aircraft and automotive industries located in Troy, Michigan.

2094 9169 16
08/17/05 MAB